Title
A Macro- and Micro-Designed Chitosan-Alginate Scaffold with Sustained Growth Factor Release for Chondrogenesis

Author
Reed, Stephanie

Publication Date
2014

Peer reviewed|Thesis/dissertation

UNIVERSITY OF CALIFORNIA

Los Angeles

A Macro- and Micro-Designed Chitosan-Alginate Scaffold with Sustained Growth Factor Release for Chondrogenesis

A dissertation submitted in partial satisfaction of the requirements for the degree Doctor of Philosophy in Biomedical Engineering

by

Stephanie M. Reed

2014

ABSTRACT OF THE DISSERTATION

A Macro- and Micro-Designed Chitosan-Alginate Scaffold

with Sustained Growth Factor Release

for Chondrogenesis

by

Stephanie M. Reed

Doctor of Philosophy in Biomedical Engineering

University of California, Los Angeles, 2014

Professor Benjamin M. Wu, Chair

Cartilage regeneration is a promising field with many attempts at creating a tissue-engineered cartilage substitute. While many tissue-engineered skin and bone products exist and continue to enter the market, there remains no FDA-approved solution to regenerate the avascular, aneural cartilage tissue other than autologous chondrocyte implantation, which is both costly and requires weeks of cell culture time, not to mention healthy cartilage from which to harvest the chondrocytes. Many attempts to create biomaterial scaffolds for implantation are being made, yet these technologies often require seeded cells, and the resulting cartilage (if there is proper cartilage regeneration and not fibrocartilage production) often lacks the zonal architecture that gives native cartilage its unique structural and functional properties. Lots of recent focus has been given to growth factor delivery from within scaffolds to assist cartilage regeneration, specifically to signal ECM production by chondrocytes. However, most diffusion-based growth factory delivery systems

suffer from a large burst release and do not provide a sustained release over the course of many weeks, which is required for cartilage production. Materials with growth factors chemically conjugated to their surface offer some advantage of a gradual release as the bulk material degrades and permanent presentation of the bioactive molecule, but certain growth factors require internalization for activation of their signaling cascades and conjugation chemistry to surfaces can be inefficient or render the protein biologically inactive. This project aims to develop an acellular scaffold implant with biomimetically designed micro- and macro-architecture that also delivers a chondrogenic growth factor via a sustained release mechanism to promote cartilage regeneration. This scaffold would be implanted into the joint during resurfacing and would facilitate the instant uptake of underlying bone marrow and residing mesenchymal stem cells, which would then be guided to differentiate into chondrocytes once in contact with the slowly diffusing chondrogenic growth factor. This system would address the many challenges facing cartilage tissue engineers today and has the potential to become an off-the-shelf solution for cartilage regeneration.

The dissertation of Stephanie M. Reed is approved.

James C. Dunn

Min Lee

David R. McAllister

Benjamin M. Wu, Committee Chair

University of California, Los Angeles

2014

I would like to dedicate this PhD dissertation to my loved ones and family who have supported me throughout this process. In addition, I would like to express my deepest gratitude to Dr. McAllister and Dr. Dunn for being a part of my committee and assisting my research over the years, Dr. Lee for his advice and involvement during our many subgroups meetings, and Dr. Wu for his unwavering support of my research and my abilities as a scientist, engineer, researcher, and contributor to the field.

Table of Contents

List of Figures

Stephanie Reed earned her Bachelor of Science from Massachusetts Institute of Technology in mechanical engineering in 2007 with a minor in biomedical engineering. She then earned her Master of Science from University of California Los Angeles in biomedical engineering in 2009. Stephanie Reed has published a review paper with Dr. Benjamin Wu titled "Sustained Growth Factor Delivery in Tissue Engineering Applications" in the Annals of Biomedical Engineering in 2013. She also has published a paper with Dr. Benjamin Wu and Debrobato Das titled "A High-Throughput Comparative Characterization of Laser-Induced Soft Tissue Damage using 3D Digital Microscopy" in Lasers in Medical Science in 2012. Her undergraduate research was published at MIT in 2007 with Dr. Paul Matsudaira and Dr. James Evans in a paper titled "Analyzing GFP-tagged Cytoskeletal Protein Colocalization in Human Carcinoma Cells". Stephanie Reed has a joint patent with Dr. Benjamin M. Wu and Emily Loughran titled "Multi-Layer Cast Systems and Methods" which was approved in November 2013.

Chapter 1

1. Introduction

1.1 Cartilage Overview

Hyaline cartilage covers the articulating surfaces of bones in condylar-type joints. This articular cartilage serves as a cushion to absorb impact and provides stable movement with little friction between joint surfaces. Despite being an avascular and non-innervated matrix, articular cartilage can modify its characteristics in response to differential loading. This complexity combined with its ability to distribute load and resist compression make articular cartilage difficult to replace with tissue engineered designs.[1]

Chondrocytes are the single cell type in articular cartilage, yet they only comprise 1% of hyaline cartilage volume. Chondrocytes are responsible for producing and maintaining the extracellular matrix (ECM), which in turn affects the mechanical properties of the tissue.[1] Chondrocyte differentiation, proliferation, and homeostasis are governed by ECM signaling mediated by integrin receptors. The ECM also regulates chondrocyte behavior by binding, storing, and releasing soluble factors. Further, chondrocyte integrins may need to be bound to the surrounding ECM molecules before chondrocytes are responsive to growth factors. This indicates a mutual dependence between chondrocyte adhesion to the ECM and chondrocyte regulation by soluble mediators.[2] In addition to signaling by growth factors and matrix molecules, cell-cell adhesion via cadherins, immunogloblins, and selectins determine chondrocyte response. Both cell-cell and cell-matrix interactions activate specific intracellular signaling pathways and actin cytoskeleton dynamics, which control chondrogenesis.[3]

Mechanical stimulus is another mechanism that motivates chondrocyte function. Chondrocytes respond to mechanical loading through multiple signaling pathways that can change transcription, translation, post-translational states, and ECM assembly and degradation. Joint loading *in vivo* is a complex combination of compressive, tensile, and shear deformations of cartilage. Dynamic compression of the ECM induces hydrostatic pressure gradients, interstitial fluid flow, and volumetric changes. Fluid convection and disruption of counterions from proteoglycan groups causes electrical streaming potentials and currents. Contrastingly, shear of a poroelastic tissue like articular cartilage does not create these effects. The compressive stiffness of chondrocytes is around three orders of magnitude less stiff than the surrounding ECM, so cells deform with the matrix and are sensitive to mechanical stimuli. Mechanotransduction has been shown to increase matrix biosynthesis and chondrogenic gene expression, but under specific loads and strains below the threshold for injury (5-10 MPa normal stress range, 300-800% body weight normal load range, ~40% normal strain).[4,5]

Many extracellular matrix molecules form the structure of articular cartilage. Collagen types II, VI, IX, X, and XI exist in native cartilage, but 90-95% of matrix collagen is made up of collagen type II. Type II collagen interacts with water more than other types due to its high amount of bound carbohydrates. Types II, IX, and XI form fibrils that interweave into a mesh, thus creating tensile strength. Glycosaminoglycans (GAGs) such as chondroitin sulfate and keratan sulfate, which together create the proteoglycan complex aggrecan, also exist in abundance in cartilage ECM. Hyaluronic acid, dermatan sulfate, and heparan sulfate are other common GAGs found in articular cartilage. The negatively-charged GAGs account for some notable cartilage properties like its resistance to compression and swollen state. Upon compression, electrostatic repulsion is generated between negatively-charged aggrecan molecules. Hyaluronic acid forms aggregates with aggrecan molecules, attracting cations and subsequently imbibing water to minimize osmotic pressure differences.[1]

The orientation of matrix and cells changes throughout four zones in mature cartilage: parallel collagen fibrils and flat chondrocytes in the superficial zone, random collagen fibrils and round chondrocytes in the middle zone, perpendicular collagen fibrils and columns of chondrocytes aligned with the fibril axis in the deep zone, and a transition from hyaline cartilage to bone in the calcified zone. The tidemark is a basophilic line between deep and calcified zones that marks the beginning of subchondral bone. Further matrix organization is found in articular cartilage within the four zones. In each zone, there are three distinct regions known as the pericellular region, the territorial region, and the interterritorial region. The pericellular and territorial regions allow for chondrocyte attachment to the ECM and protect cells during loading. The pericellular region is composed of mostly noncollagenous binding proteins. The territorial region contains collagen fibrils on the periphery of the pericellular envelope. However, as the territorial region extends away from the cells, collagen is less aligned and fibrils cross to form a square structure around chondrocytes. Fibril diameter increases and fibers align in parallel in the interterritorial region. The primary source of cartilage's strength originates in the interterritorial region.[1] It is important to note that immature cartilage is markedly different in architecture from mature cartilage. Instead of zonal structure, immature cartilage is thicker, more permeable, and contains both articular cartilage and epiphyseal growth plate features. The bulk of developing cartilage is mostly isotropic with random chondrocyte arrangement.[6]

Cartilage formation is one of the first evident morphogenetic events in embryonic development. Transient cartilage in the developing embryonic limb is classically used as a model to elucidate the maintenance of permanent articular cartilage in joints. Endochondral ossification, a strictly regulated process which gives rise to skeletal tissues that protect and structurally support vertebrates, begins with chondrogenesis. Undifferentiated mesenchymal cells condense and produce collagen type I, hyaluronic acid, tenascin, and fibronectin. Upon chondrogenic differentiation of cell condensations, ECM composition changes as chondrocytes express collagen types II, IX, and XI, Gla protein, aggrecan, and link protein, while collagen type I production is halted. After further differentiation and hypertrophy, chondrocytes produce collagen type X and decrease collagen type II expression. The region becomes vascularized, and osteoblasts transported by blood vessels replace the cartilage with mineralized bone. Mesenchymal condensation is driven by cell-cell and cell-matrix interactions, hence neural cadherin (N-cadherin), neural cell adhesion molecule (N-CAM), and fibronectin play an important role in condensing the mesenchyme but disappear upon cartilage differentiation.[7]

A number of signaling molecules such as Wnts, transforming growth factors-β (TGF-βs), and fibroblast growth factor (FGFs), as well as their downstream effectors such as mitogen-activated protein kinases (MAPKs) and homologues of *Drosophila* mothers against decapentaplegic (SMADs), are responsible for initiating and maintaining chondrogenesis in the developing limb.[7] Three major MAPK pathways specifically transmit signals necessary for chondrogenesis. Extracellular signal-regulated kinase 1/2 (ERK1/2) is one of the principal cytoplasmic signal transduction systems controlling proliferation, differentiation, and cell survival. Dual-phosphorylated ERK1/2 is abundantly present in limb buds and limb forming regions, and manipulations that reduce ERK1/2 signaling led to truncations in limb outgrowth. The p38 MAPK cascade is activated by a wide range of cellular stressors including heat shock, ultraviolet irradiation, osmotic disturbance, cytokines, and hormones. Inhibiting p38 has consistently resulted in the suppression of cartilage matrix production. C-jun N-terminal kinase (JNK) pathway is also initiated by noxious stressors, particularly stimulants like heat shock, ionizing radiation, oxidant stress, and mechanical shear. JNK has been shown to mediate cyclic loading stimulated cartilage ECM metabolism. Further, JNK may work in conjunction with p38 to regulate axial patterning and skeletogenesis.[8]

Normal limbs develop along three axes: proximodistal, dorsoventral, and anterioposterior. Limb patterning depends on the interaction of numerous proteins, specifically growth factors such as Wnts, TGF-βs (including BMPs), and FGFs and transcription factors such as engrailed (En), Sonic hedgehog (SHH), Indian hedgehog (IHH), radical fringe (rFrg), and those encoded by homeobox (Hox) and Sry-related high mobility group box (Sox).[9,10] Disruption of any of these signaling molecules will affect all developing limb axes, as the limb is an integrated structure that requires cooperative signal transduction.[7]

1.2 Cartilage Disease and Injury

Cartilage has limited regenerative capacity due to the lack of vascularization of the native tissue. Thus, when cartilage deteriorates due to aging and osteoarthritis, or when cartilage is torn in an injury, tissue is not easily replaced or repaired. Osteoarthritis is the thinning and wearing of articular cartilage. There is an overall loss of cartilage elasticity and change in underlying bone creating spurs. Particles become loose in the joint, which initiates inflammation of the synovium joint lining as well as cytokine and enzyme signaling. The end result is bone rubbing against bone, reduced motion, and pain. Arthritic change is first detectable as the cartilage surface becomes frayed and fibrillated. A loss of matrix molecules such as proteoglycans is standard.[11] Proteoglycan synthesis decreases while collagen content increases in older cartilage tissue. Moreover, aggrecan degradation by aggrecanases and metalloproteinases increases with age.[12] Various sugars in the body can accumulate and crosslink the collagen network in cartilage by a process known as non-enzymatic glycation. This creates a brittle, glycated tissue that is prone to failure or arthritic wear.[5]

At the start of osteoarthritis (OA), cartilage attempts to repair itself by initiating chondrocyte proliferation, clustering, and matrix production. As mechanical degenerative forces persist, degradative enzymes outweigh cartilage synthesis abilities. Surface fibrillation progresses causing the defect to penetrate deeper through the cartilage, and subchondral bone thickens and becomes exposed. Without a traumatic insult to the joint, the catalyst instigating degeneration in OA is difficult to identify.[10]

Biomechanical properties of cartilage are compromised during OA, but it is unclear whether this is a cause or result of the disease. The mechanical injury that occurs during OA induces swelling and deceases the compressive and shear stiffness of cartilage, most likely because of collagen network disruption. Proteoglycan content decreases in injured cartilage, and articular cartilage loses the ability to respond to physiological levels of mechanical stimuli and increase biosythesis. ECM is broken down by matrix-metalloproteinases (MMPs), particularly MMP1, MMP2, MMP3, MMP9, and MMP13, which increase in quantity after injury and may be regulated by vascular endothelial growth factor (VEGF) signaling.[13] Interestingly, chondrocytes in osteoarthritic cartilage have altered viscoelastic properties, affecting their response to mechanical stimuli.

Osteoarthritis involves an imbalance of metabolic pathway cytokines and growth factors. The resulting inflammation and MMP surplus cause matrix degradation, while resulting dedifferentiation and apoptosis cause the cessation of matrix synthesis. These events cooperatively lead to cartilage destruction. Abnormal Wnt signaling is thought to contribute to cartilage destruction in OA and rheumatoid arthritis (RA) by governing matrix remodeling, chondrocyte apoptosis, and inflammation. Wnt signaling components, such as frizzled B2 (FrzB2), are expressed at high levels in OA chondrocytes compared to control chondrocytes. β-catenin accumulates in dedifferentiated chondrocytes in arthritic cartilage by avoiding proteasomal degradation. Also, Wnt7a and Wnt16 expressions are upregulated in arthritic cartilage. However, elevated amounts of Wnt components may not prove a correlation with cartilage destruction. Further studies elucidate Wnt7a's role in ceasing collagen type II synthesis and activating cyclooxygenase 2 (COX2) expression through the β-catenin-Tcf/Lef transcriptional canonical pathway. Wnt3a-stimulated chondrocytes activate c-Jun and its phosphorylation by noncanonical JNK signaling, leading to activator protein 1 (AP1) activation. This in turn suppresses Sox9 expression which downregulates collagen type II production. Overall, Wnt3a, Wnt7a, Wnt5a, and Wnt11 contribute to the dedifferentiation of chondrocytes into fibroblastic cells via canonical and noncanonical Wnt pathways.[8]

Basic FGF (bFGF) and FGF18 have been proposed as regulators of articular cartilage homeostasis. Recent studies suggest that bFGF selectively activates FGF receptor 1 (FGFR1) to exert degradative effects in adult human articular cartilage. This ligand-receptor binding antagonizes the insulin-like growth factor 1 (IGF1)/BMP pathway, stimulates noggin expression, stimulates MMPs and aggrecanases, and also promotes cell proliferation and clustering. In contrast, FGF18 binding to FGFR3 enhances the BMP pathway, suppresses noggin expression, suppresses MMPs, and exerts anti-proliferative effects.[14]

Matrix degradation products generated by excess proteolysis in OA also contribute to cartilage destruction. Increased levels of these degradation products are found in diseased joints and partake in harmful catabolic activities that amplify the disease state. Specifically, fibronectin proteolytic fragments can activate chondrocytes and synovial fibroblasts through cell surface receptors that stimulate catabolic intracellular pathways. Central cell-binding, N-terminal gelatin-binding, N-terminal heparin-binding, and C-terminal heparin binding fibronectin fragments destroy cartilage in a number of ways: induction of chonrdrolysis, enhancement of proteoglycan loss by stimulating MMPs, enhancement of type II collagen loss by stimulating collagenases, diminishment of proteoglycan synthesis, production of nitric oxide (NO), and activation of all three MAPK families.[15]

In addition to osteoarthritic disease, acute joint injury poses serious side effects to cartilage tissue. Traumatic joint injury has been linked to developing OA later in life. Within days of an injury, MMP levels increase to 50-100 times the level in healthy athletes, yet remain 10 times higher even 10-15 years after the traumatic event.[13] Traumatic cartilage injuries are either considered microdamage, chondral fractures, or osteochondral factures. Accumulated microdamage or blunt trauma results in a biomechanical response similar to OA and eventually becomes irreparable. Chondral fracture causes chondrocyte necrosis at the site followed by increased metabolic and mitotic activity within days of injury. Fibrous tissue formation and ECM production occur for approximately two weeks post-injury. Newly synthesized matrix is typically insufficient for surface restoration and often deteriorates months later. Osteochondral fractures penetrate the tidemark and subchondral vasculature elicits the three-phase repair process seen in other tissues. However, within a year, replacement fibrous tissue and fibrocartilage producing collagen type I dominate and weaken the repair tissue.[10]

1.3 Current Treatments

Standard surgical options to repair articular cartilage are often variably successful and only a temporary fix to a chronic problem. One common surgical treatment currently used to treat OA and cartilage injury is arthroscopic chondroplasty, also called debridement. Using an arthroscopic approach, damaged tissue is trimmed away to stabilize the area. This prevents flaking off of the damaged tissue, which often irritates the lining of the joint and leads to inflammation. Arthroscopic chondroplasty may relieve pain temporarily, but it does not regenerate the cartilage defect. Another main surgical treatment is marrow stimulation, or microfracture. With this method, marrow stem cells from the subchondral region enter the defect through drilled holes or abrasion and help heal the wounded cartilage.[10] Intraarticular hyaluronic acid injections referred to as viscosupplementation have been explored as method of improving lubrication in the joint. Injections are given every 6 weeks to reduce pain and restore viscoelasticity, but clinical results are still inconclusive.

In the case of severe cartilage damage or after other methods have failed, articular cartilage can be resected and replaced with an implantable prosthesis. Partial knee resurfacing restores only the one damaged compartment of the joint, whereas total knee resurfacing restores all three articulating surface compartments. Knee replacement, which can also be either partial or total, involves greater tissue resection and replaces articular surfaces and the meniscus. The implants are titanium or cobalt/chromium alloy components that are impacted into the underlying bone and fixed with polymethylmethacrylate cement. The femoral implant is curved to mimic the natural contour of the bone, and the tibial implant is flat, often with a stem that reaches farther inside the bone for stability. A flat high density polyethylene dish is placed between the metal components to provide smooth motion and dampened loading.[1]

Other treatment modalities include soft tissue grafts using the periosteum and perichondrium. Mesenchymal progenitor cells are present in the periosteum, and local oxygen and nutrient scarcity encourage chondrogenic differentiation. Perichondrial grafts are less successful than periosteal grafts, and the periosteum is more accessible and abundant than the perichondrium. Osteochondral allograft transplantation is also available, but there is often subchondral bone collapse and creeping substitution of bone in the failed graft, thus affecting joint mechanics and destroying transplanted cartilage. These clinical studies illustrate that osteochondral transplantation only provides temporary functionality, if any improvement at all.[10]

Autologous cell transplantation as a cartilage regeneration therapy offers many benefits such as no rejection of the implanted cells and no need for donors. In autologous chondrocyte transplantation (ACT), chondrocytes are isolated from biopsies taken from a minor weight-bearing area of the injured knee. The cells are expanded in monolayer culture and injected into the cartilage defect using a periosteal patch for containment. The periosteum is sutured in place and glued with fibrin sealant before cell injection. Bilayer collagen membranes have been used in place of the periosteal flap in order to simplify surgery and reduce morbidity. Common complications include periosteal hypertrophy, delamination of the transplant, intraarticular adhesions, fibrosis, and transplant failure. Future generations of ACT that include a biomaterial matrix are in progress. Cells will be secured in the defect area with a resorbable scaffold to create a matrix-associated autologous chondrocyte transplantation (MACT). This development allows for the immediate culture of chondrocytes in the three-dimensional scaffold without monolayer expansion.[16,17] Because sutures can fail under friction from the opposing joint surface, new methods of ensuring graft fixation are desired. Cell-scaffold constructs were successfully delivered to articular cartilage defects arthroscopically using a press fit method, although defects were greatly limited in size to 7 mm.[18]

To date, none of the present cartilage replacement techniques has generated cartilage tissue that meets the functional demands of an *in vivo* environment. Major problems persist with the cell-based approaches mentioned above. Insufficient differentiation cues lead to un- or dedifferentiated cells, hypertrophy, osteogenesis, and senescence. Timed delivery of chondrogenic growth factors or gene therapy may be necessary to ensure total and directed differentiation down the chondrogenic pathway. Inhibiting known pathways can help prevent osteogenesis and hypertrophy. Senescence can be combated with low oxygen tension, anti-oxidants, and anti-inflammatories. Another obstacle with current strategies is the uncontrolled loss of transplanted cells. Cell delivery is often inefficient and inhomogeneous, and furthermore stressors can induce chondrogenic apoptosis. Necrosis due to NO, age, mechanical, chemical, and oxidative stress can be targeted with anti-oxidants, anti-inflammatories, and mechanical protection. Current Food and Drug Administration (FDA) approved approaches to cartilage regeneration have yet to overcome these challenges, but improvements incorporating biomaterials and signals are underway in both preclinical and clinical experiments.[19]

1.4 Emerging Research

The need for tissue engineered cartilage products that surpass cells-only or transplant techniques grows continuously as more people develop debilitating OA or suffer acute joint injuries. It is advantageous, for the reasons previously listed, to incorporate scaffolds and signaling molecules along with cellular therapy in cartilage tissue engineering advances. Many studies in this field explore the myriad combinations of cell types, materials, and signals in hopes of creating a construct that will regenerate or replace cartilage.

Different cell lines have distinct advantages and disadvantages. Primary chondrocytes are perhaps the most obvious cell type for cartilage regeneration, but they are limited in number and de-differentiate or lose phenotype in monolayer culture. While primary chondrocytes are a homogeneous population within the individual, autologous primary chondrocytes taken from an osteoarthritic joint for ACT may be diseased or aged, while allogeneic primary chondrocytes provided by a donor will elicit an immune response when transplanted into a patient. Adult mesenchymal stem cells (MSCs) are easily obtained from bone marrow and possess multipotency. MSC plasticity allows them to differentiate into bone, cartilage, and adipose-like cell types, even after passaging in culture. Other sources for MSCs include adipose tissue, placenta, and umbilical cord blood and Wharton's jelly. The name "multipotent stromal cell" is sometimes proposed as a more correct definition because MSCs can be derived from non-mesenchymal tissues such as muscle and dental pulp. Adipose-derived stem cells (ASCs) are easily isolated from fat, typically from liposuction. ASCs have been shown to be similar to MSCs in function and also can undergo chondrogenesis. The synovium and periosteum also contain stem cells which have demonstrated chondrogenic potential. Embryonic stem cells (ESCs) can undergo hundreds of rounds of cell doubling and can differentiate into all somatic cell types after embryoid body aggregation. However, they raise ethical concerns, and their pluripotency may be difficult to control. Induced pluripotent stem cells (iPSCs) are defined as ESC-like but avoid the ethical dilemma because they are reprogrammed somatic cells exposed to pluripotency genes. iPSCs are under heavy investigation and may lead to unwanted teratoma formation during treatment.[20,21]

Many stimulating factors have been employed to induce, accelerate, or enhance cartilage formation. Growth factors and other additives are supplemented to culture media *in vitro* and delivered within scaffolds *in vivo*. Soluble factors like BMPs, FGF2, IGF1, and TGF-βs are extensively used and investigated both independently and cooperatively. Mechanical signals can be introduced through loading regimes like hydrostatic pressure, dynamic compression, and bioreactor culture. Gene therapy is another method of local delivery in which cells are manipulated to overexpress bioactive molecules. Both viral and non-viral transfection agents can be used in *ex vivo* gene therapy to transiently overproduce and release proteins from cell-seeded scaffolds. This is an alternative to encapsulating biological agents, which have short half lives, within scaffolds.[21]

Scaffolds provide a three-dimensional environment for cell and growth factor delivery. Polymer scaffolds are commonly used in the forms of hydrogels, sponges, and fibrous meshes for cartilage regeneration. Polymeric materials are categorized as either natural or synthetic. Natural polymers include collagen, hyaluronic acid, chondroitin sulfate, fibrin, chitosan, alginate, agarose, gelatin, cellulose, and silk fibroin. Natural scaffolds are bioactive and interact with cell surface receptors to regulate cell function. However, natural materials may be mechanically inferior and subject to variable degradation by host enzymes. Synthetic polymers include polyα-hydroxy esters like polylactic acid (PLA), polyglycolic acid (PGA), and copolymer PLGA, polyethylene glycol/oxide, polyNiPAAm, polypropylene fumarate, polyurethane, and polyvinyl alcohol. Synthetic materials are more predictable, versatile, and easily modified but do not contribute to cell-scaffold interactions. Degradation products of synthetic materials may also be toxic or induce inflammation.[21,22,23]

Poly α-hydroxy esters have United States FDA approval for clinical use. Alginate has FDA approval for use in wound dressings. None of the other aforementioned polymeric materials are permitted for human use, but ongoing research will hopefully broaden the landscape.[20] Ochi et al summarized scaffolds that have potential for clinical application based on the materials' clinical experience. Prospective and retrospective clinical trials using scaffolds such as collagen type I gel, collagen type I-III membrane, hyaluronic acid, fibrin, and PLGA were reviewed. However, there was no clear ranking or firm recommendation on which cartilage repair material is preferred.[24] The ideal cartilage scaffold has many design requirements including allowance for nutrient and waste diffusion, promotion of cell viability, differentiation, and ECM production, adherence to and integration with surrounding cartilage, replacement of a variety of defect volumes, mechanical integrity, proper surface chemistry, and directed and controlled degradation.[21]

References

1. Temenoff JS, Mikos AG. Review: tissue engineering for regeneration of articular cartilage. Biomaterials 2000;21:431-440.
2. Kran PM, Buma P, Kuppevelt T, Berg WB. Interaction of chondrocytes, extracellular matrix and growth factors: relevance for articular cartilage tissue engineering. Osteoarthritis and Cartilage 2002;10:631-637.
3. Woods A, Wang G, Beier F. Regulation of Chondrocyte Differentiation by the Actin Cytoskeleton and Adhesive Interactions. Journal of Cellular Physiology 2007;213;1-8.
4. Grodzinsky AJ, Levenston ME, Jin M, Frank EH. Cartilage Tissue Remodeling in Response to Mechanical Forces. Annu Rev Biomed Eng 2000;2:691-713.
5. Kerin A, Patwari P, Keuttner K, Cole A, Grodzinsky A. Molecular basis of osteoarthritis: biomechanical aspects. Cell Mol Life Sci 2002;59:27-35.

6. Williams GM, Klisch SM, Sah RL. Bioengineering Cartilage Growth, Maturation, and Form. Pediatric Research 2008;63(5):527-534.
7. DeLise AM, Fischer L, Tuan RS. Cellular interactions and signaling in cartilage development. Osteoarthritis and Cartilage 2000;8:309-334.
8. Bobick BE, Kulyk WM. Regulation of Cartilage Formation and Maturation by Mitogen-Activated Protein Kinase Signaling. Birth Defects Research (Part C) 2008;84:131-154.
9. Chun JS, Oh H, Yang S, Park M. Wnt signaling in cartilage development and degeneration. BMB Reports 2008;41(7):485-494.
10. Yates KE, Shortkroff S, Reish RG. Wnt Influence on Chondrocyte Differentiation and Cartilage Function. DNA and Cell Biology 2005;24(7):446-457.
11. Frenkel SR, Di Cesare PE. Degradation and Repair of Articular Cartilage. Frontiers in Bioscience 1999;4:671-685.
12. Sztrolovics R, Alini M, Roughley PJ, Mort JS. Aggrecan degradation in human intervertebral disc and articular cartilage. Biochem J 1997;326:235-241.
13. Kurz B, Lemke AK, Grodzinky AJ, Schunke M, et al. Pathomechanisms of cartilage destruction by mechanical injury. Ann Anat 2005:187:473-485.
14. Ellman MB, An HS, Muddasani P, Im HJ. Biological impact of the fibroblast growth factor family on articular cartilage and intervertebral disc homeostasis. Gene 2008;420:82-89.
15. Yasuda T. Cartilage destruction by matrix degradation products. Mod Rheumatol 2006;16:197-205.
16. Marlovits S, Zeller P, Vecsei V, et al. Cartilage repair: Generations of autologous chondrocyte transplantation. European Journal of Radiology 2006;57:24-31.
17. Brittberg M, Peterson L, Lindahl A, et al. Articular Cartilage Engineering with Autologous Chondrocyte Transplantation. Journal of Bone and Joint Surgery 2003;85A(3S):109-115.

18. Grande DA, Breitbart AS, Schwartz RE, et al. Cartilage Tissue Engineering: Current Limitations and Solutions. Clinical Orthopaedics and Related Research 1999;367S:S176-S185.
19. Steinert AF, Ghivizzani SC, Tuan RS, Noth U, et al. Major biological obstacles for persistent cell-based regeneration of articular cartilage. Arthritis Research & Therapy 2007;9:213-227.
20. Kuo CK, Li WJ, Mauck RL, Tuan RS. Cartilage tissue engineering: its potential and uses. Current Opinion in Rheumatology 2006;18:64-73.
21. Chung C, Burdick JA. Engineering cartilage tissue. Advanced Drug Delivery Reviews 2008;60:243-262.
22. Nesic D, Whiteside R, Mainil-Varlet P, et al. Cartilage tissue engineering for degenerative joint disease. Advanced Drug Delivery Reviews 2006;58:300-322.
23. Frenkel SF, Di Cesare PE. Scaffolds for Articular Cartilage Repair. Annals of Biomedical Engineering 2004;32(1):26-34.
24. Iwasa J, Engebretsen L, Shima Y, Ochi M. Clinical application of scaffolds for cartilage tissue engineering. Knee Surg Sports Traumatol Arthrosc 2008.

Chapter 2

2. Design Considerations

2.1 Acellular Osteochondral Constructs

While many tissue-engineered constructs aimed to treat cartilage defects are being researched, most involve chondrocytes or stem cells (mesenchymal or adipose-derived) seeded on a scaffold and provided with proper signaling molecules to maintain phenotype and function. Various cell-loaded natural and synthetic scaffolds in conjunction with delivered growth factors are being studied both *in vitro* and *in vivo*, but the clinical application of these techniques is limited due to the cost of maintaining cellular constructs on the shelf. There also exists the potential immune response to allogeneic cell lines, and autologous cell sources require biopsy from an already diseased, scarce tissue as well as extensive culture time to grow a large enough cell population for therapy. Thus an acellular scaffold that can induce the endogenous influx of native stem cells from the marrow cavity holds great promise for cartilage regeneration.

One acellular osteochondral scaffold aimed to mimic the native articular joint by cosynthesizing two distinct layers, one type II collagen-GAG cartilaginous layer and one type I collagen-GAG-calcium phosphate osseous layer, interdiffused together in a gradual, continuous interface.[1-3] Collagen fibrils extended across the interface, bonding the two compartments together, but the structure far from replicated tidemark and zonal architecture. Marrow stimulation and delivery of cells from the lesion into the construct were not addressed, and absorption of marrow-derived stem cells throughout the finely porous bilayered scaffold seemed improbable. A more practical design tackling the bone marrow delivery feature would greatly benefit current osteochondral scaffold research.

2.2 Channeled Constructs

Channeled scaffolds have been implemented for blood vessel, cardiac, neural, bone, and tendon tissue engineering to guide cells, bundles, and fibers in a defined orientation.[4-10] Channels also improve nutrient and oxygen delivery as well as waste removal from within large scale constructs where diffusion is insufficient to sustain cells.[11] Agarose gels cast in polytetrafluoroethylene (PTFE) molds were seeded with chondrocytes cultured under dynamic rotation, and GAG production was substantially greater around channel circumference due to forced convective flow carrying nutrients and oxygen to maintain cell metabolism and ECM production.[12] A PLGA osteochondral implant was fabricated with staggered microchannels in the cartilage portion to aid seeded cell distribution.[13]

The benefits of channeled scaffolds may also extend to improving the ability to absorb fluid by adding a capillary action driving force to the normal wettability of the polymer scaffold. The design of an acellular scaffold relies on endogenous infiltration of host cells for successful regeneration. Chondrocytes are unlikely to migrate from native cartilage into an implanted construct, so channeled architecture that can wick bone marrow and distribute bone marrow stromal cells throughout an implanted scaffold holds a considerable advantage over other acellular designs.

2.3 Degradation and In Vivo *Response of Chitosan and Alginate*

2.3.1 Overview

There are a vast array of materials, both biologic and synthetic, currently being studied for uses in cartilage tissue repair and regeneration. While the mechanical properties, differentiation potential, and cellular compatibility of these materials are under thorough investigation, *in vivo* biodegradability is often ignored or not properly assessed. Detailed parameters are required to evaluate scaffolds based on their ability to degrade reliably, quickly but within the time scale of new matrix production, and completely without byproducts or particles inciting a sustained inflammatory and immune response. With regard to reliability and rate, widely ranging degradation profiles for a given material have been reported, often with little accuracy or quantification of new cartilage formation. Complete scaffold volume loss depends on the scaffold pore size, presence of seeded cells, animal model, implant site, and method of repair (intrinsic or extrinsic). Different architectures for delivery such as hydrogels, meshes, sponges, membranes, and injectables further complicate the predictability of degradation.

Matrix degradation is important because regenerating tissue requires space to completely repair the defect and lingering matrix fragments cause damage to the surrounding environment that can counteract the repair process. The ideal degradation profile would be one that has a defined kinetic profile, a reliable time scale, optimized scaffold properties like architecture, pore size, and permeability, predictable behavior under mechanical stimuli, integration with surrounding tissue, minimal inflammatory response, and biocompatible byproducts and wear particles. However, no material currently meets all of these parameters. Often materials are referred to as biodegradable without further detail on the mechanism or *in vivo* response.

Material biodegradation can be hydrolytic or enzymatic. Synthetic polyα-hydroxy esters are commonly used as implants because they are degraded by hydrolysis. Nonspecific hydrolytic scission is the cleaving polymer chains by simple hydrolysis of their ester linkages. PGA is highly hydrophilic and quickly degrades by hydrolysis or by nonspecific esterases and carboxypeptidases. PLA, with an additional methyl group, is more hydrophobic, less crystalline, and degrades at a slower rate through hydrolytic scission.[14] PLGA copolymer degradation rate can therefore be controlled by altering PLA:PGA ratios. This is greatly beneficial because researchers can prevent the acid homopolymers from releasing unacceptable amounts of acid byproducts upon their degradation.[15]

Toxicity and biological incompatibility are major drawbacks to consider when using synthetic materials. Natural materials are biocompatible and may not generate the severe immune response that synthetic materials can. Natural polymers also have matrix-specific enzymes and thus a higher probability of total degradation compared to synthetic polymers. For example, collagen is recognized by cellular enzymes like collagenases and can be remodeled and degraded to provide space for neocartilage.[16] Chitosan is degraded *in vivo* by enzymatic hydrolysis driven by lysozymes, which target acetylated residues. Proteolytic enzymes may also exhibit some activity with chitosan. Resulting degradation products are chitosan oligosaccharides of different lengths. Degradation kinetics are inversely related to the degree of crystallinity, which is controlled by the degree of deacetylation. Highly deacetylated forms of chitosan, typically greater than 85%, show the lowest degradation rates and may last months *in vivo*. Less deacetylated and therefore less crystalline chitosan degrades more rapidly. To achieve desired rapid degradation, side chains have been added to alter molecular chain packing and increase the amorphous fraction.[17] Chitosan degradation is naturally accelerated by plasma and lysozyme.

GAGs like chondroitin sulfate and dermatan sulfate have a high charge density and lack of crystallinity, making them highly water soluble. Ethyl and benzyl esterified hyaluronic acid scaffolds have demonstrated *in vivo* lifetimes of several months, while partially esterified hyaluronic acid scaffolds degraded within a few weeks and attracted many more macrophages that phagocytosed the material.[17,18] In contrast, alginate gels do not possess an easily controlled degradation.[19] A de-crosslinking hydrolysis mechanism occurs, in which the divalent cations are exchanged with monovalent cations from surrounding media.

2.3.2 Time Scale of Biodegradation

Long term degradation kinetics must be ascertained in order to control material behavior at later stages after implantation. Chung et al performed an *in vivo* comparison of PLGA, 2.5%, and 5% chitosan chondrocyte-seeded scaffolds implanted in 40 nude mice. Constructs were retrieved at various time points and their gross appearance and volume were recorded. The 5% chitosan degraded slower than 2.5% chitosan scaffold, with 2.5% chitosan present at half its original volume by 24 weeks and 5% chitosan present at 75% its original volume. PLGA, on the other hand, rapidly degraded to 15% its original volume within 12 weeks.[20]

Degradation of alginate has been shown to be slow and uncontrollable, releasing high molecular weight strands that may have difficulty being cleared from the body. Partially oxidized alginate may exhibit faster degradation because the cleaved carbon-carbon bond in the uronate residue alters chain conformation and may promote hydrolysis. 5% oxidized alginate backbones degraded with a dependence on pH and temperature, and ionically crosslinked gels degraded within 9 days. Lower pH values substantially retarded partially oxidized alginate degradation.[21]

Scaffold degradation must be controlled temporally and spatially to direct new cartilage growth. Studies have demonstrated that scaffolds with degradable and non-degradable regions enhance ECM distribution over purely non-degradable scaffolds. This brings up the issue of balancing fast degradation, which may impede new ECM synthesis, and slow degradation, which may compromise structural support.[22]

When comparing PLGA (65:35) with 2% and 5% chitosan, western blot for collagen type II and reverse transcription-polymerase chain reaction (RT-PCR) for Col2A1 both illustrate that expression is strong initially in chondrocyte-PLGA complexes but weakens with time, whereas expression is strong in chondrocyte-chitosan complexes and increases with time for the entire 24 week period.[20]

Different ratios of degradable PEG-LA-DA and non-degradable PEG-DM were encapsulated uniformly with chondrocytes. GAG synthesis decreased with increasing degradable crosslinks, but collagen synthesis increased with increasing degradability. Thus it seems that higher degradable crosslink content, and therefore faster degradation, promotes collagen production, but slower degradation encourages GAG production.[23]

2.3.3 Scaffold Properties and Biodegradation

Scaffold architectures such as high surface area to polymer mass ratio as well as high surface area to volume ratio allow for tissue ingrowth, uniform cell delivery, and development of high cell density.[16] Pore size affects cell metabolic activities, specifically matrix biosynthesis. Moreover, chondrocyte ingrowth into and chondrocyte survival within the scaffold depend strongly on pore size. Nutrient, waste, oxygen, and enzyme diffusion are regulated by scaffold permeability. High permeability also allows for the evacuation of degradation byproducts. Permeability is defined as the degree of ease or difficulty for fluid to move in and out of the scaffold, thus influencing the viscoelastic response of the scaffold.[24] Permeability is not synonymous for porosity, although high porosity does typically translate to high permeability and vice versa.[25] It is useful to note that altering porosity or permeability can significantly impact the degradation characteristics of the scaffold.

The pH of the local environment in the joint can drastically alter tissue behavior as well as material integrity. Products of scaffold degradation often change pH which hinders repair or even destroys neocartilage. For example, polyα-hydroxy esters lower the pH around the scaffold due to the release of PLA and PGA upon hydrolytic degradation. In an acidic environment, hydrolysis can be accelerated.[24] Lee et al fabricated a homogeneous chitosan-PLGA composite (C/Pc) matrix from a one-phase solution and compared it to a PLGA-dispersed chitosan (C/Pd) matrix, in which PLGA was emulsified in a chitosan solution. Scaffolds were subjected to *in vitro* degradation at 37 C in PBS.

Homogeneous C/Pc scaffolds degraded less quickly than C/Pd scaffolds, indicating that homogeneous chitosan more effectively protects against PLGA degradation, likely due to the acid-neutralizing function of chitosan. Investigation of the pH change over time revealed that degradation of PLGA alone rapidly decreased pH, but degradation of C/Pc demonstrated substantial resistance to pH change for 4 weeks.[26]

2.3.4 Integration with Host Tissue

Cartilage to cartilage and cartilage to bone integration impacts degradation since the bonding of an implant to surrounding tissue allows endogenous cell, enzyme, and soluble factor influx. The integration of an implanted cartilage construct with surrounding cartilage, and subchondral bone if repairing an osteochondral defect, is also imperative for joint integrity and function. Research has implied that osteochondral scaffolds should be of similar stiffness to native bone tissue and not too flexible as that might compromise healing.[27] Few studies assess the bond strength of an implant to adjacent cartilage and bone. Native chondrocyte migration, scaffold adhesion, signaling molecule flow, and ECM biosynthesis all have roles in graft integration *in vivo*. Adult chondrocytes seem to have a limited ability to infiltrate existing cartilage matrix and even empty lacunae. Potential therapeutic strategies to encourage integration include crosslinking or gluing native cartilage matrix to the construct. Ensuring tidemark formation, whether by artificial creation or biological cues, is also beneficial. Another approach is to stimulate cell migration, particularly chondrocytes above the tidemark and osteoblasts below the tidemark.[28] Integration comes with potential drawbacks as well, however. The nature and status of the tissue at the wound lesion edge is paramount. Delivered cells may exhibit degenerative changes once in the osteoarthritic environment. Signaling from adjacent diseased cartilage can initiate destructive effects and degrade the newly implanted construct.

Scaffolds composed of PLA-alginate amalgams seeded with bone marrow-derived MSCs and dosed with TGF-β were implanted in osteochondral defects in canine femoral condyles. After 6 weeks *in vivo*, cell-seeded and cell-free constructs both assisted in filling defects with cartilaginous tissue. However, the cell-seeded scaffolds produced higher quality tissue in terms of matrix characteristics, cell distribution, and proteoglycan staining that more closely resembled native cartilage than cell-free scaffolds. Constructs were rated based on the gross visibility of defect margins and histological evaluation of surface regularity or cleft presence. Defect margins were between 50% and 75% visible in both cell-seeded and cell-free conditions. Surface regularity was somewhat smooth but at times irregular for both scaffolds, and no clefts in the cartilage or clefts to the bone were present.[29]

2.3.5 In Vivo *Response during Biodegradation*

Implantation of materials *in vivo* incites an inflammatory response involving cytokines such as interleukin 1 (IL1) and tumor necrosis factor-α (TNF-α). These cytokines regulate ECM degradation by stimulating proteolytic enzyme, MMP, aggrecanase, and NO secretion.[28] Anti-inflammatory cytokines or matrix molecules may offer a method of reducing uncontrolled matrix degradation. Inflammation further leads to matrix degradation by macrophage phagocytosis. Signals released during this process recruit neutrophils and granulocytes which lay down granulation tissue. Later stages of inflammation, if prolonged, can result in fibrous tissue formation. Foreign body reaction is stimulated if an implant or implant fragments persist in the body. Foreign body giant cells, or fused macrophages that are able ingest very large foreign bodies, are created, and the foreign object is encapsulated by fibrous tissue. This results in chronic inflammation for the duration of the material's residence *in vivo*.

It is of significant interest to understand how the host responds to chitosan and alginate, specifically what pathways are involved and whether the response will affect tissue regeneration. Chitosan implants are categorized as causing sub-acute inflammatory reactions. The acetylated residues on chitosan oligosaccharides have been shown to stimulate macrophages. Further, chitosan has been shown to exert chemoattractive effects on neutrophils both *in vitro* and *in vivo*, but neutrophil accumulation dissipates rapidly, and chronic inflammation and chronic lymphocyte presence does not develop. Chitosan generally does not elicit a strong foreign body reaction or foreign body giant cell attraction, and it activates coagulation as fibrinogen and plasma proteins bind it but not acetylated chitosan.[30,31] Major fibrous encapsulation is not typically seen with chitosan-based materials, and the usual course of healing supports normal granulation tissue formation and often accelerated angiogenesis.[17] Both chitin and chitosan activate the complement system via the alternative pathway. Chitin and chitosan activate C3 and C5 but not C4. After C3 is turned on, C3b is produced and binds to chitosan particles. The stabilized C3b then acts as a binder for factor B. One study reported that chitosan induced a 50% increase of C3 levels.[32] C3 activation increased with chain length and the number of amines. Moreover, chitosan acetylation has been found to increase activation of the alternative pathway.

Alginate implants cause an acute inflammatory response involving neutrophils, macrophages, lymphocytes, eosinophils, and mastocytes.[33] Inflammatory cells such as CD4+, CD8+, and CD11b+ are also associated with the host response to alginate.[34] Alginate causes persistent fibroblast presence, fibroplasia, and fibrosis, which can prevent nutrient and oxygen diffusion. Further, granulation tissue and blood vessels form in response to alginate. However, alginate with low mannuronic acid content evokes minimal cytokine signaling and fibroplasia, and alginate removed of impurities can improve its biocompatibility.[35]

2.3.6 Degradation Products and Wear Particles

Harmful byproducts and residual fragments of scaffold degradation can advance cartilage decay, but the exact byproduct composition and degradation mechanism are rarely known and are frequently monitored indirectly via inflammatory response. Scaffold degradation byproducts can be generated by excessive proteolysis, either from arthritis or inflammatory response to an implant, and can negate the benefits of the construct. Proteolytic fragments activate chondrocytes and synovial fibroblasts, and the signal is propagated through cell surface receptors to intracellular pathways, leading to the more scaffold degradation and the production of such catalysts. Because reduced biocompatibility is most often detected in the latter stages of implant degradation, it is believed that degradation byproducts are responsible for tissue reactions. This implies that a large amount of byproducts released per unit time cannot be sufficiently handled by the clearing capacity of surrounding tissue. Thus, degradation kinetics are important for determining the time scale required to study *in vivo* response and graft behavior.[36]

Often implant materials are not fully degraded and resorbed. The residual fragments elicit inflammatory and foreign body responses. PLA-alginate amalgams treated with TGF-β showed residual fragments in both scaffolds seeded with bone marrow-derived MSCs and acellular scaffolds. After 6 weeks, significant PLA-alginate material remained. While newly generated tissue was a combination of articular cartilage and fibrous tissue, macrophages and granulocytes were absent in the defects, constructs, and surrounding tissue, pointing to minimal inflammatory response.[29] Implants in the joint, whether prosthetic or tissue engineered, encounter friction with contact surfaces, and this produces wear particles. Frictional wear debris in the joint and micromotion can lead to deleterious effects such as osteolysis. In osteochondral implants, osteolysis eventually leads to loosening of the implant due to subchondral bone deterioration. The first reaction at the implant site involves bone resorption stimulated by degradation byproducts. This is difficult to assess, however, because of the reactive region surrounding the final implant degradation. Osteolysis can vary from mild osteolytic changes to cystic-like extended resorption cavities. Mild osteolytic changes likely do not interfere with fracture healing, soft-tissue fixation, or static properties of the bone unless changes exceed a certain level, at which point they most likely will impede fracture healing and graft fixation. In severe cases, osteolysis can disturb regeneration by fracture displacement, fragment sequestration, or healing failure of soft tissue.[36]

In order to more precisely control biodegradation and consequently integration, future techniques could incorporate enzyme cleavage sites within the polymer backbone or crosslinks. Choosing materials like chitosan and alginate with fairly well defined degradation profiles and behaviors will be helpful in preparing for and predicting host response to an implant. Chitosan and alginate are not quickly degraded, and their persistence may improve the success of an implant by providing long-term structural support for the prolonged phases of cartilage regeneration.

References

1. Lynn AK, Bonfield W, et al. Design of a Multiphase Osteochondral Scaffold. I. Control of Chemical Composition. J Biomed Mater Res 2010;92A:1057-1065.
2. Harley BA, Gibson LJ, et al Design of a Multiphase Osteochondral Scaffold. II. Fabrication of a Mineralized Collagen-Glycosaminoglycan Scaffold. J Biomed Mater Res 2010;92A:1066-1077.
3. Harley BA, Gibson LJ, et al. Design of a Multiphase Osteochondral Scaffold. III. Fabrication of Layered Scaffolds with Continuous Interfaces. J Biomed Mater Res 2010;92A:1078-1093.
4. Kaully T, Levenberg S, et al. Vascularization—The Conduit to Viable Engineered Tissues. Tissue Engineering: Part B 2009;15(2):159-169.
5. Madden LR, Ratner BD, et al. Prioangiogenic Scaffolds as Functional Templates for Cardiac Tissue Engineering. PNAS 2010;107(34):15211-15216.

6. Moore JM, Yaszemski MJ, at al. Multiple-Channel Scaffolds to Promote Spinal Cord Axon Regneration. Biomaterials 2006;27:419-429.
7. Wahl DA, Czernuszka JT, et al. Controlling the Processing of Collagen-Hydroxyapatite Scaffolds for Bone Tissue Engineering. J Mater Sci: Mater Med 2007;18:201-209.
8. Seitz H, Ziegler G, et al. Different Calcium Phosphate Granules for 3-D Printing of Bone Tissue Engineering Scaffolds. Advanced Engineering Materials 2009;11(5):B41-B46.
9. Bagnaninchi PO, El Haj AJ, et al. Chitosan Microchannel Scaffolds for Tendon Tissue Engineering Characterized Using Optical Coherence Tomography. Tissue Engineering 2007;13(2):323-331.
10. Bryant SJ, Ratner BD, et al. Photo-Patterning of Porous Hydrogels for Tissue Engineering. Biomaterials 2007;28:2987-2986.
11. Grayson WL, Vunjak-Novakovic G, et al. Biomimetic Approach to Tissue Engineering. Seminars in Cell & Developmental Biology 2009;20:665-673.
12. Buckley CT, Kelly DJ, et al. Engineering of Large Cartilaginous Tissues Through the Use of Microchanneled Hydrogels and Rotational Culture. Tissue Engineering: Part A 2009;15(11):3213-3220.
13. Sherwood JK, Ratcliffe A, et al. A Three-Dimensional Osteochondral Composite Scaffold for Articular Cartilage Repair. Biomaterials 2002;23:4739-4751.
14. Agrawal CM, Ray RB. Biodegradable polymeric scaffolds for musculoskeletal engineering. J Biomed Mater Res 2001;55:141-150.
15. Frenkel SF, Di Cesare PE. Scaffolds for Articular Cartilage Repair. Annals of Biomedical Engineering 2004;32(1):26-34.
16. Temenoff JS, Mikos AG. Review: tissue engineering for regeneration of articular cartilage. Biomaterials 2000;21:431-440.

17. Suh JKF, Matthew HWT. Application of chitosan-based polysaccharide biomaterials in cartilage tissue engineering: a review. Biomaterials 2000;21:2589-2598.

18. Campoccia D, Hunt JA, Williams DF, et al. Quantitative assessment of the tissue response to films of hyaluronan derivatives. Biomaterials 1996;17:963-975.

19. Eiselt P, Mooney DJ, et al. Porous Carriers for Biomedical Applications Based on Alginate Hydrogels. Biomaterials 2000;21(19):1921-1927.

20. Jeon YH, Choi JH, Chung HY, et al. Different Effects of PLGA and Chitosan Scaffolds on Human Cartilage Tissue Engineering. The Journal of Craniofacial Surgery 2007;18(6):1249-1258.

21. Bouhadir KH, Lee KY, Mooney DJ, et al. Degradation of Partially Oxidized Alginate and Its Potential Application for Tissue Engineering. Biotechnol Prog 2001;17:945-950.

22. Chung C, Burdick JA. Engineering cartilage tissue. Advanced Drug Delivery Reviews 2008;60:243-262.

23. Bryant SJ, Anseth KS. Controlling the spatial distribution of ECM components in degradable PEG hydrogels for tissue engineering cartilage. J Biomed Mater Res 2003;64A:70-79.

24. LeBaron RG, Athanasiou KA. Ex vivo synthesis of articular cartilage. Biomaterials 2000;21:2575-2587.

25. Agrawal CM, McKinney JS, Lanctot D, Athanasiou KA. Effects of fluid flow on the in vitro degradation kinetics of biodegradable scaffolds for tissue engineering. Biomaterials 2000;21:2443-2452.

26. Shim IK, Lee SY, Park YJ, Lee, Lee SJ, et al. Homogeneous chitosan-PLGA composite fibrous scaffolds for tissue regeneration. J Biomed Mater Res 2008;84A:247-255.

27. Schlichting K, Schell H, Epari DR, et al. Influence of Scaffold Stiffness on Subchondral Bone and Subsequent Cartilage Regeneration in an Ovine Model of Osteochondral Defect Healing. The American Journal of Sports Medicine 2008;36(12):2379-2391.

28. Steinert AF, Ghivizzani SC, Tuan RS, Noth U, et al. Major biological obstacles for persistent cell-based regeneration of articular cartilage. Arthritis Research & Therapy 2007;9:213-227.
29. Wayne JS, McDowell CL, Shields KJ, Tuan RS. *In Vivo* Response of Polylactic Acid-Alginate Scaffolds and Bone Marrow-Derived Cells for Cartilage Tissue Engineering. Tissue Engineering 2005;11(5/6):953-963.
30. Okamato Y, Minami S, et al. Effects of Chitin and Chitosan on Blood Coagulation. Carbohydrate Polymers 2003;53(3):337-342.
31. Benesch J, Tengvall P. Blood Protein Adsorption onto Chitosan. Biomaterials 2002;23(12):2561-2568.
32. Minami S, Shigemasa Y, et al. Chitin and Chitosan Activate Complement via the Alternative Pathway. Carbohydrate Polymers 1998;36(2-3):151-155.
33. Robitaille R, Halle JP, et al. Inflammatory Response to Peritoneal Implantation of Alginate-poly-L-Lysine Microcapsules. Biomaterials 2005;26(19):4119-4217.
34. Babensee JE, Miko AG, et al. Host Response to Tissue Engineering Devices. Advanced Drug Delivery Reviews 1998;33(1-2):111-139.
35. Atala A, Lanza RP. Methods of Tissue Engineering. Gulf Professional Publishing 2002; 796.
36. Weiler A, Hoffmann RFG, Sudkamp NP, et al. Biodegradable Implants in Sports: The Biological Base. Arthroscopy: The Journal of Arthroscopic and Related Surgery 2000;16(3):305-321.

Chapter 3

3. Sustained Growth Factor Delivery in Tissue Engineering Applications

3.1 Abstract

While tissue engineering often involves the delivery of stimulating growth factors to accelerate tissue regeneration, the use of growth factors as a therapeutically viable alternative to treat degenerative diseases remains limited. Systemic and bolus administration both lack tissue specificity and sustained protein localization, and large amounts of protein are required to produce the desired cell activation. These attributes can lead to dangerous tissue overgrowth, toxicity, and even tumor formation. In addition, the short biological half-life of proteins restricts their effect to a time scale insufficient for regeneration. Growth factor delivery within an implanted scaffold is a very attractive way to modulate cell behavior both in the scaffold and in endogenous tissue. Carrier materials have been widely used to deliver growth factors to the injury site and assist regeneration structurally and biochemically. Proteins can be non-specifically adsorbed to the material surface or simply entrapped within the bulk scaffold, but release kinetics of these methods often begin with a diffusive burst and require more precise spatial and temporal control. This review focuses on the development of sustained growth factor delivery techniques used in tissue engineering. Noncovalent and covalent immobilization techniques will be reviewed in terms of design, efficacy of encapsulation or conjugation, release mechanism and profile, concentration dose dependence, spatial distribution, and local duration and timing. Further, the biological response to sustained growth factor delivery will also be covered, such as retained protein bioactivity and stability, cell interaction, cell responsiveness, proliferation, differentiation, extracellular matrix production, and tissue regeneration.

3.2 Introduction

Tissue engineering regularly employs growth factors to heal injuries and chronic degenerative diseases. While a main requirement of tissue engineering is the selection of proper cell types and material scaffold properties to successfully rebuild damaged tissue and restore its function, equal attention needs to be paid to the cellular microenvironment including the biochemical signals involved in tissue growth[1]. Cellular fate is governed by numerous factors and interactions that require robust control in order for tissue regeneration to be safe and effective[1]. Interactions between cells, extracellular matrix (ECM), and soluble factors all contribute to the local microenvironment. As cells sense this microenvironment, for example as growth factors bind to target cell receptors and transfer information, their function and fate are dynamically regulated, affecting such processes as proliferation, metabolism, adhesion, chemotaxis, gene expression, differentiation, and even apoptosis[1,2]. Systemic administration and local bolus injection as methods of exogenous growth factor delivery can be unpredictable and lack tissue specificity. Moreover, bolus injections often do not maintain localization and are cleared too quickly. Preserving the bioactivity of proteins is challenging because of protein instability in the protease-rich wound site environment, leading to enzymatic digestion or deactivation[3]. The short biological half-life and lack of long-term instability *in vivo* demand high doses of protein, which is not only inefficient but also can lead to tissue overgrowth, toxicity, and carcinogenicity. Systemic and bolus administration share the problem of slow tissue penetration due to large molecular weight proteins in addition to the long-standing question of protein aggregation or denaturation occurring once injected.

To combat these issues, researchers have turned to implantable scaffolds as delivery vehicles. A variety of synthetic and natural materials have been used as carriers to not only deliver growth factors, but also to provide structural support, allow host cell invasion, and supply biochemical cues with the end goal of tissue regeneration. For the purpose of regenerative medicine, it is crucial to engineer a biochemical and mechanical niche that carefully orchestrates molecular and cellular wound healing events. Tissue repair, however, is not instantaneous but rather a long-term process lasting the course of many weeks, and therefore the role of growth factors remains activated over a long period of time in the native wound healing cascade. Growth factor delivery carriers should reflect this prolonged period of time required for healing and correspondingly extend release for multiple weeks, catering to the specific tissue.

Thus, there is a need for sustained delivery of growth factors in which release of signaling molecules from delivery vehicles is synchronized with natural tissue healing. Growth factor delivery mechanisms should work synergistically with tissue engineered carriers. Growth factor local concentration and spatiotemporal gradients rely on a balance between scaffold transport properties, protein binding, degradation, and generation rates[4]. Further, released growth factors may interact with matrix proteins in the scaffold or tissue, which could enhance bioavailability or stability. Minimalized host response to the scaffold may reduce fibrosis, inflammation, and immune response, which could improve effectiveness of growth factor delivery. Ultimately, the carrier in conjunction with the delivery mechanism should act as a local regulator to control the doses and kinetics of the released growth factor and increase the potential retention time at therapeutic concentration levels. Tissue regeneration is an intricate, biological process that depends on highly regulated signaling molecules at exact times, locations, and concentrations. By providing the proper biological cues that mimic or even enhance native healing with precise control in a sustained manner, the repair of more complex and functional tissues can be improved drastically.

Early attempts at growth factor delivery from carriers exhibited poor modulation of release characteristics and no protection from detrimental conditions in the environment[5]. Many strategies have since been developed to extend and control the release of growth factors from scaffolds *in vivo* and in translatable *in vitro* models. Signaling molecules can be noncovalently or covalently attached to the scaffold surface as a way to implement sustained release with better spatiotemporal control. Noncovalent immobilization techniques rely on electrostatic interactions, in the architectural form of particles or bulk scaffolds, or physical encapsulation, in the form of fibers, microspheres, or coatings. Covalent immobilization methods must be assessed in terms of gradients, spatial distribution and density, conjugation efficiency, dose dependence, downstream signaling, heparin/affinity-based delivery, dual delivery, and cleavable linkers. For the purpose of this review, 100% delivery within 30 days is considered successful sustained release.

3.3 Emerging Research

3.3.1 Noncovalent Immobilization

A number of parameters need to be considered when evaluating noncovalent immobilization techniques. The protein loading efficiency and the efficacy of delivery from the scaffold to the site will influence the starting amount of protein. Concentration ranges have not been well defined but are necessary to elucidate any dose dependent effects that may lead to tissue overgrowth, carcinogenesis, or toxicity. Local duration of exposure can further contribute to adverse growth effects if not carefully designed. Growth factor delivery gradients can be achieved using noncovalent immobilization, but these release mechanisms and kinetics require careful timing to stimulate and mimic the healing process. Once delivered *in vivo* through noncovalent techniques, growth factors can become unstable, and the limitation of their lifetime must be examined. Proteins may need to bind to matrix molecules or undergo proteolysis to be active or stable. Finally, the degradation profiles of hydrogels will significantly impact how growth factors are freed into the environment.

3.3.1.1 Electrostatic Interaction

Often growth factors are added to scaffolds through non-specific adsorption of the protein to the material surface. Signaling molecules are adsorbed via electrostatic interaction, or ionic complexation, when ionic bonding occurs between oppositely charged functional groups on proteins and substrate polymer chains. Adsorption can result in a burst release of growth factor, and release is based on the protein interaction strength with the matrix. In protein-surface interactions, the elements that govern kinetics include bound ions, surface charge, surface roughness, surface elemental composition and surface energetics[6]. If scaffolds exhibit charge, electrostatic interactions will dominate protein adsorption kinetics. This is true for even neutral or like-charged proteins, as charge distribution is not usually uniform. During non-specific adsorption, protein interaction with the scaffold may block cellular binding sites on the growth factor, potentially disrupting its bioactivity. Due to the various ways proteins can interact with a surface, it would be difficult to determine which binding sites need to be available, and loss of activity due to inactive configurations would require a greater amount of initial protein, decreasing the efficiency of delivery.

3.3.1.1.1 Particles

Nano-and microparticles are often fabricated using natural polymers that, due to their inherent charge, are known to electrostatically bind proteins or small molecules as an attempt to delay their release over time. Hydroxyapatite is a main component of bone and known for its biocompatibility, osteoconductivity, and osteoinductivity. Its role as a protein delivery carrier has been receiving more attention in recent years due to the fact that hydroxyapatite particles bind many chemicals and proteins. Hydroxyapatite nanoparticles sustained the release of bone morphogenetic protein-2 (BMP-2)[7,8] and steroidal drug triamcinolone acetonide from poly(d,l-lactide-co-glycolide) (PLGA)[9].

Similar to hydroxyapatite in composition of inorganic calcium and phosphate, β-tricalcium phosphate (β-TCP) is a commonly used osteogenic material for bone substitutes and protein carriers. Bose and Tarafder provide a comprehensive review of calcium phosphates used in growth factor and drug delivery for bone tissue engineering[10]. β-TCP microparticles were modified by Lee et al with an apatite coating to improve their protein carrying capacity and burst release profiles of

Nell1, a novel osteogenic protein[11]. Lee and Wu et al also investigated chitosan/alginate microparticles coated with apatite for sustained release of Nell1, and these microparticles combined with demineralized bone powder and hyaluronan formed a moldable putty that was implanted in a rat spinal fusion model, resulting in improved fusion within 4 weeks[12]. For cartilage regeneration applications, Lee et al further fabricated chitosan/tripolyphosphate/chondroitin sulfate nanoparticles to reduce the burst release of Nell1 while retaining a loading association efficiency of 90%[13]. Chitosan/dextran sulfate nanoparticles encapsulating vascular endothelial growth factor (VEGF) with a ~75% efficiency significantly reduced cumulative release when incorporated into Matrigel scaffolds and improved *in vivo* angiogenesis[14].

3.3.1.1.2 Bulk Scaffolds

As an alternative to particles, bulk scaffolds generated out of similar natural materials can also electrostatically bind growth factors. These bulk scaffolds serve as stand-alone three-dimensional scaffolds and can also offer sustained release. Mesoporous hydroxyapatite, which offers 9 times greater surface area and 4 times greater pore volume than commercial hydroxyapatite, reduced burst and sustained release of VEGF in an attempt to restore the vascular supply in bone implants to improve osteointegration[15]. Silica xerogels synthesized using the sol-gel process were hybridized with chitosan in order to control the release of basic fibroblast growth factor (bFGF) and reduce mechanical brittleness[16]. Further, this hybrid coating was loaded with BMP-2 and applied to a porous hydroxyapatite scaffold, enhancing osteoblast response and also new bone formation when implanted in rabbit calvarial defects[17].

3.3.1.2 Physical encapsulation

Another noncovalent immobilization method, physical encapsulation, allows growth factors to be loaded into gels. Physical entrapment is a technique of delivering growth factors inside a hydrogel by forming the gel from a solution containing those growth factors. Proteins that are interspersed are released through free diffusion and if possible, during degradation. Encapsulation designs come in many 3D hydrogel geometries, such as homogeneous blocks, layers, spheres, shells, and fibers. Crosslinking density and diffusive properties of the network, such as porosity, tortuosity, and pore size, dictate the rate of diffusion[5]. If the diffusing protein's molecular size is much smaller than the hydrogel mesh size, diffusion kinetics govern and release is quick within days. Contrastingly, when the molecule's hydrodynamic radius is near the hydrogel mesh size, release is based on polymer degradation, either hydrolytic or enzymatic[18]. Diffusion-based release is largely insensitive to the surrounding environment and biological signals, with the exception of release due to environment-mediated degradation of the encapsulating carrier. Another exception can occur if environmental pH affects the solubility of proteins, which in turn determines the release rate in diffusion, dissolution, and osmotic controlled approaches[18]. While growth factor release using these noncovalent immobilization techniques is somewhat extended, a burst release can be typical and the time scale of release is often insufficient to mimic or coincide with native cues during healing.

3.3.1.2.1 Fibers

Many different synthetic polymers have been electrospun for the sustained delivery of growth factors, with common examples being polycaprolactone (PCL) and PLGA. A review by Yoo et al covers different surface modifications applied to electrospun nanofibers as well as methods of growth factor loading on the surface of these nanofibers using simple physical adsorption, nanoparticles, multilayer assembly, or chemical immobilization[19].

Emulsion electrospinning is a method of fabricating core-shell nanofibers that attempts to reduce burst release and protect the encapsulated protein. Growth factors incorporated into the core of nanofibers using coaxial electrospinning have been shown to release more slowly, compared to blend electrospinning with the growth factor randomly distributed in the fiber. In approaches for cardiac or vascular tissue engineering, respectively, VEGF was entrapped into the cores of poly(L-lactic acid-co-ε-caprolactone) (PLCL) nanofibers[20] or dextran core/PLGA shell coaxial electrospun membranes to lower burst and sustain cumulative release[21]. Poly(L-lactide-co-caprolactone) (PLLACL) and collagen electrospun into nanofibrous mats sustained the release of BMP-2 and dexamethasone from the fiber core[22], while PLGA nanofibers also sustained the release of bFGF from the central core when coaxially electrospun[23].

Hybrid fibrous scaffolds containing both micro- and nanofibers can potentially offer superior mechanical strength, which is useful in engineering certain tissues such as ligaments and tendons. bFGF-releasing PLGA fibers were coated over mechanically robust microfibrous silk scaffolds, stimulating mesenchymal progenitor cells to undergo tenogeneic differentiation, which included collagen production that increased failure load and stiffness[24].

3.3.1.2.2 Microspheres

Biodegradable nano- and microspheres fabricated using synthetic polymers such as PLGA are commonly used to encapsulate and deliver different agents such as DNA, proteins, and small molecules[25]. By relying on diffusion out of the microsphere as the polymer degrades, microspheres can provide a slow release of growth factors. 50:50 PLGA microspheres entrapped between PCL nanofibers offered a controlled release of BSA or chondroitin sulfate[26], while 50:50 PLGA microspheres embedded in polyvinyl alcohol (PVA) hydrogels slowly released an important cartilage growth factor, insulin-like growth factor-1 (IGF-1)[27]. 85:15 PLGA microspheres releasing biologically active VEGF improved capillary density and epithelial proliferation when implanted within a polyglycolic acid (PGA) scaffold in rat omentum[28]. BMP-2 was incorporated into PLGA/polyethylene glycol (PEG) spheres, and the temperature-sensitive spheres were sintered into scaffolds that sustained released of BMP-2 and increased bone volume 55% in mouse calvarial defects *in vivo*[29]. Porous PLGA microspheres slowly releasing dexamethasone were added to a blend of hyaluronic acid/Pluronic F127 and promoted chondrogenic differentiation of mesenchymal stem cells *in vivo*[30]. Composite PLGA/silicon microspheres decreased burst release of BSA while maintaining a loading efficiency up to 86%, depending on protein concentration[31].

Dual growth factory delivery can offer many advantages over single growth factor delivery in that more sophisticated signaling with multiple, distinct functional effects on cells can be attained. Simultaneous delivery of multiple growth factors is a practical strategy that may be feasibly employed in clinical applications. However, sequential release of multiple growth factors with different release kinetic profiles may be preferential to simultaneous delivery. This type of approach has been realized by manipulating diffusion constants. Spatial and temporal control can be achieved by using microspheres embedded in bulk hydrogels, or any other engineered system that harnesses the diffusivity differences between various materials, and distinct growth factors can be loaded in the different materials. Chen et al provides a comprehensive review on dual growth factor diffusion delivery systems up to 2010[3].

In order to obtain a sequential delivery of two distinct growth factors, PLG microspheres encapsulating platelet-derived growth factor (PDGF) were mixed into alginate hydrogels containing VEGF. The resulting sustained, biphasic release increased vessel diameter and formed arterioles with smooth muscle lining when injected into ischemic hindlimb intramuscular regions of mice[32]. In an attempt to create an osteochondral construct that guides differentiation of mesenchymal stem cells, a dual delivery silk scaffold with BMP-2- or IGF-1-loaded PLGA or silk microspheres in various gradients reduced burst and sustained the release of BMP-2, and mesenchymal stem cells osteogenically and chondrogenically differentiated along IGF-1/BMP-2 dual gradient scaffolds[33].

3.3.1.2.3 Coatings

Coatings loaded with growth factors can be applied to pre-existing, three-dimensional scaffolds of any shape or material and allow for controlled release of growth factors as the coating swells and degrades over time. Since the amount of BSA that can be loaded onto pure TCP is limited, porous TCP sintered scaffolds were coated with PCL containing BSA to allow for longer release with greater initial payload[34].

3.3.2 Covalent Immobilization

Polymer scaffolds can be functionalized to interact with bioactive molecules, and the resulting covalent immobilizing hinders free diffusion and prolongs growth factor release[18]. For covalent immobilization, conjugation chemistry is important to consider when designing the proper functional groups to target and protect. Functional groups such as hydroxyl-, amino-, or carboxyl groups are introduced to each other through blending, copolymerization, chemical solutions, or physical treatment[2]. Conjugating signaling molecules to a scaffold using specified linker chemistry holds some advantages over noncovalent immobilization. Namely, the options for linking, lifetime, and controlled release of growth factors within a scaffold may be improved. Though, when a growth factor is chemically conjugated to the scaffold through a specific functional group, that blocked functional group may compromise the protein bioactivity. Further, the efficacy of this conjugation reaction dictates how much initial protein is required, and the conjugation efficiency may be insufficient using some covalent immobilization techniques. When further considering covalent linkers, linker spacing and arm length need to be optimized to maintain active proteins that are not sterically hindered, and in the case of cleavable linkers, allow protease intrusion. It is important to note that covalent immobilization of a signaling molecule prevents its internalization by cells, thus lengthening the protein's active lifetime as an extracellular trigger until the linker bond is broken or the scaffold is degraded. However, some signaling molecules need to be internalized to activate downstream signaling. Moreover, permanent presentation of a ligand that continuously stimulates cells can also lead to serious problems such as tissue overgrowth.

Still, conjugation chemistry is truly modular and can be used to design custom linkages between surfaces and proteins. It allows researchers to choose qualities of interest and couple these building blocks using controlled reactions. Bifunctional chemical linkers can be bound on one end to a growth factor and on the other end to a scaffold. The tether in between can be composed of a variety of polymers and can contain a number of desired components such as peptides, fluorescent tags, cytokines, and proteins.

Conjugating growth factors to a stabilizing molecule incorporated in the linker chain may also extend the protein's lifetime. For example, dextran- and PEG-based conjugates have been shown to stabilize proteins by increasing the circulation half-life time *in vivo*, namely by increasing the protein hydrodynamic radius which protects it from renal clearance, proteolysis, and immune system recognition[35,36]. Further, the retention time of dextran-based conjugates once internalized within a cell is prolonged[35]. Both stabilization and retention can be modified by choosing different polymer lengths and branching architectures[35]. Conjugating polymers like dextran or PEG to various growth factors may help maintain the growth factor in its active state for longer periods of time.

3.3.2.1 Gradients, Spatial Distribution, and Density

Growth factors can be tethered to scaffolds in concentration gradients, spatial distributions, and various densities to direct cell adhesion, migration, and differentiation of progenitor cells. This points to the importance of growth factor patterning in ECM maintenance and equilibrium. Cells can be organized into complex structures based on cues from both bioactive molecule arrangement and ECM architectural features[4]. Specific ligand distribution required for tissue regeneration differs between growth factors and can even be distinct for the same growth factor during various phases of tissue formation. Biomaterials engineered to present ligands in patterns may be critical for regulating desired cell interactions and responses.

Integrin-binding peptide sequence fragments are often conjugated to materials to assist cell adhesion. Often polymer spacers are covalently attached to solid surfaces to serve as a way to immobilize growth factors or peptide fragments at defined concentrations while minimizing loss of bioactivity due to steric hindrance. Using avidin-biotin affinity binding, biotinylated ligands, either fibronectin fragment Arg-Gly-Asp (RGD) or laminin fragment Ile-Lys-Val-Ala-Val (IKVAV), were patterned with nanometer precision on block copolymer polylactide-poly(ethylene glycol) (PLA-PEG) matrices via flexible PEG chains, spatially confining aortic endothelial cells or PC12 nerve cells to the RGD or IKVAV micropatterned lines, respectively[37]. Leukemia inhibitory factor (LIF) and stem cell factor were immobilized using PEG spacers in wide range of concentrations, and this method lends itself to tethering regulated amounts of signaling molecules at specific densities[38]. In another example, poly(methacrylic acid) (PMAA) linkers immobilized in a gradient on a substrate were functionalized with RGD to induce cell adhesion as the ligand gradient increased[39].

Gly-Arg-Gly-Asp-Ser-Pro (GRGDSP) was conjugated to an acrylamide-PEG-based interpenetrating network at various surface densities using the heterobifunctional crosslinker sulfosuccinimidyl 4-(N-maleimidomethyl)cyclohexane-1-carboxylate (sulfo-SMCC), and endothelial cell adhesion and spreading increased with GRGDSP density, activating extracellular signal-regulated kinase (ERK)[40]. Alginate was modified with RGD using carbodiimide chemistry to determine the effect of ligand density on proliferation and differentiation of skeletal myoblasts[41], and osteoblast-seeded RGD-alginate gels formed bone *in vivo* at 16 and 24 weeks[42]. RGD was covalently immobilized on PEG hydrogels in gradients at different concentrations using photopolymerization, and human dermal fibroblasts aligned along the RGD gradient and migrated toward increasing concentration[43]. In a similar example, both RGD and linearly graded bFGF were covalently tethered on photopolymerizable PEG gels, and smooth muscle cells (SMCs) aligned and migrated along the growth factor gradient in the direction of increasing bFGF concentration[44]. Immobilized epidermal growth factor (EGF) was micropatterned in a gradient on polystyrene, and Chinese hamster ovary (CHO) cells with overexpressed EGF receptor (EGFR) preferentially grew on high EGF density regions[45].

Chemotactic and haptotactic agent concentration gradients have been shown to guide axons, and this model was translated to a poly(2-hydroxyethyl-methacrylate) [p(HEMA)] implant with nerve growth factor (NGF) immobilized in a gradient, which stimulated PC12 neurite growth towards greater NGF concentrations[46]. Moreover, immobilized NGF and neutrotrophin-3 (NT-3) concentration gradients showed synergistic effects in guiding dorsal root ganglion neurons[47]. Such implants with spatially distributed growth factors may be critical to enhancing axonal guidance and regenerating the injured nerve.

3.3.2.2 Conjugation Efficiency

To decrease the cost and waste associated with lost protein, the conjugation efficiency between growth factors and carriers is a priority. Efficiency is especially important because larger amounts of initial protein do not necessarily correspond with larger amounts of conjugated or loaded protein. Thus scaling up is not always the answer. One study found that conjugation efficiency of BMP-2 immobilized on PCL scaffolds was greatly improved over BMP-2 that was physically adsorbed onto PCL[48]. Greater loading efficiency of BMP-7 derived peptide was exhibited when covalently grafted onto nano-hydroxyapatite using aminosilane chemistry versus the peptide being non-specifically adsorbed. Peptide-functionalized nano-hydroxyapatite was dispersed in PLGA, resulting in a sustained release over 3 months[49,50].

3.3.2.3 Dose Dependence

Growth factors usually influence cell behavior at very low concentrations around 10^{-9} to 10^{-11}M[51]. Moreover, the elicited response is typically biphasic, with low concentrations insufficient to activate cells and high concentrations excessive for saturated receptors[52]. Because the role of morphogens is often dose dependent, spatial control is intrinsically achieved since only tissues within a certain distance from the release point contact active growth factor concentrations[1]. Thus, the local concentration in the microenvironment, not the total dose of delivered growth factor, dictates the degree of cellular response[1].

Ephrin-A1, a ligand critical for vascular development and angiogenic remodeling, was covalently modified and photopolymerized onto PEG hydrogels, stimulating endothelial cell adhesion in a positively correlated, dose-dependent manner and forming endothelial tubules with luminal diameters between 5-30um[53]. Neural stem/progenitor cells (NSPCs) were induced down the neuronal lineage most effectively with the single growth factor interferon-γ (IFN-γ), compared to brain-derived neurotrophic factor (BDNF) and erythropoietin, and neuronal differentiation of NSPCs on IFN-γ-immobilized methacrylamide chitosan scaffolds exhibited dose dependence on IFN-γ, with the most effective dose occurring at the highest tested concentration[54].

3.3.2.4 Downstream Signaling

Physical presentation of growth factors to cells, whether in immobilized or soluble form, directly affects cell function from the onset of ligand-receptor binding to the activation of downstream signaling. It is important to look at cell signaling pathways when assessing the cellular response to delivered growth factors. Whether protein conjugation has masked active binding sites necessary for bioactivity must be ascertained. The level of cell responsiveness, such as the level of growth factor receptor expression, is important for cell-protein interactions. Cell binding to growth factors and resulting downstream signaling must remain intact. A bind-and-lock strategy was used to orient VEGF in its bioactive state through its heparin-binding domain before the addition of a secondary functional group covalently coupling VEGF onto the heparin-functionalized surface. Covalently bound VEGF phosphorylated VEGF receptor-2 (VEGFR-2) in cells and affected human umbilical vein endothelial cell (HUVEC) morphology[55].

When contacting immobilized EGF, keratinocytes expressed high levels of EGFR, low ERK1/2 and Akt phosphorylation, decreased proliferation, and increased migratory and aligned phenotype. However, keratinocytes in the presence of soluble EGF displayed low EGFR, high ERK1/2 and Akt phosphorylation, and exhibited proliferative rather than migratory behavior[56]. EGFR signaling is known to assist cell survival and may have a role in bone development and homeostasis. Scaffolds designed to promote survival and proliferation of aspirated marrow cells were tethered with EGF to sustain its local delivery and helped differentiate human bone marrow cells into osteogenic colonies[57]. NHS-activated chitosan covalently reacted with EGF promoted chondrocyte proliferation and increased glycosaminoglycan content[58].

BMP-2 localized on PLG scaffolds using a heterobifunctional PEG spacer enhanced bone formation when bone marrow-derived mesenchymal stromal cells were seeded on constructs and implanted into bilateral, full-thickness rabbit cranial defects[59]. BMP-2 was also immobilized on silk fibroin matrices using carbodiimide chemistry, improving osteogenic differentiation of human bone marrow stromal cells[60].

Fibroblast differentiation into myofibroblasts during soft tissue healing is mediated by transforming growth factor-β1 (TGF-β1)[61]. Surfaces functionalized with aldehyde and epoxy groups were covalently immobilized with TGF-β1 while maintaining the ability to induce normal human dermal fibroblast differentiation into myofibroblasts[62]. While scaffolds containing peptide adhesion substrates improve cell adhesion, this modification often compromises ECM production and requires additional growth factors to counteract the decrease in matrix synthesis. Covalently bound adhesive ligands and TGF-β1 within PEG hydrogels synergistically increased vascular SMCs to increase matrix production over soluble TGF-β1 or tethered TGF-β1 alone[63].

3.3.2.5 Heparin/Affinity-Based Delivery

In affinity binding, a substrate specific to the protein of interest is conjugated to a scaffold. Protein affinity toward that substrate receptor, along with total receptor capacity, drive the delivery and release. Heparin, a highly sulfated glycosaminoglycan, can be physically or covalently immobilized on a scaffold and presented for secondary associations with heparin-binding growth factors. The basic heparin-binding domains on growth factors interact electrostatically with the acidic sulfate and carboxylic acid moieties on heparin. Heparin protects proteins from degradation, and growth factor release in this system is moderated by enzymatic degradation of the scaffold[2].

Delivered growth factors can be stabilized by the physical structure and chemical composition of the carrier. Hyaluronic acid, a stabilizing polymer, was conjugated to heparin, which has inherent binding sites for the FGF family of proteins, and rapidly bound FGF-2 was released upon enzymatic digestion in a fully functional state as seen by fibroblast growth and with increased stability and activity over free form FGF-2[64]. Hyaluronan was also crosslinked with gelatin and chitosan into a porous scaffold upon which heparin was then covalently immobilized using carbodiimide chemistry. bFGF was bound to heparin by affinity force, and heparin-bFGF-ternary scaffolds provided a favored environment for chondrocyte viability[65].

Heparin-functionalized chitosan-alginate scaffolds, created using N-(3-dimethylaminopropyl)-N'-ethylcarbodiimide (EDC) and N-hydroxysuccinimide (NHS) conjugation chemistry, increased bFGF binding efficiency 15-fold over that of bare chitosan-alginate[66]. Hydroxyapatite scaffolds vacuum-coated with a thin film of collagen type I were immobilized with heparin using EDC/NHS, reducing the release of loaded BMP-2 approximately four-fold[67]. Thiol-modified hyaluronic acid hydrogels were crosslinked with polyethylene glycol diacrylate (PEGDA) and thiol-modified heparin, attenuating the release of BMP-2 and maintaining ALP activity by mesenchymal precursor cells for up to 28 days[68]. Calcium phosphate/poly(hydroxybutyrate-co-hydroxyvalerate) (PHBV) nanocomposite microspheres were laser sintered into intricate scaffolds based on computer-aided design (CAD) models and computer tomography (CT) scans, and after gelatin coating heparin was immobilized using EDC/NHS so that BMP-2 could be affinity bound onto the scaffold, thus increasing ALP and osteocalcin expression by mesenchymal stem cells[69].

Heparin was conjugated to PCL/gelatin scaffolds using EDC/NHS chemistry, while allowing the negatively charged sulfonic groups on heparin to remain free to trap PDGF via electrostatic interaction, which promoted SMC proliferation and infiltration[70].

Differentiation of human embryonic stem cells into neural cells is dictated by EGF and bFGF, although EGF has been shown to be more potent in inducing neuronal and glial markers and cell extensions[71]. When EGF and bFGF were immobilized onto PLA nanofibers using covalently functionalized heparin, axon growth was significantly longer than with simply adsorbed growth factor[71]. Heparin was functionalized on PLLA nanofibers using homobifunctional PEG, allowing the heparin to then bind laminin and bFGF, and these immobilized factors in addition to aligned nanofibers synergistically improved neurite extension and dermal fibroblast migration in wound healing[72]. Heparin was similarly functionalized on PLLACL nanofibers, followed by immobilization of stromal cell-derived factor-1α (SDF-1α), and anastomosed vascular grafts recruited endothelial cells and smooth muscle cells, accelerating endothelialization and improving patency[73].

Covalently coupled heparin on PLGA was engineered to release bFGF with maintained bioactivity as demonstrated by HUVEC proliferation and blood vessel formation in the PLGA subcutaneous implant[74]. Covalent loading of heparin onto PLGA was increased over three-fold by using star-shaped versus linear PLGA polymer for scaffolds. Bioactive BMP-2 was continuously delivered from heparin-PLGA and induced nine-fold greater bone formation and four-fold greater calcium content *in vivo* than BMP-2 released without heparin modification[75].

PLGA was functionalized with diamino-PEG to combat uncontrolled, non-specific protein adsorption, and the PEG end amine group was further coupled to heparin to provide a substrate for growth factor tethering that permitted the natural binding and presentation of bioactive, matrix-sequestered molecules[76]. Collagen matrices crosslinked and heparinized with EDC/NHS bound and released bFGF with variable kinetics depending on the molar ratio between EDC and heparin carboxylic acid groups[61]. Vinyl-conjugated heparin and terminally di-acrylated Pluronic were photo-crosslinked with bFGF into a hydrogel, and the resulting sustained release produced greater neovascularization *in vivo* than carriers without heparin[77].

3.3.2.6 Dual Delivery

Because tissue development is a complex process involving numerous growth factors, tissue engineered constructs designed for multi-protein delivery are likely more effective for regeneration and more clinically applicable. Due to current challenges with single factor delivery, only a few studies have explored dual growth factor delivery. Even so, properly timed and controlled release kinetics of multiple signaling molecules can increase construct utility and mimic natural repair mechanisms. Growth factors play key roles at different stages in the tissue development and repair process, and orchestrating the delicate balance may improve regeneration and should be strongly considered in carrier design. Simultaneous or sequential delivery of multiple growth factors can be achieved by using different methods of immobilization or by changing polymer degradation rates through molecular weight and ratio formulations.

PLGA microspheres loaded with dexamethasone and immobilized with TGF-β3 through heparin simultaneously released both molecules with approximately zero order kinetics, leading to dramatic lacunae phenotype formation by mesenchymal stem cells[78]. With the aim of therapeutic angiogenesis, PDGF was encapsulated in PLG microspheres with different degradation rates which were embedded within a bulk PLG-alginate scaffold containing VEGF via surface association. Dual delivery led to the rapid formation of mature vascular networks in a non-obese diabetic (NOD) mouse femoral artery and vein ligation model[79].

Elicited angiogenesis was also targeted with *in situ* crosslinked PEG-hyaluronan-based hydrogels delivering VEGF, angiopoietin-1 (Ang-1), keratinocyte growth factor (KGF), and PDGF via covalently bound, thiol-modified heparin. Gels injected into mouse ear pinnae showed vascularization with all combinations of growth factors, as quantified by microvessel density[80]. VEGF and FGF2 dually incorporated within acellular, porous heparin-collagen scaffolds led to the most mature and highest density of blood vessels when subcutaneously implanted in rats, with no hypoxic cells after 3 weeks[81].

Despite the benefits of dual delivery, some combinations of growth factors have been shown to be detrimental and in some examples inhibited bone formation and ingrowth[82-86]. This points out that tissue regeneration mechanisms may require still more precise spatial and temporal control beyond sequential delivery to mimic complex biological processes.

3.3.2.7 Cleavable Linkers

In contrast to covalent conjugation schemes that provide permanent presentation of a growth factor, growth factors can be released from the carrier as demanded by the tissue repair process upon encountering cues from the *in vivo* environment. Since proteases like matrix metalloproteinase (MMP) and plasmin are present in wound and chronic degeneration environments as well as remodeling environments, they make desirable targets for triggering growth factor release. Peptide sequences that act as substrates for specific enzymes can be covalently immobilized on scaffolds and render the linker both biologically responsive and cleavable. Peptide sequence linkers are cleaved, freeing downstream growth factors that promote tissue formation into the environment as demanded by cells. This leads to a "release as needed" system. As cells produce proteases to assist ECM breakdown during either degeneration or remodeling, appropriate growth factors are released to counteract degeneration or support remodeling. Such enzyme-sensitive hydrogels are mediated by the local release of enzymes from active cells, and release is governed by enzyme concentration. A cleavable conjugation scheme allows for a sustained release of growth factor into the environment and also for protein internalization by cells. Recently, a bioartificial hydrogel scheme to induce vascularization included an MMP cleavable crosslinker bifunctionalized with two PEG-acrylates, mono-PEG-acrylated RGD and VEGF, and all three PEG components were photopolymerized under ultraviolet light with a photoinitiator. Degradable hydrogels implanted subcutaneously in Lewis rats released VEGF gradually and increased blood vessel density, and implants in a mouse ischemic hind-limb model demonstrated strongly encouraged reperfusion[87].

Alternatively, cleavable peptide sequences can be embedded in the matrix itself within the polymer backbone. Growth factors that are covalently or noncovalently immobilized within the matrix will be released upon cleavage of peptide sequences. In this type of cleavable scaffold scheme, release is impacted by enzyme concentration and bulk scaffold degradation rate, followed by poorly controlled diffusion. This approach to growth factor release is accompanied by a loss in overall scaffold mechanical properties during enzymatic cleavage but allows improved cell infiltration as the scaffold degrades.

3.4 Discussion

As the field of tissue engineering aims to tackle more ambitious regeneration endeavors, more sophisticated advancements in controllable, biomimetic cell signaling are required. Advances in growth factor delivery using noncovalent and covalent immobilization offer more precise spatiotemporal regulation than ever before. Diffusion-based strategies are becoming more sophisticated, such as multi-polymer delivery systems and platforms that manipulate polymer characteristics, leading to reduced burst release and sustained multi-week kinetics. Chemical conjugation of biological molecules allows the possibility of bioresponsive release mechanisms. Enzyme-mediated cleavage of scaffolds and tethers is a promising way for growth factors to stimulate local cells within the carrier and later enter the injury site upon demand by the environment. Although not covered in this review, gene therapy in the form of DNA and RNA release systems[4], DNA-based coatings functionalized with growth factors[88], and therapeutic transgenes encoding tissue-specific transcription factors or soluble growth factors[1] may be used to initiate and sustain tissue repair.

Growth factor delivery is moving toward the direction of multiple growth factor systems with spatial and temporal control to stimulate different healing responses tailored to specific tissues[1]. Examples include engineering osteochondral constructs, complex multi-functional tissues, and implants requiring angiogenesis to sustain growth of the tissue of interest. The field of tissue engineering will surely benefit from emerging developments in both noncovalent and covalent methods of growth factor delivery that allow for more refined control of regeneration stimuli.

References

1. Chen, F. M., Z. F. Wu, et al. Toward delivery of multiple growth factors in tissue engineering. Biomaterials 31:6279-6308, 2010.
2. Tayalia, P., and D. J. Mooney. Controlled growth factory delivery for tissue engineering. Adv. Mater. 21:3269-3285, 2009.
3. Geer, D. J., S. T. Andreadis, et al. Biomimetic delivery of keratinocyte growth factor upon cellular demand for accelerated wound healing in vitro and in vivo. American J. Pathology 167(6):1575-1586, 2005.
4. Biondi, M., A. Netti, et al. Controlled drug delivery in tissue engineering. Advanced Drug Delivery Reviews 60:229-242, 2008.
5. Quaglia, F. Bioinspired tissue engineering: the great promise of protein delivery technologies. Intl. J. Pharmaceuticals 364:281-297, 2008.
6. Israelachvili, J. Intermolecular and Surface Forces, 2nd edition. London: Academic Press, 1992.
7. Xie, G., J. Sun, J. Wei, et al. Hydroxyapatite nanoparticles as a controlled-release carrier of BMP-2: absorption and release kinetics in vitro. J. Mater. Sci.: Mater. Med. 21:1875-1880, 2010.

8. Davis, H. E., E. M. Case, J. K. Leach, et al. Osteogenic response to BMP-2 of hMSCs grown on apatite-coated scaffolds. Biotechnol. Bioeng. 108:2727-2735, 2011.
9. Koocheki S., S. S. Madaeni, and P. Niroomandi. Application of hydroxyapatite nanoparticles in development of an enhanced formulation for delivering sustained release of triamcinolone acetonide. Intl. J. Nanomedicine 6:825-833, 2011.
10. Bose, S., and S. Tarafder. Calcium phosphate ceramic systems in growth factor and drug delivery for bone tissue engineering: a review. Acta Biomaterialia 8:1401-1421, 2012.
11. Hu, J., Y. Hou, M. Lee, et al. Beta-tricalcium phosphate particles as a controlled release carrier of osteogenic proteins for bone tissue engineering. J. Biomed. Mater. Res. Part A 100A:1680-1686, 2012.
12. Lee, M., W. Li, B. M. Wu, et al. Biomimetic apatite-coated alginate/chitosan microparticles as osteogenic protein carriers. Biomaterials 30(30):6094-6101, 2009.
13. Hou, Y., J. Hu, M. Lee, et al. Chitosan-based nanoparticles as a sustained protein release carrier for tissue engineering applications. J. Biomed. Mater. Res. Part A 100A:939-947, 2012.
14. des Rieux, A., B. Ucakar, V. Preat, et al. 3D systems delivering VEGF to promote angiogenesis for tissue engineering. J. Controlled Release 150:272-278, 2011.
15. Poh, C. K., S. Ng, W. Wang, et al. In vitro characterizations of mesoporous hydroxyapatite as a controlled release delivery device for VEGF in orthopedic applications. J. Biomed. Mater. Res. Part A 100A:3134-3150, 2012.
16. Jun, S. H., E. J. Lee, Y. H. Koh, et al. Silica-chitosan hybrid coating on Ti for controlled release of growth factors. J. Mater. Sci.: Mater. Med. 22:2757-2764, 2011.
17. Jun, S. H., E. J. Lee, Y. H. Koh, et al. Bone morphogenic protein-2 (BMP-2) loaded hybrid coating on porous hydroxyapatite scaffolds for bone tissue engineering. J. Mater. Sci.: Mater. Med. 24:773-782, 2013.

18. Langer, R., and M. Moses. Biocompatible controlled release polymers for delivery of polypeptides and growth factors. J. Cellular Biochemistry 45:340-345, 1991.

19. Yoo, H. S., T. G. Kim, and T. G. Park. Surface-functionalized electrospun nanofibers for tissue engineering and drug delivery. Advanced Drug Delivery Reviews 61:1033-1042, 2009.

20. Tian, L., M. P. Prabhakaran, S. Ramakrishna, et al. Emulsion electrospun vascular endothelial growth factor encapsulated by poly(l-lactic acid-co-ε-caprolactone) nanofibers for sustained release in cardiac tissue engineering. J. Mater. Sci. 47:3272-3281, 2012.

21. Jia, X., C. Zhao, Y. Fan, et al. Sustained release of VEGF by coaxial electrospun dextran/PLGA fibrous membranes in vascular tissue engineering. J. Biomaterials Science 22:1811-1827, 2011.

22. Su, Y., Q. Su, M. El-Newehy, et al. Controlled release of bone morphogenetic protein 2 and dexamethasone loaded in core-shell PLLACL-collagen fibers for use in bone tissue engineering. Acta Biomaterialia 8:763-771, 2012.

23. Sahoo, S., L. T. Ang, S. L. Toh, et al. Growth factor delivery through electrospun nanofibers in scaffolds for tissue engineering applications. J. Biomed. Mater. Res. 93A:1539-1550, 2010.

24. Sahoo, S., S. L. Toh, and J. C. H. Goh. A bFGF-releasing silk/PLGA-based biohybrid scaffold for ligament/tendon tissue engineering using mesenchymal progenitor cells. Biomaterials 31:2990-2998, 2010.

25. Panyam, J., and V. Labhasetwar. Biodegradable nanoparticles for drug and gene delivery to cells and tissue. Advanced Drug Delivery Reviews 55:329-347, 2003.

26. Ionescu, L. C., G. C. Lee, R. L. Mauck, et al. An anisotropic nanofiber/microsphere composite with controlled release of biomolecules for fibrous tissue engineering. Biomaterials 31:4113-4120, 2010.

27. Spiller, K. L., Y. Liu, A. M. Lowman, et al. A novel method for the direct fabrication of growth factor-loaded microspheres within porous nondegradable hydrogels: controlled release for cartilage tissue engineering. J. Controlled Release 157:39-45, 2012.

28. Rocha, F. G., C. A. Sundback, E. E. Whang, et al. The effect of sustained delivery of vascular endothelial growth factor on angiogenesis in tissue-engineered intestine. Biomaterials 29:2884-2890, 2008.

29. Rahman, C. V., D. Ben-David, E. Rahman, et al. Controlled release of BMP-2 from a sintered polymer scaffold enhances bone repair in a mouse calvarial defect model. J. Tissue Eng. Regen. Med., 2012. doi: 10.1002/term.1497

30. Bae, S. E., D. H. Choi, K. Park, et al. Effect of temporally controlled release of dexamethasone on in vivo chondrogenic differentiation of mesenchymal stromal cells. J. Controlled Release 143:23-30, 2010.

31. Fan, D., E. De Rosa, E. Tasciotti, et al. Mesoporous silicon-PLGA composite microspheres for the double controlled release of biomolecules for orthopedic tissue engineering. Adv. Funct. Mater. 22:282-293, 2012.

32. Sun, Q., E. A. Silva, S. Rajagopalan, et al. Sustained release of multiple growth factors from injectable polymeric system as a novel therapeutic approach towards angiogenesis. Pharmaceutical Research 27(2):264-271, 2010.

33. Wang, X., E. Wenk, D. L. Kaplan, et al. Growth factor gradients via microsphere delivery in biopolymer scaffolds for osteochondral tissue engineering. J. Controlled Release 134:81-90, 2009.

34. Xue, W., A. Bandyopadhyay, and S. Bose. Polycaprolactone coated porous tricalcium phosphate scaffolds for controlled release of protein for tissue engineering. J. Biomed. Mater. Res. Part B: Appl. Biomater. 91B:831-838, 2009.

35. Carlsson, J., H. Lundqvist, et al. Conjugate chemistry and cellular processing of EGF-dextran. Acta Oncologica 38(3):313-321, 1999.

36. Molineux, G. Pegylation: engineering improved pharmaceuticals for enhanced therapy. Cancer Treatment Reviews 28(Supplement 1):13-16, 2002.

37. Patel, N., K. M. Shakesheff, et al. Spatially controlled cell engineering on biodegradable polymer surfaces. FASEB J. 12:1447-1454, 1998.

38. Pompe, T., C. Werner, et al. Immobilization of growth factors on solid support for the modulation of stem cell fate. Nature Protocols 5(6):1042-1050, 2010.

39. Harris, B. P., A. T. Metters, et al. Photopatterned polymer brushes promoting cell adhesion gradients. Langmuir 22(10):4467-4471, 2006.

40. Patel, S., S. Li, et al. Regulation of endothelial cell function by GRDGSP peptide grafted onto interpenetrating polymers. J. Biomed. Mater. Res. 83A:423-433, 2007.

41. Rowley, J. A., and D. J. Mooney. Alginate type and RGD density control myoblast phenotype. J. Biomed. Mater. Res. 60:217-223, 2002.

42. Alsberg, E., D. J. Mooney, et al. Cell-interactive alginate hydrogels for bone tissue engineering. J. Dent. Res. 80(11):2025-2029, 2001.

43. DeLong, S. A., A. S. Gobin, and J. L. West. Covalent immobilization of RGDS on hydrogel surfaces to direct cell alignment and migration. J. Controlled Release 109:139-148, 2005.

44. DeLong, S. A., J. J. Moon, and J. L. West. Covalently immobilized gradients of bFGF on hydrogel scaffolds for directed cell migration. Biomaterials 26:3227-3234, 2005.

45. Chen, G., and Y. Ito. Gradient micropattern immobilization of EGF to investigate the effect of artificial juxtacrine stimulation. Biomaterials 22:2453-2457, 2001.

46. Kapur, T. A., and M. S. Shoichet. Immobilized concentration gradients of nerve growth factor guide neurite outgrowth. J. Biomed. Mater. Res. 68A:235-243, 2004.

47. Moore, K., M. S. Shoichet, et al. Immobilized concentration gradients of neurotrophic factors guide neurite outgrowth of primary neurons in macroporous scaffolds. Tissue Eng. 12:267-278, 2006.

48. Zhang, H., S. J. Hollister, et al. Chemically-conjugated bone morphogenetic protein-2 on three-dimensional polycaprolactone (PCL) scaffolds stimulates osteogenic activity in bone marrow stromal cells. Tissue Eng.: Part A 16(11):3441-3448, 2010.

49. Liu, H., and T. J. Webster. Ceramic/polymer nanocomposites with tunable drug delivery capability at specific disease sites. J. Biomed. Mater. Res. 93A:1180-1192, 2010.

50. Lock, J., T. Y. Nguyen, and H. Liu. Nanophase hydroxyapatite and poly(lactide-co-glycolide) composites promote human mesenchymal stem cell adhesion and osteogenic differentiation in vitro. J. Mater. Sci.: Mater. Med. 23:2543-2552, 2012.

51. Gurdon, J. B., and P. Y. Bourillot. Moprhogen gradient interpretation. Nature 413:797-803, 2001.

52. Gurdon, J. B., H. Standley, et al. Single cells can sense their position in a morphogen gradient. Development 126:5309-5317, 1999.

53. Moon, J. J., S. H. Lee, and J. L. West. Synthetic biomimetic hydrogels incorporated with ephrin-A1 for therapeutic angiogenesis. Biomacromolecules 8:42-49, 2007.

54. Leipzig, N. D., M. S. Shoichet, et al. Functional immobilization of interferon-gamma induces neuronal differentiation of neural stem cells. J. Biomed. Mater. Res. 93A:625-633, 2010.

55. Anderson, S. M., T. Segura, et al. The phosphorylation of vascular endothelial growth factor receptor-2 (VEGFR-2) by engineered surfaces with electrostatically or covalently immobilized VEGF. Biomaterials 30:4618-4628, 2009.

56. Puccinelli, T. J., P. J. Bertics, and K. S. Masters. Regulation of keratinocyte signaling and function via changes in epidermal growth factor presentation. Acta Biomaterialia 6(9):3415-3425, 2010.

57. Marcantonio, N. A., L. G. Griffith, et al. The influence of tethered epidermal growth factor on connective tissue progenitor colony formation. Biomaterials 30:4629-4638, 2009.

58. Tigli, R. S., and M. Gumusderelioglu. Evaluation of RGD- or EGF-immobilized chitosan scaffolds for chondrogenic activity. Intl. J. Biological Macromolecules 43:121-128, 2008.

59. Liu, H. W., G. H. Hsiue, et al. Heterobifunctional poly(ethylene glycol)-tethered bone morphogenetic protein-2-stimulated bone marrow mesenchymal stromal cell differentiation and osteogenesis. Tissue Eng. 13(5):1113-1124, 2007.

60. Karageorgiou, V., D. Kaplan, et al. Bone morphogenetic protein-2 decorated silk fibroin films induce osteogenic differentiation of human bone marrow stromal cells. J. Biomed. Mater. Res. A 71A:528-537, 2004.

61. Wissink, M. J. B., J. Feijen, et al. Binding and release of basic fibroblast growth factor from heparinized collagen matrices. Biomaterials 22(16):2291-2299, 2001.

62. Metzger, W., M. Oberringer, et al. Induction of myofibroblastic differentiation in vitro by covalently immobilized transforming growth factor-B1. Tissue Eng. 13(11):2751-2760, 2007.

63. Mann, B. K., R. H. Schmedlen, and J. L. West. Tethered-TGF-β increases extracellular matrix production of vascular smooth muscle cells. Biomaterials 22:439-444, 2001.

64. Liu, L. S., R. C. Spiro, et al. Hyaluronate-heparin conjugate gels for the delivery of basic fibroblast growth factor (FGF-2). J. Biomed. Mater. Res. 62:128-135, 2002.

65. Tan, H., C. Gao, et al. Gelatin/chitosan/hyaluronan ternary complex scaffold containing basic fibroblast growth factor for cartilage tissue engineering. J. Mater. Sci.: Mater. Med. 18:1961-1968, 2007.

66. Ho, Y., F. Mi, H. Sung, and P. Kuo. Heparin-functionalized chitosan-alginate scaffolds for controlled release of growth factor. Intl. J. Pharmaceutics 376:69-75, 2009.

67. Teixeira, S., L. Yang, F. J. Monteiro, et al. Heparinized hydroxyapatite/collagen three-dimensional scaffolds for tissue engineering. J. Mater. Sci.: Mater. Med. 21:2385-2392, 2010.

68. Bhakta, G., B. Rai, S. M. Cool, et al. Hyaluronic acid-based hydrogels functionalized with heparin that support controlled release of bioactive BMP-2. Biomaterials 33:6113-6122, 2012.

69. Duan, B., and M. Wang. Customized Ca-P/PHBV nanocomposite scaffolds for bone tissue engineering: design, fabrication, surface modification and sustained release of growth factor. J. R. Soc. Interface 7:S615-S629, 2010.

70. Lee, J., J. J. Yoo, A. Atala, and S. J. Lee. The effect of controlled release of PDGF-BB from heparin-conjugated electrospun PCL/gelatin scaffolds on cellular bioactivity and infiltration. Biomaterials 33:6709-6720, 2012.

71. Lam, H. J., S. Li, et al. In vitro regulation of neural differentiation and axon growth by growth factors and bioactive nanofibers. Tissue Eng. Part A 16(8):2641-2648, 2010.

72. Patel, S., S. Li, et al. Bioactive nanofibers: synergistic effects of nanotopography and chemical signaling on cell guidance. Nano Lett. 7(7):2122-2128, 2007.

73. Yu, J., S. Li, et al. The effect of stromal cell-derived factor-1α/heparin coating of biodegradable vascular grafts on the recruitment of both endothelial and smooth muscle progenitor cells for accelerated regeneration. Biomaterials 33:8062-8074, 2012.

74. Yoon, J. J., T. G. Park, et al. Heparin-immobilized biodegradable scaffolds for local and sustained release of angiogenic growth factor. J. Biomed. Mater. Res. Part A 79A(4):934-942, 2006.

75. Jeon, O., B. S. Kim, et al. Enhancement of ectopic bone formation by bone morphogenetic protein-2 released from a heparin-conjugated poly(L-lactic-co-glycolic acid) scaffold. Biomaterials 28(17):2763-2771, 2007.
76. Rohman, G., N. R. Cameron, et al. Heparin functionalization of porous PLGA scaffolds for controlled, biologically relevant delivery of growth factors for soft tissue engineering. J. Mater. Chem. 12:9265-9273, 2009.
77. Yoon, J. J., T. G. Park, et al. Photo-crosslinkable and biodegradable Pluronic/heparin hydrogels for local delivery of angiogenic growth factor. J. Biomed. Mater. Res. A 83A(3):597-605, 2007.
78. Park, J. S., K. H. Park, et al. Determination of dual delivery for stem cell differentiation using dexamethasone and TGF-beta3 in/on polymeric microspheres. Biomaterials 30:4796-4805, 2009.
79. Richardson, T. P., D. J. Mooney, et al. Polymeric system for dual growth factory delivery. Nature Biotechnology 19:1029-1034, 2001.
80. Elia, R., R. A. Peattie, et al. Stimulation of in vivo angiogenesis by an in situ crosslinked, dual growth factor-loaded, glycosaminoglycan hydrogels. Biomaterials 31:4630-4638, 2010.
81. Nillesen, S. T., T. H. van Kuppevelt, et al. Increased angiogenesis and blood vessel maturation in acellular collagen heparin scaffolds containing both FGF2 and VEGF. Biomaterials 28:1123-1131, 2007.
82. Vonau, R. L., A. E Sams, et al. Combination of growth factors inhibits bone ingrowth in the bone harvest chamber. Clin. Orthop. 386:243-251, 2001.
83. Ripamonti, U., D. C. Rueger, et al. Periodontal tissue regeneration by combined applications of recombinant human osteogenic protein-1 and bone morphogenetic protein-2. A pilot study in Chacma baboons (Papio ursinus). Eur. J. Oral Sci. 109:241-248, 2001.

84. Marden, L. J., and J. O. Hollinger. Platelet-derived growth factor inhibits bone regeneration induced by osteogenin, a bone morphogenetic protein, in rat craniotomy defects. J. Clin. Invest. 92:2897-2905, 1993.
85. Raiche, A. T., and D. A. Puleo. In vitro effects of combined and sequential delivery of two bone growth factors. Biomaterials 25:677-685, 2004.
86. Young, S., L. S. Baggett, et al. Dose effect of dual delivery of vascular endothelial growth factor and bone morphogenetic protein-2 on bone regeneration in a rat critical-size defect model. Tissue Eng. Part A 15:2347-2362, 2009.
87. Phelps, E. A., A. J. Garcia, et al. Bioartificial matrices for therapeutic vascularization. PNAS 107(8):3323-3328, 2010.
88. Van Den Beucken, J. J. J. P., J. A. Jansen, et al. In vitro and in vivo effects of deoxyribonucleic acid-based coatings functionalized with vascular endothelial growth factor. Tissue Eng. 13(4):711-720, 2007.

Chapter 4

4. Biological and Mechanical Characterization of Chitosan-Alginate Scaffolds for Growth Factor Delivery and Chondrogenesis

4.1 Abstract

Cartilage regeneration using tissue engineering is a highly sought after research and commercial endeavor. A myriad of scaffold types, cell types, and growth factors have been utilized in attempt to achieve successful chondrogenesis. However, not enough attention is paid to the mechanical strength requirements of scaffolds as implants that need to be handled, manipulated, and dynamically compressed in vivo. Moreover, growth factors are often haphazardly embedded in scaffolds without careful engineering or characterization of release, leading to poor control over their delivery. This initial phase of work focuses on creating a biocompatible, mechanically robust scaffold that can promote chondrocyte cartilage production initiated by nonspecifically adsorbed chondrogenic growth factors.

Chitosan-alginate (Ch-Al) scaffolds provided a favorable environment, both mechanical and biological, for chondrogenesis. Ch-Al scaffold fabrication resulted in a highly porous, tortuous, and interconnected structure, with pores ranging from 20-200 um and 78% ± 13% porosity. Hydrated 2%-2% w/v Ch-Al demonstrated 83.1 ± 14.6 kPa compressive elastic modulus, and dry 2%-2% w/v Ch-Al resulted in 337.8 ± 61.6 kPa elastic modulus. The mechanical properties of chitosan-alginate scaffolds could be varied by changing the ratio and concentration of the chitosan and alginate solutions. 1%, 2%, and 3% w/v chitosan and alginate mixed at various ratios resulted in different elastic moduli, and Ch-Al scaffolds were able to be handled above ~20 kPa. Hydrated 2:1 ratio 2%-2% w/v Ch-Al scaffolds crosslinked with 1% w/v chondroitin sulfate (CS) measured up to 450 kPa, the peak elastic modulus of all tested formulations. Ch-Al scaffolds exhibited springback after

compression, and this resiliency improved with hydration. Ch-Al maintained mouse bone marrow stromal cell (mBMSC) viability and proliferation, with initial cell clusters forming at day 5 and cellular protrusions and spreading after 21 days. Adding dilute concentrations of fibrin to the mBMSC suspension during seeding improved cell spreading on Ch-Al scaffolds drastically. Ch-Al supported primary rabbit joint chondrocyte (RJC) chondrogenesis at weeks 3 and 6 without any growth factors, although Ch-Al coated with fibrin supported more homogeneous RJC chondrogenesis at week 6, also without any growth factor supplements.

Ch-Al scaffolds provided a favorable template for growth factor delivery, which promoted chondrogenesis. Ch-Al nonspecifically adsorbed bovine serum albumin (BSA) and histone with <5% burst release at 1ug and 100ug loading, sustaining release for >30 days. 1ug and 100ug BSA released 60% of total loaded protein at day 28, while 100ug histone released merely 5%. Further, Ch-Al nonspecifically adsorbed transforming growth factor-β1 (TGF-β1) with 2% burst release at 100ng loading, sustaining release for >42 days in complete DMEM at 37C. Ch-Al with 200ng TGF-β1 nonspecifically adsorbed demonstrated homogeneous and expedited RJC chondrogenesis at week 3, a significant improvement over the spatially sporadic extracelluar matrix (ECM) production seen at weeks 3 and 6 when no growth factor was added. These results illustrate the potential of Ch-Al scaffolds as a framework for growth factor delivery and chondrogenesis.

4.2 Introduction

Articular cartilage has limited regenerative capacity due to the lack of vascularization of the native tissue and the limited proliferation capacity of chondrocytes. Despite being an avascular and non-innervated matrix, articular cartilage can modify its characteristics in response to differential loading. Mechanotransduction has been shown to increase matrix biosynthesis and chondrogenic gene expression under specific loads and strains below the threshold for injury (5-10 MPa normal stress range, ~40% normal strain).[1,2] This complexity combined with its ability to distribute load, resist compression, and accommodate extreme strain make articular cartilage difficult to replace with tissue engineered designs.[3]

Chitosan-alginate (Ch-Al) scaffolds have been used in cartilage tissue engineering because they are naturally occurring polysaccharides similar in chemical structure to articular cartilage extracellular matrix (ECM) glycosaminoglycans (GAGs) like chondroitin sulfate (CS), keratan sulfate, and hyaluronic acid.[4] Thus chitosan and alginate can serve as less expensive GAG analogs in tissue engineered constructs. Positively charged chitosan amine groups and negatively charged alginate carboxylic acid groups can electrostatically crosslink[5] or be further crosslinked with a divalent cation like Ca^{2+}, Ba^{2+}, or Sr^{2+}, which cooperatively interact with blocks of G monomers within alginate to form ionic bridges between different polymer chains.[6-8] Ultimately, the mechanical properties of hybrid Ch-Al scaffolds are superior to those of either polymer alone, with 1.5% w/v chitosan and 1% w/v alginate exhibiting equilibrium compressive moduli of 1.5kPa[9] and 1kPa[10], respectively. Li et al reported 4.8%-4.8% w/v dry Ch-Al scaffolds to exhibit a compressive Young's modulus of 8.16MPa, while in comparison, pure chitosan measured a compressive modulus of 2.56MPa.[6] Further, Ch-Al scaffolds can be prepared at neutral pH, allowing growth factors and drugs to be uniformly incorporated without denaturation.[7]

Here we proposed using mechanically resilient Ch-Al scaffolds to mimic the native robust properties of articular cartilage. By altering the concentrations and ratios of chitosan and alginate during the Ch-Al fabrication process, we hoped to identify an optimal working region that could be tailored for various tissue engineering applications.

CS is a GAG that, alongside keratan sulfate, makes up the proteoglycan molecule, which in turn binds to hyaluronic acid through link protein. When incorporated into highly crystalline scaffolds, the negatively charged CS molecule introduces amorphous regions that increase the rate of hydrolytic degradation of the scaffolds. Because CS is an anionic molecule that exhibits electrostatic repulsion upon compression, giving native cartilage its resistance to impact, it was hypothesized that adding CS into Ch-Al scaffolds would increase the stiffness to even more closely match that of articular cartilage.

In previous in vitro studies, Ch-Al hybrid scaffolds have been shown to serve as a template to modulate chondrocyte phenotype and support chondrogenesis, as well as promote osteogenesis.[6,7] Ch-Al was shown to improve collagen type II production over chitosan, as shown by western blot but without any supporting evidence of ECM laydown in histological images.[7] In this study, we first aimed to demonstrate chondrogenesis by normal primary chondrocytes on Ch-Al using zero growth factors. Next, we hoped to achieve more homogeneous chondrogenesis when Ch-Al scaffolds were coated with plasma proteins naturally present in the implant site like fibrinogen and thrombin, also cultured in the absence of supplemental growth factors.

Timed delivery of chondrogenic growth factors or gene therapy may be necessary to ensure total and directed differentiation down the chondrogenic pathway. Cartilage healing in canine defects is characterized by a proliferative phase at 1.5 months followed by a remodeling phase lasting 3-6 months.[11] Thus a sustained release of chondrogenic growth factor with a release profile coinciding with the natural healing timeline of cartilage is desirable. Previously, Ch-Al polyelectrolyte complexes in various forms have been used to encapsulate and deliver proteins or drugs by manipulating the degree of association between the two polymers' functional groups as well as their pH-dependent charge density.[5,12] For example, Ch-Al self-assembling polyelectrolyte multilayer films have been used to immobilize antibodies[12], Ch-Al blend gel beads with dual crosslinking were shown to have gastrointestinal site-specific protein release[13], and drug-loaded, polyelectrolyte complexed Ch-Al fibers released charged compounds such as bovine serium albumin (BSA), platelet-derived growth factor-bb (PDGF-bb), and avidin over the course of 3 weeks.[14] As the final study concerning the chondrogenic potential of Ch-Al, we hypothesized that utilizing the charged nature of Ch-Al to deliver growth factors in a sustained manner would improve chondrogenesis beyond the inherent cues of the scaffold alone.

4.3 Materials and Methods

4.3.1 Materials

Mouse bone marrow stromal cells (mBMSCs, C57BL/6 mouse mesenchymal stem cells from Bone Marrow, Cat # S1502-100), live/dead calcein AM/ethidium homodimer-1 stain (Cat # L-3224), collagenase type II (Cat # 17101-015), antibiotic-antimycotic (ABAM, Cat # 15240-062), and histone H1 from calf thymus Alexa Fluor 488 conjugate (Cat # H-13188) were obtained from Life Technologies (Grand Island, NY).

Chitosan (practical grade, Cat # 41763), alginate from brown algae (Cat # A7003), calcium chloride ($CaCl_2$-$2H_2O$, Cat # 12022), 50% sodium hydroxide in water (Cat # 415413), chondroitin sulfate sodium salt from shark cartilage (Cat # C4384), and bovine serum albumin fluorescein isothiocyanate conjugate (BSA-FITC, Cat # A9771) were obtained from Sigma-Aldrich (St. Louis, MO).

Acetic acid (glacial, Cat # A38 SI-212), ethanol (reagent alcohol, Cat # A962P-4), optimal cutting temperature Compound (OCT, Tissue-Tek, Cat # 4583), Dulbecco's Modification of Eagle's Medium w/ 4.5 g/L glucose, L-glutamine & sodium pyruvate (DMEM 1X, Cellgro, Cat # 10-013-CV), fetal bovine serum (FBS, Cat # MT35015CV), and 70 um nylon meshes (Cat # 22363548) were obtained from Fisher Scientific (Waltham, MA).

Fibrinogen sealer protein (Lot # 08P1498C), fibrinolysis inhibitor solution (bovine, 3,000KIU of aprotonin/mL, Lot # 76B0698C), thrombin (Lot # 78H1198D), and calcium chloride solution (40mmol/L, Lot # 810498D) were all obtained from Haemacure (Sarasota, FL).

Transforming growth factor-β1 (TGF-β1, 25kDa, Cat # 100-21) was obtained from PeproTech (Rocky Hill, NJ).

4.3.2 Scaffold fabrication

Adapted and modified from Li et al[6,7], Ch-Al scaffolds were fabricated with 2% w/v chitosan dissolved in 2% v/v acetic acid in dH_2O and 2% w/v alginate dissolved in dH_2O, mixed at 1:1 ratio. The solution was ultrasonically homogenized for 1min, titrated to pH 7.4 with 50% sodium hydroxide, ultrasonically homogenized for 5min, poured into molds, and frozen at -80C overnight. The resulting frozen scaffolds were lyophilized overnight, crosslinked for 15min with 1% w/v $CaCl_2$, washed three times with dH_2O, and lyophilized overnight. For all experiments, except the mechanical characterization when various concentrations and ratios of Ch and Al are used, 2%-2% Ch-Al at 1:1 ratio was the chosen scaffold formulation. For viability and chondrogenesis experiments, scaffolds were soaked in 70% v/v ethanol for 1hr for sterilization, followed by washing three times with dH_2O.

4.3.3 Porosity

Porosity was calculated using the liquid displacement method, with dH_2O as the displacing fluid.[15,16] Scaffolds were fabricated using a 96-well plate as a mold, and different batches of scaffolds were tested and averaged. Ch-Al scaffolds were imaged using a Nova Nano scanning electron microscope (SEM) 230 (FEI, Hillsboro, OR) under low vacuum detector, 5-10keV accelerating voltage, and 3.0 spot size.

4.3.4 Mechanical Characterization

Ch-Al scaffolds were fabricated with 0.5%, 1%, or 2% w/v chitosan dissolved in 2% v/v acetic acid in dH_2O and 0.5%, 1%, or 2% w/v alginate dissolved in dH_2O, mixed at various ratios (1:1, 1:2, 1:3, 2:1, 2:2, 2:3, 3:1, 3:2, and 3:3). The scaffolds were processed the same as above, except crosslinking was with 1% w/v $CaCl_2$ alone or 1% w/v $CaCl_2$ with 2% w/v CS. Scaffolds were fabricated using 6-well plates as molds. For testing the various concentrations and ratios, scaffolds were hydrated in dH_2O prior to mechanical testing. For comparing the mechanical properties (both Young's modulus and resiliency) under hydrated or dry conditions, 2%-2% Ch-Al scaffolds were either hydrated in dH_2O or left dry after lyophilization.

Young's modulus was determined using an elastic compression test (Instron, Norwood, MA) in which a probe indented the scaffold surface 1 mm at a rate of 2 mm/s. Sneddon's equation describing flat punch indentation was used for calculating Young's modulus E from force F (Eq 1). Poisson's ratio was taken to be ν=0.45, as reported for polysaccharide hydrogels[17]. Probe diameter a was 3 mm. F and h values were taken from the linear region of the force-displacement curve generated by the Instron. Values were taken from 3 different scaffolds, with 3 locations on each scaffold.

$$F = \frac{2aEh}{(1-\nu^2)} \qquad \text{Eq (1)}$$

For determining Ch-Al resiliency, Instron flat punch indentation compression was performed as described above but with 1, 2, 3, or 5mm indentation, which was 20%, 40%, 60%, and 100% of the height of the scaffold, respectively. 20% compression was tested at 1mm/min strain rate, while all other % compressions were tested at 10mm/min strain rate. For 100% compression, the Instron compressed the scaffolds as far as possible, but the remaining thickness of the scaffolds renders this condition nearly 100%, not fully 100%. Scaffolds were fabricated using a 96-well plate as a mold. Springback was measured immediately after compression, within 5 s. Some dry scaffolds were compressed 60% or 100% and then immediately after their springback, were rehydrated with water, and additional springback was observed.

4.3.5 Cell Viability

Mouse bone marrow stromal cells (mBMSCs) cultured under standard conditions using DMEM with 10% FBS and 1% ABAM were seeded on Ch-Al scaffolds at a density of 101.9 cells/mm^3 (40,000 mBMSCs in 392.5mm^3 scaffold) and allowed to proliferate for over 3 weeks. Scaffolds were fabricated using a 48-well plate. Viability was performed using a 1:1000 live/dead calcein AM/ethidium homodimer-1 stain at various time points.

4.3.6 Chondrocyte Isolation

Primary rabbit joint chondrocytes (RJCs) were harvested from the knee and acetabulofemoral joints of 3 month old New Zealand White rabbits. Briefly, the femurs of sacrificed rabbits were isolated, surgically removed, and soaked in PBS. Cartilage was carefully scraped off the femoral condyles, patellar groove, and femoral head, and immediately soaked in DMEM with 10% FBS and 1% ABAM. The cartilage flakes were diced into 1mm^3 pieces and digested in 200 U/mL collagenase type II for 6 hr at 37 C. The solution was filtered through a 70 um nylon mesh to isolate the RJCs from any undigested cartilage or debris. RJCs were seeded at an initial density of 13,000 cells/cm^2 (1,000,000 RJCs on 10 cm plate) using DMEM with 10% FBS and 1% ABAM. Plated RJCs were allowed to recover and form adhesions for 3 days before changing medium. Approximately 50% of plated RJCs survived by day 3, and they exhibited a 1 week doubling time. RJCs were trypsinized and used for chondrogenesis experiments after this 1 week in culture.

4.3.7 Chondrogenesis

Ch-Al scaffolds fabricated in a 96-well plate seeded with RJCs at a density of 5095.5 cells/mm^3 (500,000 RJCs in 98.125mm^3 scaffold) were cultured under standard conditions using DMEM containing 10% FBS and 1% ABAM. Constructs were collected, fixed, embedded in OCT, and sectioned at weeks 3 and 6 for histology.

4.3.8 Chondrogenesis with Fibrin

A dilute fibrin solution containing resuspended RJCs was pipetted onto pre-fabricated Ch-Al scaffolds made in a 96-well plate. Physiological concentrations of 0.67 mg/mL fibrinogen and 3.33 IU/mL thrombin were chosen. The RJC seeding density was 5095.5 cells/mm^3 (500,000 RJCs in 98.125mm^3 scaffold), and constructs were cultured under standard conditions using DMEM containing 10% FBS and 1% ABAM. Constructs were collected, fixed, embedded in OCT, and sectioned at weeks 3 and 6 for histology.

4.3.9 Histology

Chondrogenesis was examined via ECM production, specifically H&E stain for nuclei and collagen, 0.1% SafraninO stain for GAGs, 1% Alcian blue stain at pH 1.5 for proteoglycans, and immunohistochemistry for collagen type II.

4.3.10 Nonspecific Adsorption of Model Proteins

Ch-Al scaffolds fabricated in a 96-well plate were nonspecifically loaded with 1ug, 100ug, or 10mg BSA-FITC or 100ug histone AlexaFluor 488 (histone488) by pipetting 50ul of protein solution in PBS directly onto the scaffold. Scaffolds were incubated in dH_2O for 4 weeks, and the fluorescence of collected supernatants containing protein released during that time was quantified using a plate reader (Tecan, Männedorf, Switzerland).

4.3.11 Nonspecific Adsorption of TGF-β1

Ch-Al scaffolds fabricated in a 96-well plate were nonspecifically loaded with 100ng transforming growth factor-β1 (TGF-β1) by pipetting 50ul of protein solution in PBS directly onto the scaffold. Scaffolds were incubated in DMEM with 10% FBS and 1% ABAM at 37C for 6 weeks, and ELISA was used to quantify release.

4.3.12 Chondrogenesis with TGF-β1

Ch-Al scaffolds fabricated in a 96-well plate were nonspecifically loaded with 200ng TGF-β1 and seeded with RJCs at a density of 5095.5 cells/mm^3 (500,000 RJCs in 98.125mm^3 scaffold). Constructs were cultured under standard conditions using DMEM containing 10% FBS and 1% ABAM. Constructs were collected, fixed, embedded in OCT, and sectioned at week 3 for histology.

4.4 Results

4.4.1 Porosity

Chitosan-alginate hybrid scaffolds were porous, with tortuous interconnected pores ranging between 20 and 200um, as illustrated by SEM in Figure 4.1. Previous work by Li and Zhang has shown chitosan alginate scaffolds to be similarly porous with open structures between 50 and 200um.[6,7] Porosity was quantified based on the liquid displacement method and calculated to be 78% ± 13%. The high standard deviation can be attributed to averaging across different batches of Ch-Al solution.

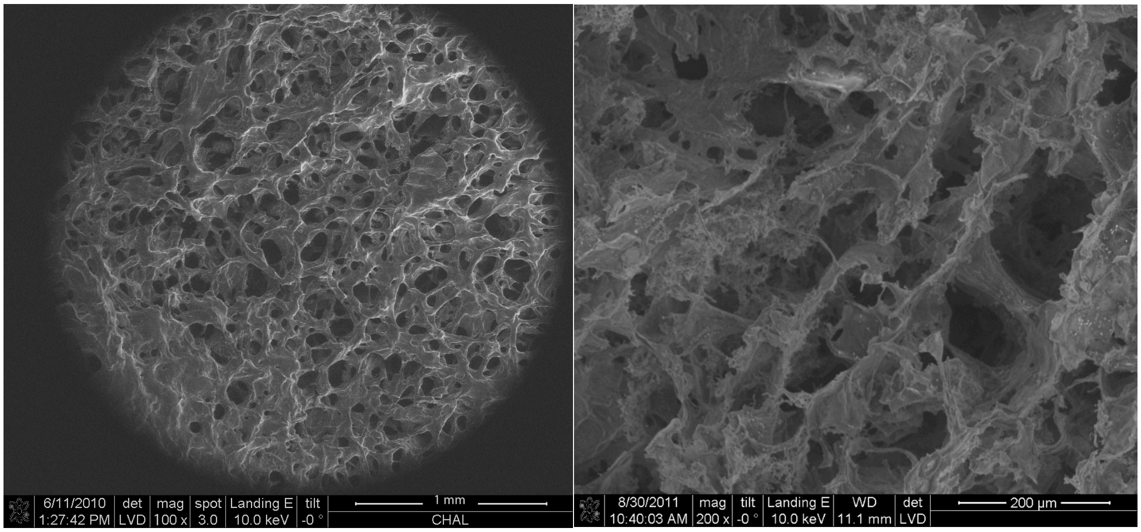

Figure 4.1 SEM images showing porosity, tortuosity, and interconnectivity of cross-sectioned chitosan-alginate (Ch-Al) scaffolds.

4.4.2 Mechanical Characterization

Hydrated 2%-2% Ch-Al exhibited 83.1 ± 14.6 kPa compressive elastic modulus, and dry 2%-2% Ch-Al demonstrated a modulus of 337.8 ± 61.6 kPa, as shown in Figure 4.2a. Further, the mechanical properties of Ch-Al scaffolds could be varied by changing the ratio and concentration of the chitosan and alginate solutions. Various weight % ratios resulted in different elastic moduli, and Ch-Al was able to be handled above ~20 kPa. Heat maps in Figure 4.2b and 4.2c illustrate the dependence of scaffold stiffness on Al, Ch, and CS content when crosslinked with $CaCl_2$ alone or CS in $CaCl_2$. Comparison showed that the addition of CS significantly increased scaffold stiffness. A 2:1 Ch:Al ratio crosslinked with CS resulted in a peak stiffness of ~450 kPa elastic moduli when hydrated.

A

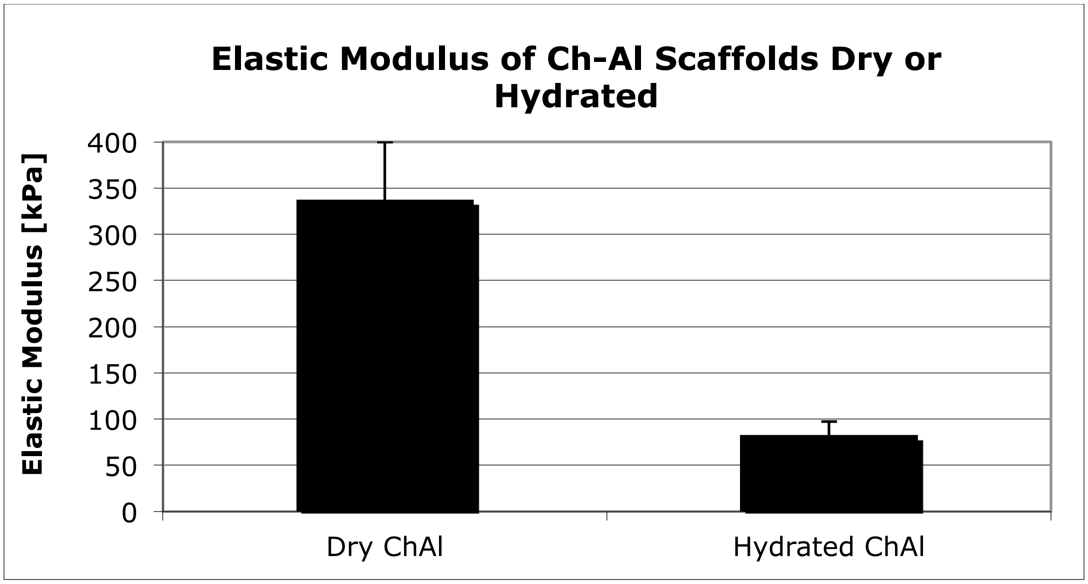
Elastic Modulus of Ch-Al Scaffolds Dry or Hydrated
Elastic Modulus [kPa]
400
350
300
250
200
150
100
50
0
Dry ChAl
Hydrated ChAl

B

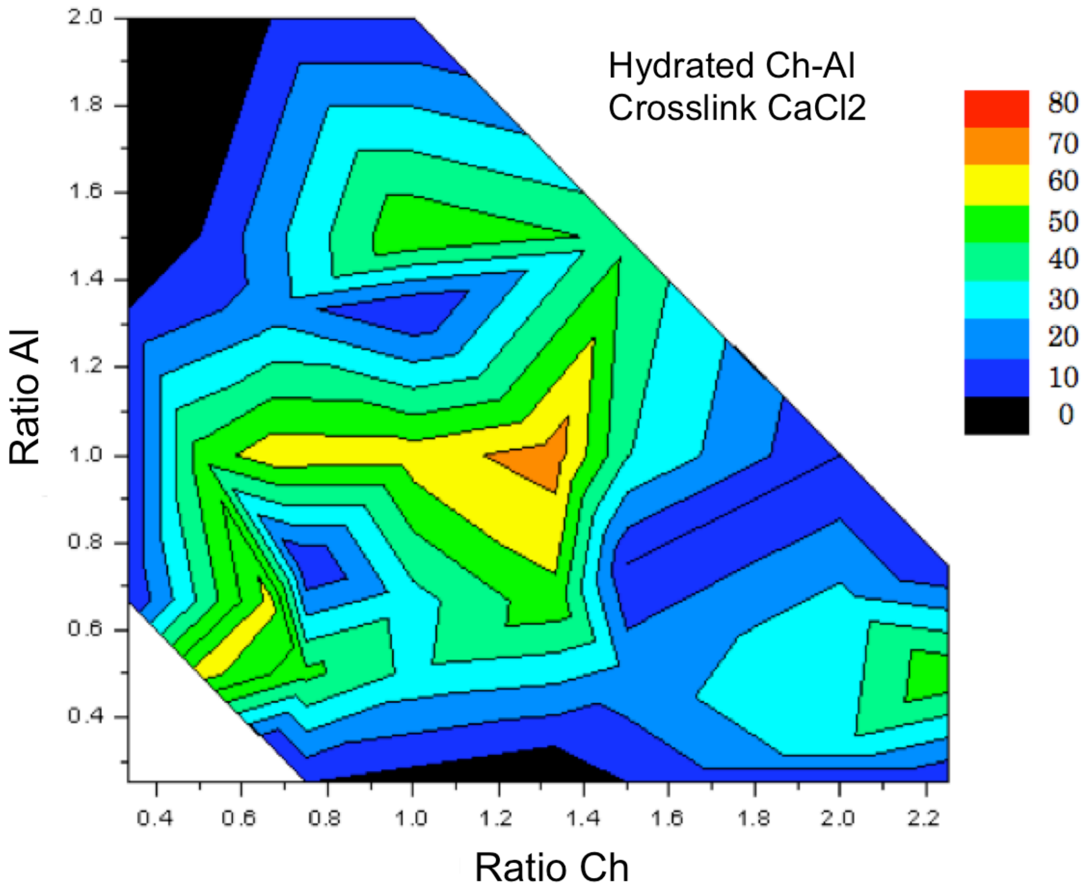
Hydrated Ch-Al
Crosslink CaCl2
80
70
60
50
40
30
20
10
0
Ratio Al
2.0
1.8
1.6
1.4
1.2
1.0
0.8
0.6
0.4
Ratio Ch
0.4
0.6
0.8
1.0
1.2
1.4
1.6
1.8
2.0
2.2

C

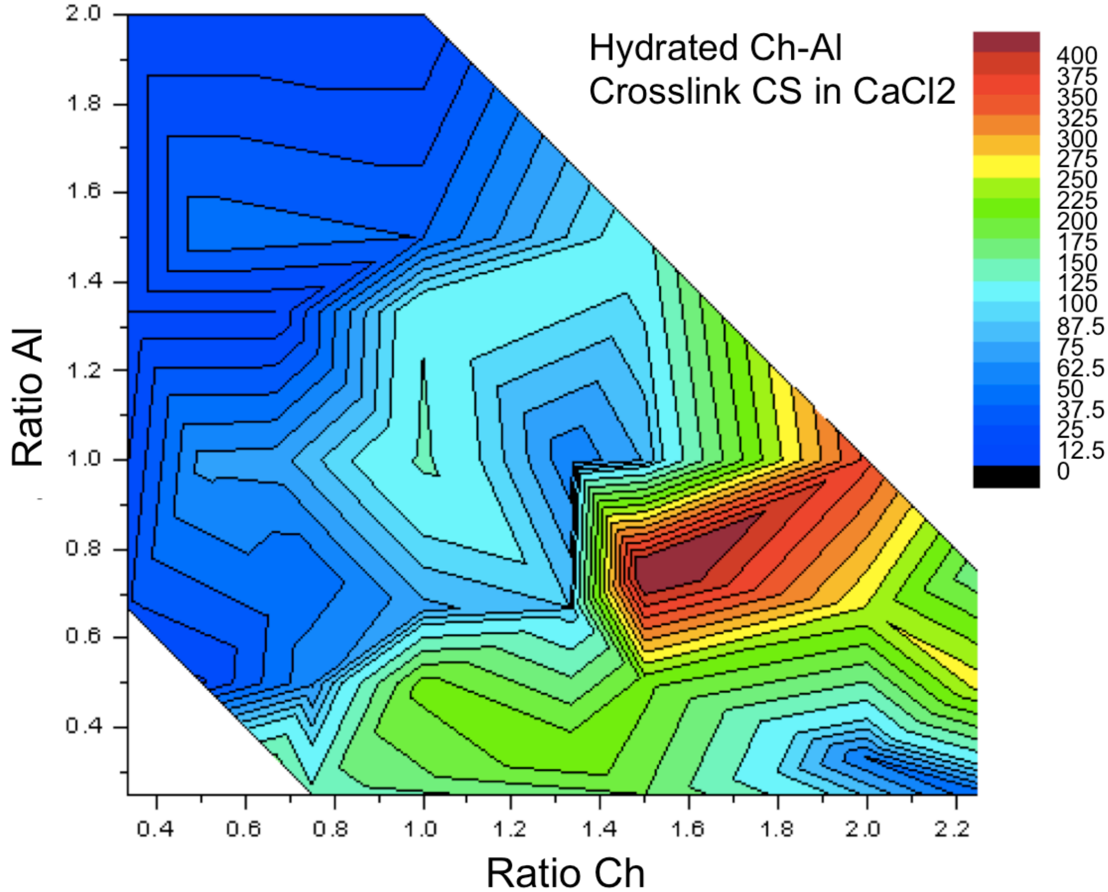

Figure 4.2 Elastic modulus of Ch-Al hydrated or dry under compression (a). Formulational dependence of hydrated scaffold stiffness on alginate, chitosan, and chondroitin sulfate (CS) content (b, c). 0.5%, 1%, and 2% formulations of chitosan (x axis) and alginate (y axis) were mixed at 1:1, 1:2, 1:3, 2:1, 2:2, 2:3, 3:1, 3:2, and 3:3 ratios. The stiffness of different Ch-Al scaffolds varied when crosslinked with calcium chloride (b) or 2% w/v CS in calcium chloride (c). Heat map color scale indicates values of Young's Modulus in kPa.

Ch-Al scaffolds exhibited springback after compression, and this resiliency was improved when scaffolds were hydrated compared to dry (Figure 4.3). Ch-Al scaffolds were compressed at different strains and their springback was measured as resiliency. Hydrated scaffolds showed greater resiliency than dry scaffolds, but only at 60% and 100% compressive strains (Figure 4.3a). Both dry and hydrated scaffolds were fairly resilient at 20% and 40% strain, with nearly entirely elastic springback at 20% strain. Plastic deformation was substantial for dry scaffolds at 60% and 100%

compression (only 40% and 10% height regained, respectively), while plastic deformation was only substantial for hydrated scaffolds at 100% compression (40% height regained). Moreover, when plastically deformed scaffolds compressed to 60% and 100% were rehydrated in water, some recovery of plastic deformation was seen by recovery in scaffold height—40$ height recovered to 70% height and 10% height recovered to 17% height, respectively (Figure 4.3b). This may be due to swelling of scaffold when wetted. These results show that by hydrating a dry scaffold that has hardly any springback after compression, additional springback can be recovered.

A

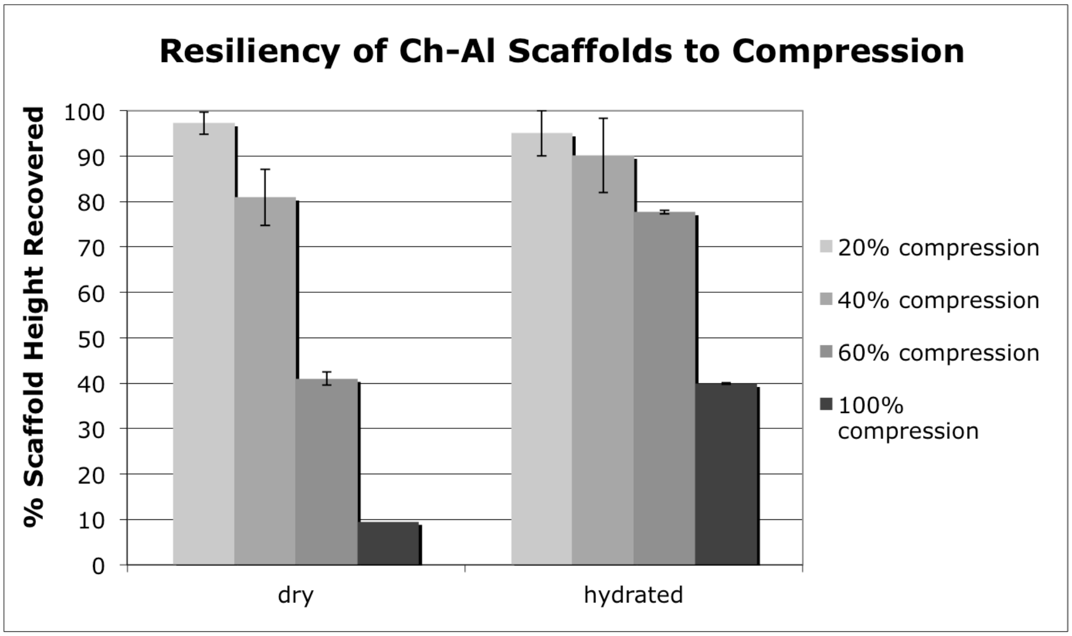

B

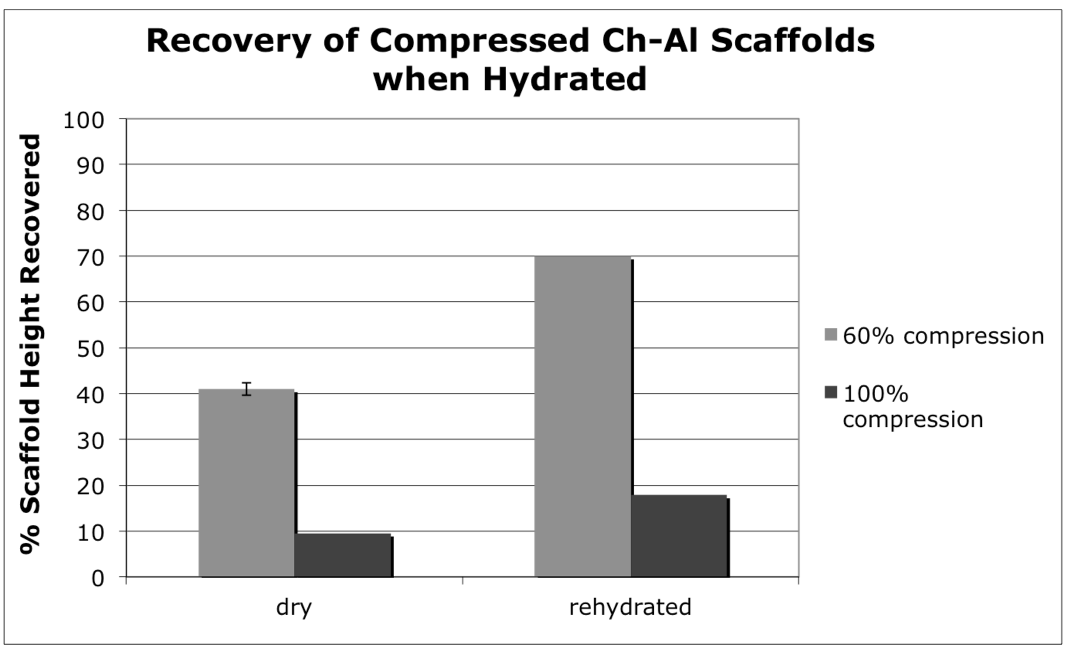

Figure 4.3 Resiliency of Ch-Al scaffolds after being compressed at different strains (a). 20% compression occurred at 1mm/min strain rate, while all other % compressions occurred at 10mm/min strain rate. Compressed scaffolds showed some recovery when hydrated (b).

4.4.3 Cell Viability

Ch-Al supports mBMSC viability and proliferation, with spreading after 21 days. Live/dead fluorescently stained images in Figure 4.4 show mBMSC viability and proliferation on Ch-Al scaffolds up to 23 days in vitro. Cell proliferation over time was substantial, with an estimated doubling rate of approximately four days. Alamar blue confirmed proliferation for the first week of culture (data not shown). Cells quickly adhered to Ch-Al scaffolds, but spreading was uncommon initially. Cellular protrusions from clusters did not appear until 3 weeks in vitro. Cryosections confirmed the characteristic clustering seen in live/dead experiments (data not shown). Although spreading was not substantial until 3 weeks, when seeded at a higher cell density (5095.5 cells/mm^3 vs 101.9 cells/mm^3, 500,000 cells in 98.125mm^3 scaffold vs 40,000 cells in 392.5mm^3 scaffold), cell spreading occurred much earlier at 5 days (data not shown).

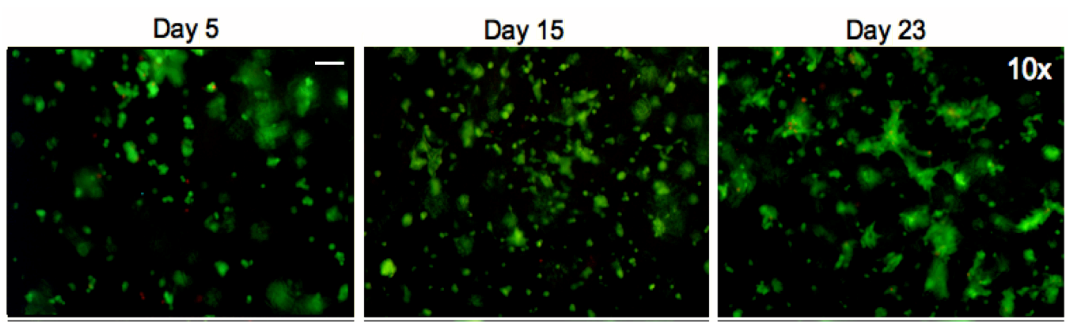

Figure 4.4 Live/dead fluorescently stained images showing mouse bone marrow stromal cell (mBMSC) viability and proliferation on Ch-Al scaffolds. Live cells appear green while dead cells appear red. Viability was assessed up to day 23. 40,000 mBMSCs were seeded on Day 0. Images were taken at 10x from the scaffold center. Scale bar equals 100um.

4.4.4 Chondrogenesis

Ch-Al supported RJC chondrogenesis at weeks 3 and 6 without any growth factor. Using plain medium with no chondrogenic growth factors, RJC constructs showed positive aggrecan staining by Alcian blue and collagen staining by H&E, as seen in Figure 4.5. Cell-secreted matrix was inhomogeneous but covered approximately 40% of the scaffold volume at week 3 and 60% of the scaffold volume at week 6.

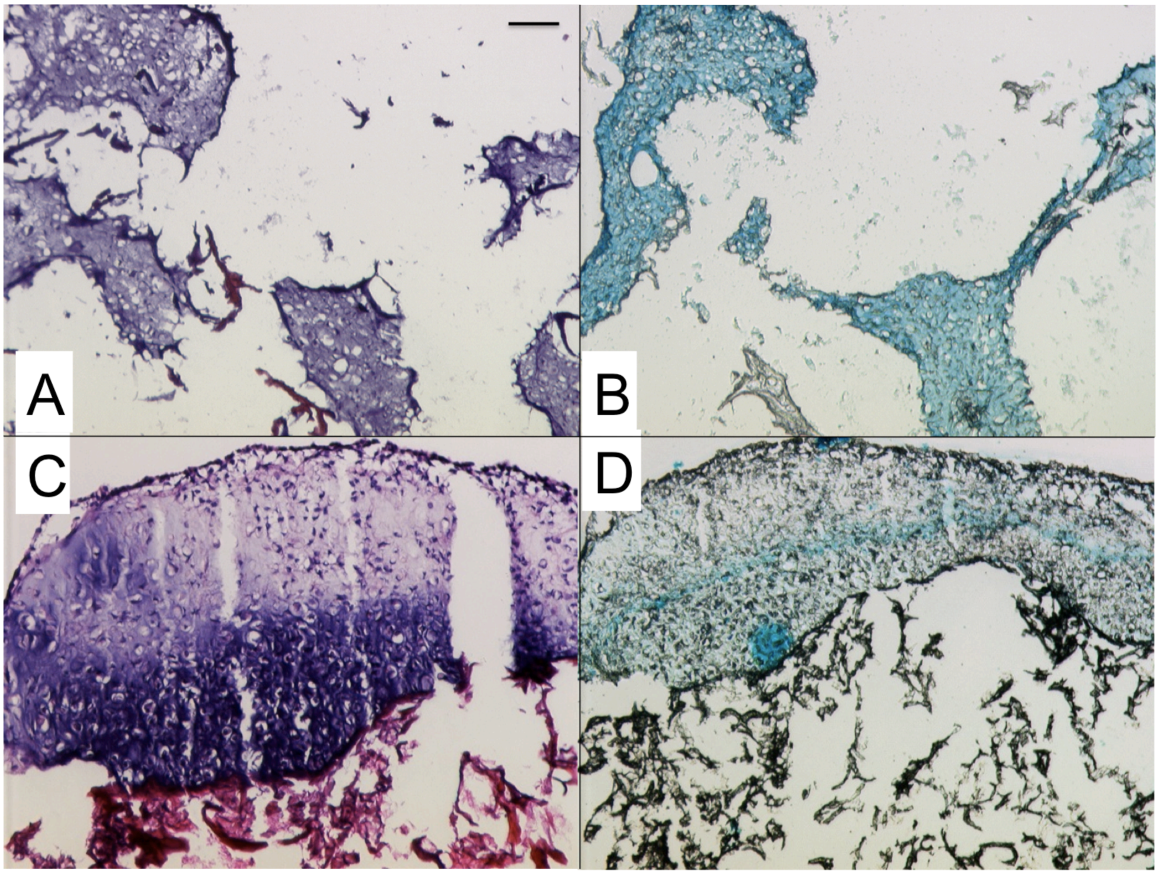

Figure 4.5 Rabbit joint chondrocytes (RJCs) cultured on Ch-Al scaffolds at a density of 500,000 cells per construct. Constructs were collected at weeks 3 (a, b) and 6 (c, d). H&E (a, c) and Alcian blue (b, d) stained slides were imaged at 10x. Scale bar equals 100um.

4.4.5 Chondrogenesis with Fibrin

In an attempt to simulate the in vivo implant site environment where blood plasma proteins, such as fibrinogen and thrombin, will be present, a dilute fibrin solution was added to Ch-Al to improve chondrogenesis. Fibrin has been used widely as a chondrogenic matrix for chondrocytes as well as BMSCs.[18,19] Ch-Al coated with fibrin supported RJC chondrogenesis at week 3 (Figure 4.6a) and homogeneous RJC chondrogenesis at week 6 without any supplemental growth factors (Figure 4.6b). At week 6, the presence of fibrin within chondrocyte-seeded Ch-Al drastically enhanced chondrogenic ECM production, namely collagen type II and proteoglycans seen explicitly with specific staining. These scaffolds showed improved chondrogenesis by RJCS that covered 95% of the volume of the construct, as seen by positive staining with SafraninO for GAGs, Alcian blue for aggrecan, H&E for collagen, and immunohistochemistry for collagen type II. The morphology of generated chondrocyte lacunae matched the morphology typical of native tissue.

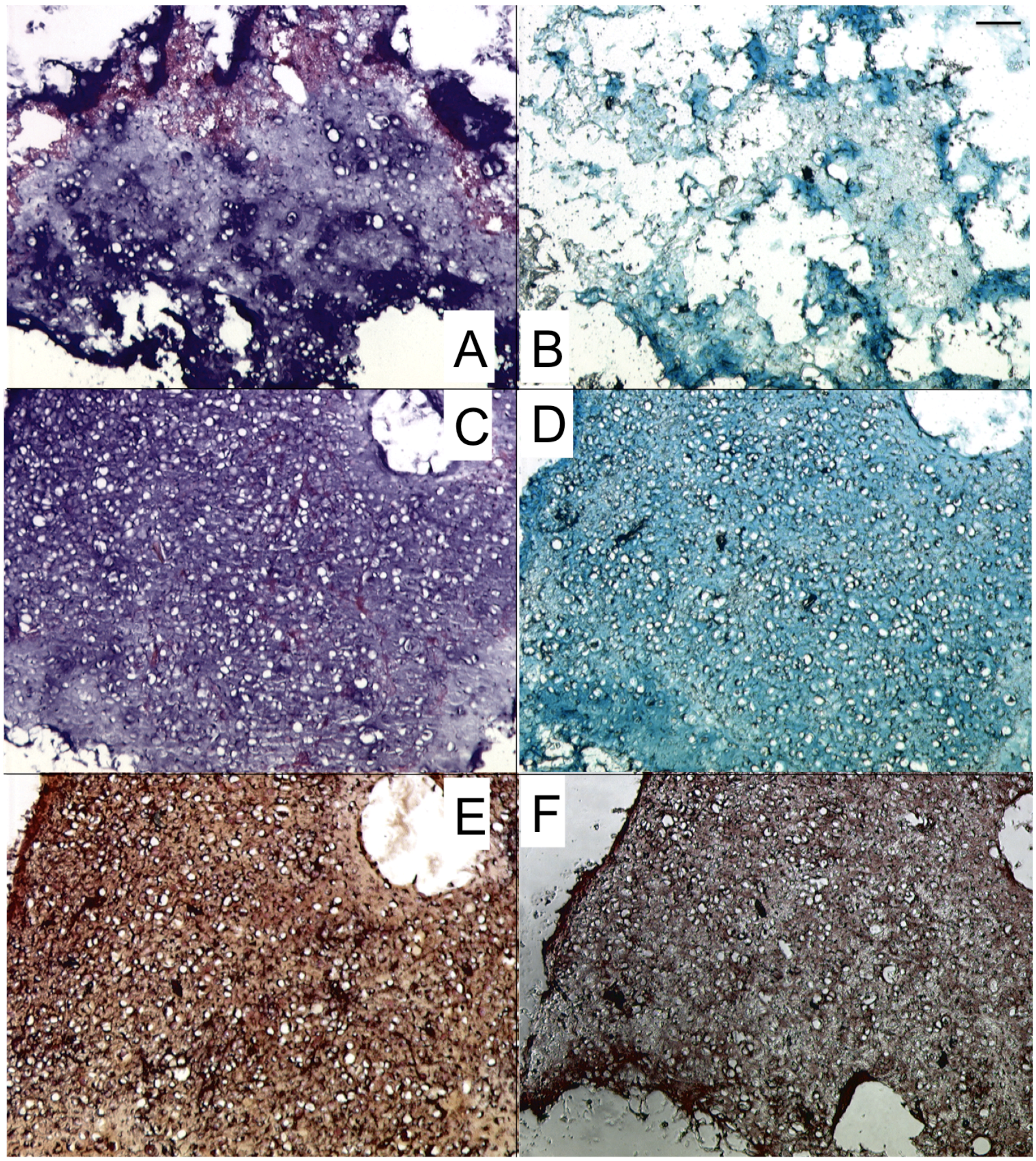

Figure 4.6 RJCs cultured on Ch-Al scaffolds coated with dilute fibrin at a density of 500,000 cells per construct. Constructs were collected at weeks 3 (a, b) and 6 (c-f). H&E (a, c), Alcian blue (b, d), SafraninO (e), and collagen type II immunohistochemistry (f) stained slides were imaged at 10x. Scale bar equals 100um.

4.4.6 Nonspecific Adsorption of Model Proteins

At neutral pH, both negatively-charged BSA and positively-charged histone nonspecifically adsorbed to Ch-Al scaffolds with minimal loss on day 0 (Figure 4.7a). Ch-Al nonspecifically adsorbed BSA and histone with 5% and 1% burst release at 100 ug loading, sustaining 60% and 5% total release for >30 days, respectively (Figure 4.7b). BSA loaded at 1ug also displayed 5% burst release and 60% total release, while BSA loaded at 10mg displayed 30% burst release followed by 80% total release by day 30 (Figure 4.7c).

4.4.7 Nonspecific Adsorption of TGF-β1

Ch-Al nonspecifically adsorbed TGF-β1 with 2% burst release at 100ng loading, sustaining release for >42 days in complete DMEM at 37C (Figure 4.7d). TGF-β1 is positively charged at physiological pH, and thus the release profile more closely matched that of positively-charged model protein histone. TGF-β1 release rate was slightly increased over the histone release profile extrapolated to 42 days, most likely due to the increased temperature conditions and serum in the release medium displacing the TGF-β1.

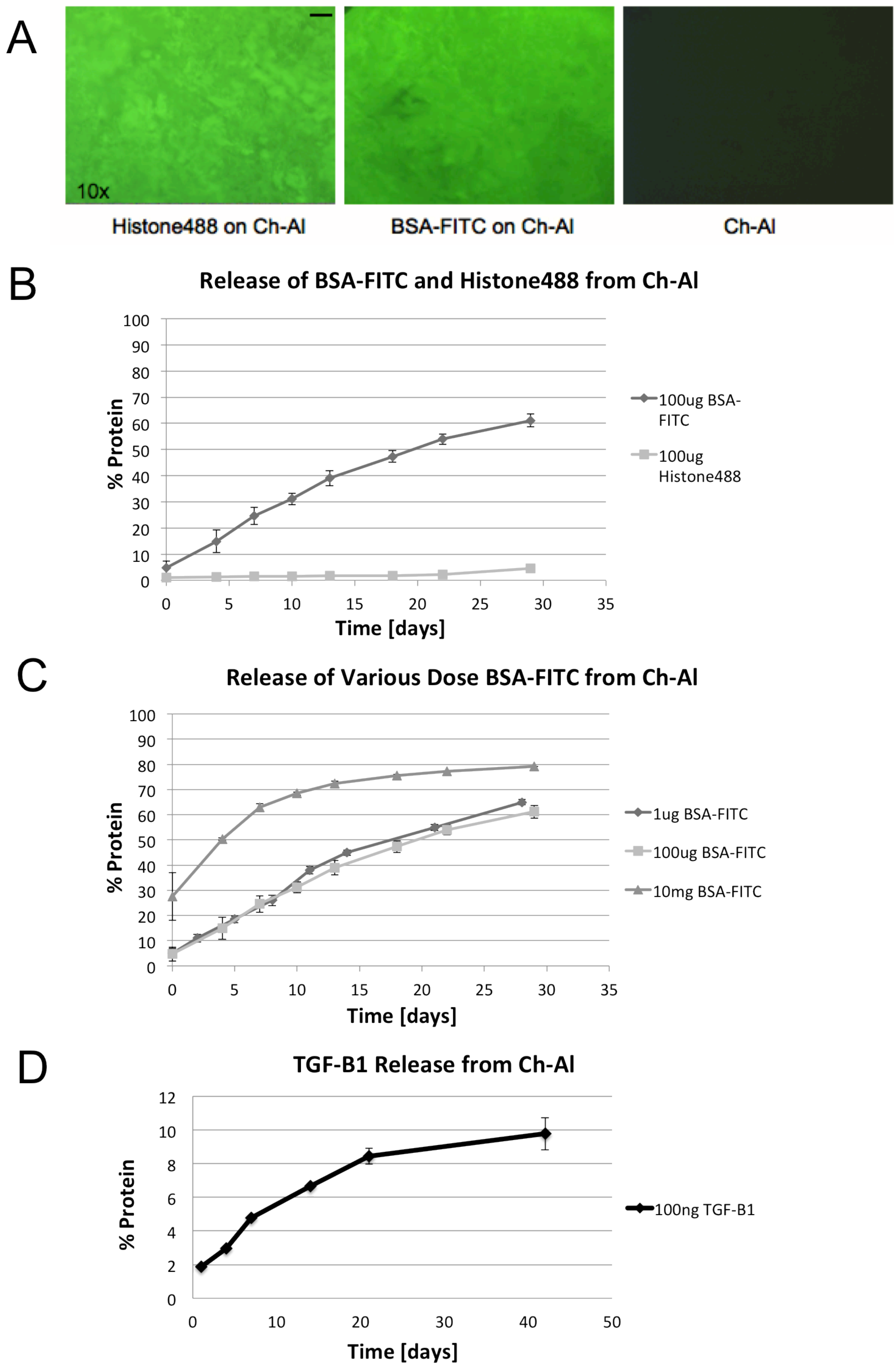
A
10x
Histone488 on Ch-Al
BSA-FITC on Ch-Al
Ch-Al
B
Release of BSA-FITC and Histone488 from Ch-Al
% Protein
Time [days]
100ug BSA-FITC
100ug Histone488
C
Release of Various Dose BSA-FITC from Ch-Al
% Protein
Time [days]
1ug BSA-FITC
100ug BSA-FITC
10mg BSA-FITC
D
TGF-B1 Release from Ch-Al
% Protein
Time [days]
100ng TGF-B1

Figure 4.7 Fluorescent images of 100ug Histone488 or BSA-FITC nonspecifically adsorbed on Ch-Al scaffolds compared to blank Ch-Al (a). Images were taken at 100x. Scale bar equals 100um. Release profiles of 100ug BSA-FITC or Histone488 nonspecifically adsorbed onto Ch-Al scaffolds (b). Release profiles of different doses (1ug, 100ug, 1mg) of BSA-FITC nonspecifically adsorbed onto Ch-Al scaffolds (c). Release profile of 100ng TGF-β1 nonspecifically adsorbed onto Ch-Al scaffolds. TGF-β1 was released in complete DMEM at 37C.

4.4.8 Chondrogenesis with TGF-β1

TGF-β1 nonspecifically adsorbed at 200ng onto Ch-Al promoted homogeneous RJC chondrogenesis at week 3, as illustrated in Figure 4.8. Chondrogenic matrix secretion covered 95% of the construct volume, and this condition of TGF-β1 release resulted in the earliest that a mature lacunae morphology covering nearly the entirety of the scaffold was seen. Chondrogenesis was more homogeneous and occurred significantly earlier than scaffolds cultured without growth factor or scaffolds coated with fibrin. Cartilaginous ECM production was confirmed with aggrecan staining by Alcian blue and collagen staining by H&E.

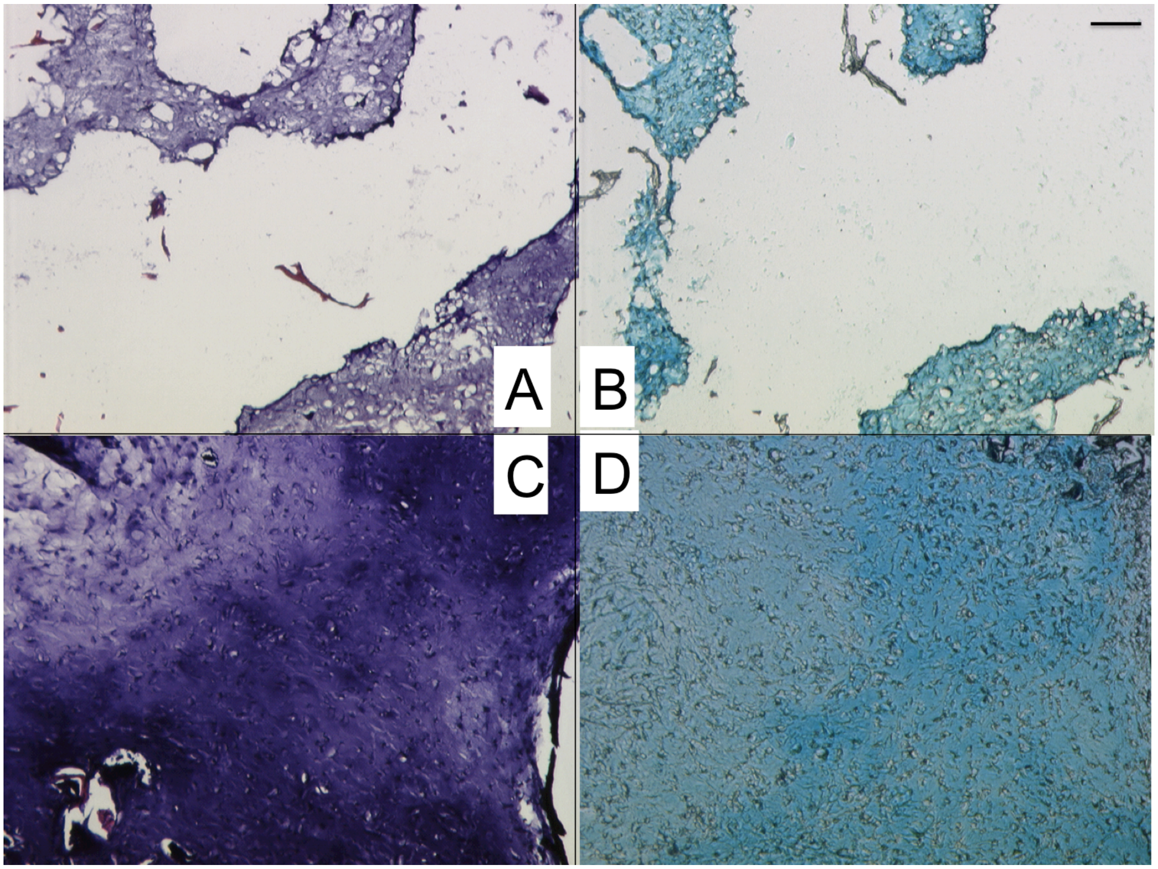

Figure 4.8 RJCs cultured on Ch-Al scaffolds with 200ng TGF-β1 nonspecifically adsorbed at a density of 500,000 cells per construct. Ch-Al without growth factor (a, b) showed less homogeneous cartilage formation than Ch-Al with TGF-β1 (c, d). Constructs were collected at week 3. H&E (a, c) and Alcian blue (b, d) stained slides were imaged at 10x. Scale bar equals 100um.

4.5 Discussion

Ch-Al scaffolds exhibited significant open porosity with interconnected and tortuous pores ranging from 20-200um. Scaffold architectures such as high surface area to polymer mass ratio as well as high surface area to volume ratio allow for tissue ingrowth, uniform cell delivery, and development of high cell density.[20] Pore size affects cell metabolic activities, specifically matrix biosynthesis. Moreover, chondrocyte ingrowth into and chondrocyte survival within the scaffold depend strongly on pore size. Nutrient, waste, oxygen, and enzyme diffusion are regulated by scaffold permeability. High permeability also allows for the evacuation of degradation byproducts.

Permeability is defined as the degree of ease or difficulty for fluid to move in and out of the scaffold, thus influencing the viscoelastic response of the scaffold.[21] Permeability is not synonymous for porosity, although high porosity does typically translate to high permeability and vice versa.[22] Literature shows 1.5% chitosan and 1% alginate elastic moduli to be 1.5 kPa and 1 kPa, respectively.[9,10] Thus, the combination of these two polysaccharides shown in this study improves the mechanical strength over either of the individual polymers, due to the ionic interactions between negatively charged alginate carboxylate groups and some positively charged chitosan amine groups at pH 7.4, based on the two polymers' acid dissociation constants being 3.4-3.7 and 6.3, respectively.[5] Native cartilage elastic modulus ranges from 1-20 MPa[23,24], but this value does not need to be matched in the blank scaffold as the presence of cells and their secreted matrix will increase the elastic modulus over time during healing. The significant amount of strain Ch-Al scaffolds can accommodate, as shown here by resiliency, is likely to assist mechanotransduction and subsequent ECM production. Mechanotransduction has been shown to increase matrix biosynthesis and chondrogenic gene expression, but under specific loads and strains below the threshold for injury (5-10 MPa normal stress range, 300-800% body weight normal load range, ~40% normal strain).[1,2] Ch-Al scaffolds under 40% normal strain, comparable to the maximum physiological in vivo level before injury, rebounded 90% of their original height when compressed while hydrated. However during the healing phase after implantation, it is likely that the joint will not be load bearing, and thus much smaller strains will be experienced initially, upon which Ch-Al scaffolds can recover 100% height. The resiliency Ch-Al can accommodate is likely due to the swollen nature of the polymer chains at pH 7.4, where negatively charged alginate carboxylate groups attract counterions and water molecules along with them, providing resistance to compression that is heavily dependent on water repulsion, as evidenced by the difference in dry and hydrated springback. This mechanism of water imbibement during counterion influx occurs in native cartilage to neutralize negatively charged hyaluronic acid and chondroitin sulfate and accounts for cartilage's compressive resiliency.

The mechanical strength of chitosan-alginate scaffolds can be tailored depending on the formulation of each component. Peak stiffness of ~70 kPa was determined to be in the 1:1 Ch:Al region where ionic interactions between positive chitosan and negative alginate are maximized. Figure 4.4 illustrates how the addition of CS greatly increased scaffold stiffness. In particular, the 2:1 ratio of Ch:Al experienced the most dramatic effects when CS was incorporated during crosslinking. This may be due to an optimal charge ratio occurring at this formulation, where two parts positively charged chitosan is balanced by one part negatively charged alginate and one part negatively charged CS. In other words, the maximum amount of interaction occurs when there is twice as much chitosan as alginate and available positive binding sites remain for CS. Alginate hydrogels, when crosslinked by chelation of Ca^{2+} ions, form an egg-box structure due to the stacking of guluronic acid groups when divalent cations bind to the guluronic acid groups in a highly cooperative manner.[25] When anionic CS is incorporated into the calcium chloride crosslinking process, CS acts as a third polymer strand which will engage in physical entanglements within the polymer network, and there will be more negative charges to create electrostatic repulsion upon scaffold compression. Moreover, CS may also bind to free cationic chitosan amine groups, particularly at the 2:1 Ch:Al ratio, consequently resulting in an increased ionic interactions, and thus a greater elastic modulus.

Even though spreading by mBMSCs was uncommon until 3 weeks of culture, studies actually show that a lack of cellular protrusions may be beneficial for chondrogenesis. How BMSCs interact with their microenvironment plays an important role in their morphogenesis and downstream differentiation commitment. These interactions can be mediated by cell surface receptors, like cadherins and integrins, and ECM components.[26] Round cellular morphology as well as cell aggregation can be indicative of chondrocytic phenotype and chondrogenic behavior such as mesenchymal condensation.[26-28] The round BMSC morphology and immediate cell clustering observed on Ch-Al scaffolds may indicate that Ch-Al serves as a conducive chondrogenic microenvironment, and this may explain the spatially sporadic cartilaginous ECM produced on bare Ch-Al without any growth factors.

Reasons fibrin made such a difference in cartilage ECM secretion could be physical and/or chemical. RJCs were initially resuspended in fibrinogen, followed by the addition of thrombin, before adding the suspension to Ch-Al scaffolds. Chemically, the RGD binding sequences on fibrin may be preferential to the way chondrocytes adhere to chitosan and alginate polysaccharides. Physically, the ability of cells to spread and migrate at earlier time points has been shown to lead to enhanced chondrogenic condensation. Further, the surface tension due to being surrounded by fibrin hydrogel, the increased number of RJC integrins bound to fibrin due to being surrounded by the hydrogel, the smaller pore size needing to be filled with deposited ECM, and the smaller pore size and thus closer contact with nearby cells may all play a role in this dramatic result.

Both positively and negatively charged growth factors adsorbed very well to Ch-Al due to ionic complexation with the charged chitosan and alginate functional groups, specifically positive amine and negative carboxylate groups, respectively. Ch-Al polyelectrolyte complexes have been shown to be able to delivery a variety of drugs and proteins, such as insulin, indomethacin, and hemoglobin.[25,29-35] In this study, however, protein is not encapsulated within the Ch-Al complex, but rather nonspecifically adsorbed to its surface. Because the Ch-Al solution is titrated to pH 7.4, the net charge of the scaffold surface is likely negative due to the acid dissociation constants of chitosan and alginate being 6.3 and 3.4-3.7, respectively.[5] This would explain why positively charged proteins like histone and TGF-β1 released so slowly over the course of many weeks. Comparatively, negatively charged BSA released more quickly, but the release kinetics were still favorable to match the timeline of cartilage tissue healing across various doses. This may be explained by residual free, charged amine groups able to electrostatically bind BSA. Because pH 7.4 is near that of the pKa for chitosan, 6.3, not every amine functional group may be deprotonated, allowing some amine groups to remain protonated and cationic. Also, although BSA has a net negative charge, the charge distribution of the protein is likely not uniform, and some positively charged moieties may be able to bind to the negative surface of Ch-Al.

TGF-β1 is a common chondrogenic growth factor used in cartilage tissue engineering to encourage cellular clustering and cartilaginous ECM deposition, by both chondrocytes and mesenchymal precursors.[26,36] Many studies in multiple model systems have shown that TGF-βs stimulate early chondrocyte differentiation, repress abnormal terminal differentiation leading to osteoarthritis, and are essential for articular cartilage maintenance.[37] TGF-β1 has been shown to initiate and maintain chondrogenesis of BMSCs through the differential chondro-stimulatory activities of p38, extracellular signal-regulated kinase-1 (ERK-1), and c-Jun N-terminal kinase (JNK). This regulation of chondrogenic differentiation by the (mitogen-activated protein) MAP kinases involves the modulation of N-cadherin expression levels. MAP kinases likely control the cell-cell interactions during condensation and the following progression to chondrogenic differentiation, by sequentially up-regulating and down-regulating N-cadherin. TGF-β1-mediated MAP kinase activation also controls Wnt gene expression and Wnt-mediated signaling, which leads to regulation of N-cadherin expression and subsequent cell-adhesion complexes formed during the early steps of BMSC chondrogenesis.[38] Here, improved chondrogenesis on Ch-Al likely occurred at earlier time points due to the pro-chondrogenic effects of TGF-β1, such as its ability to induce N-cadherin-mediated cell-adhesion complexes, condensation, and directed chondrogenic lineage.

4.6 Conclusion

Ch-Al scaffolds have the potential to mimic the native robust properties of articular cartilage, namely because its chemical polysaccharide structure serves as an analog to GAGs, its mechanical stiffness and resistance to compression can be tailored to be as strong as 450 kPa when hydrated, and its springback after compression is extremely resilient and can handle physiological strains. Moreover, Ch-Al scaffolds biologically support a round cellular phenotype and cell aggregation, which can encourage mesenchymal condensation. These chemical, mechanical, and biological properties of Ch-Al explain why chondrogenesis on bare scaffolds occurs at 3 and 6 weeks of chondrocyte culture. To improve this level of chondrogenesis to be more homogeneous, growth factors of various charges and molecular weights can be delivered in a sustained manner from Ch-Al scaffolds via nonspecific adsorption, as shown by enhanced and expedited chondrogenesis when TGF-β1 was loaded onto Ch-Al and cultured for merely 3 weeks.

References

1. Grodzinsky AJ, Levenston ME, Jin M, Frank EH. Cartilage Tissue Remodeling in Response to Mechanical Forces. Annu Rev Biomed Eng 2000;2:691-713.
2. Kerin A, Patwari P, Keuttner K, Cole A, Grodzinsky A. Molecular basis of osteoarthritis: biomechanical aspects. Cell Mol Life Sci 2002;59:27-35.
3. Temenoff JS, Mikos AG. Review: tissue engineering for regeneration of articular cartilage. Biomaterials 2000;21:431-440.
4. Wan Y, Wu H, Wen D. Porous-Conductive Chitosan Scaffolds for Tissue Engineering, 1: Preparation and Characterization. Macromol Biosci 2004;4:882-890.
5. Lawrie G, Keen I, Grondahl L, et al. Interactions between alginate and chitosan biopolymers characterized using FTIR and XPS. Biomacromolecules 2007;8:2533-2541.

6. Li Z, Zhang M, et al. Chitosan-Alginate Hybrid Scaffolds for Bone Tissue Engineering. Biomaterials 2005;26:3919-3928.
7. Li Z, Zhang M. Chitosan-Alginate as Scaffolding Material for Cartilage Tissue Engineering. J Biomed Mater Res 2005;75A:485-493.
8. Drury JL, Mooney DJ. Hydrogels for tissue engineering: scaffold design variables and applications. Biomaterials 2003;24(24):4337-4351.
9. Hoemann CD, Sun J, Buschmann MD, et al. Tissue engineering of cartilage using an injectable and adhesive chitosan-based cell-delivery vehicle. Osteoarthritis and Cartilage 2005;13(4):318-329.
10. Draget KI, et al. Homogeneous alginate gels: A technical approach. Carbohydrate Polymers 1991;14:159-178.
11. Breinan, H. A., T. Minas, M. Spector, et al. Histological evaluation of the course of healing of canine articular cartilage defects treated with cultured autologous chondrocytes. Tissue Eng. 1998;4(1):101-113.
12. Yuan W, Dong H, Zhou Q, et al. pH-controlled construction of chitosan/alginate multilayer film: characterization and application for antibody immobilization. Langmuir 2007;23:13046-13052.
13. Xu Y, Zhan C, Zheng H, et al. Preparation of dual crosslinked alginate-chitosan blend gel beads and in vitro controlled release in oral site-specific drug delivery system. International Journal of Pharmaceuticals 2007;336:329-337.
14. Liao IC, Wan ACA, Leong KW, et al. Controlled release from fibers of polyelectrolyte complexes. Journal of Controlled Release 2005;104:347-358.

15. Zhang Y, Zhang M. Synthesis and characterization of macroporous chitosan/calcium phosphate composite scaffolds for tissue engineering. J Biomed Mater Res 2001;55:304-312.

16. Zhang Y, Zhang M. Calcium phosphate/chitosan composite scaffolds for controlled in vitro antibiotic drug release. J Biomed Mater Res 2002;62:378-386.

17. Cheng JMC. Biomimetic, polymeric transistor-based biosensor technology. University of California, Berkeley, 2009.

18. Ho STB, et al. The influence of fibrin based hydrogels on the chondrogenic differentiation of human bone marrow stromal cells. Biomaterials 2010;31(1):38-47.

19. Hendrickson DA, et al. Chondrocyte-fibrin matrix transplants for resurfacing extensive articular cartilage defects. J Orthop Res 1994;4:485-497.

20. Agrawal CM, Ray RB. Biodegradable polymeric scaffolds for musculoskeletal engineering. J Biomed Mater Res 2001;55:141-150.

21. LeBaron RG, Athanasiou KA. Ex vivo synthesis of articular cartilage. Biomaterials 2000;21:2575-2587.

22. Agrawal CM, McKinney JS, Lanctot D, Athanasiou KA. Effects of fluid flow on the in vitro degradation kinetics of biodegradable scaffolds for tissue engineering. Biomaterials 2000;21:2443-2452.

23. Shepherd DET, Seedhom BB. The 'instantaneous' compressive modulus of human articular cartilage in joints of the lower limb. Rheumatology 1999;38:124-132.

24. Mansour JM. Biomechanics of cartilage. Biomechanical Principles. Part 1. Chapter 5:66-79.

25. George M, Abraham TE. Polyionic hydrocolloids for the intestinal delivery of protein drugs: Alginate and chitosan—a review. Journal of Controlled Release 2006;114(1):1-14.

26. Varghese S, Hwang NS, Elisseeff J, et al. Chondroitin sulfate based niches for chondrogenic differentiation of mesenchymal stem cells. Matrix Biology 2008;27(1):12-21.

27. Sechriest VF, Miao YJ, Suh JK, et al. GAG-augmented polysaccharide hydrogel: A novel biocompatible and biodegradable material to support chondrogenesis. J of Biomedical Materials Research 2000;49(4):534-541.

28. Lee M, Siu RK, Wu BM, et al. Effect of Nell-1 delivery on chondrocyte proliferation and cartilaginous extracellular matrix deposition. Tissue Engineering Part A 2010;16(5):1791-1800.

29. Sezer AD, Akbuga J. Release characteristics of chitosan treated alginate beads: I. Sustained release of a macromolecular drug from chitosan treated alginate beads. J Microencapsul 1999;16:195-203.

30. Hari PR, Chandy T, Sharma CP. Chitosan/calcium alginate beads for oral delivery of insulin. J Appl Polym Sci 1996;59:1795-1801

31. Huguet ML, Groboillot A, Dellacherie E, et al. Hemoglobin encapsulation in chitosan/calcium alginate beads. J Appl Polym Sci 1994;51:1427-1432.

32. Mi FL, Sung HW, Shyu SS. Drug release from chitosan-alginate complex beads reinforced by a naturally occurring crosslinking agent. Carbohydr Polym 2002;48:61-72.

33. Ramadas M, Paul W, Sharma CP, et al. Lipoinsulin encapsulated alginate-chitosan capsules: intestinal delivery in diabetic rats. J Microencapsul 2000;17:405-411.

34. Vandenberg GW, De La Noue J. Evaluation of protein release from chitosan-alginate microcapsules using external or internal gelation. J Microencapsul 2001;18:433-441.

35. Wheatley MA, Chang M, Langer R, et al. Coated alginate microspheres: factors influencing the controlled delivery of macromolecules. J Appl Polym Sci 1991;43:2123-2135.

36. Han F, Adams CS, Hickok NJ, et al. Transforming growth factor-β1 (TGF-β1) regulates ATDC5 chondrogenic differentiation and fibronectin isoform expression. Journal of Cellular Biochemistry 2005;95(4):750-762.

37. Yang X, Chen L, Deng CX, et al. TGF-β/Smad3 signals repress chondrocyte hypertrophic differentiation and are required for maintaining articular cartilage. Journal of Cell Biology 2001;153(1):35-46.

38. Tuli R, Tuli S, Tuan RS, et al. Transforming growth factor-β-mediated chondrogenesis of human mesenchymal progenitor cells involves N-cadherin and mitogen-activated protein kinase and Wnt signaling cross-talk. Journal of Biological Chemistry 2003;278(42):41227-41236.

Chapter 5

5. Macro- and Micro-designed Chitosan-Alginate Scaffold Architecture by Three-Dimensional Printing and Directional Freezing

5.1 Abstract

While many tissue-engineered constructs aimed to treat cartilage defects are being researched, most involve chondrocytes seeded on a scaffold. Various cell-loaded scaffolds in conjunction with delivered growth factors are being studied both *in vitro* and *in vivo*, but the clinical application of these techniques is limited due to the cost of maintaining cellular constructs on the shelf, the potential immune response to allogeneic cell lines, and autologous cell sources requiring biopsy from already diseased, scarce tissue. Thus an acellular scaffold that can induce the endogenous influx of native stem cells from bone marrow holds great promise for cartilage regeneration. The overall aim of this study was to develop an acellular scaffold with designed, channeled architecture to increase wicking and model the native zones of articular cartilage and subchondral bone.

Chitosan-alginate (Ch-Al) scaffolds were fabricated in three-dimensionally printed (3DP) negative molds designed to produce macro-channels, which improved aqueous solution uptake with a maximum wicking volumetric flow rate of 448.9 ± 15.8mm^3/s, blood uptake with a maximum volumetric flow rate of 171.7 ± 25.6mm^3/s, and also cell suspension uptake and distribution within the scaffold, compared to scaffolds without channels. Implementing a positive molding approach, Ch-Al solution was centrifuge infused into synthetic polymer preform shells cast from sugar 3D prints with macro-channels, and the resulting macro-channeled Ch-Al scaffolds also improved cell uptake and distribution over scaffolds without channels. Directional freezing was applied to Ch-Al scaffolds for the first time, resulting in lamellar pores measuring 300um on the long axis and 30um

on the short axis, thus creating micro-channels. Macro- and micro-channeled Ch-Al scaffolds were achieved by directionally freezing Ch-Al solution cast in 3DP negative molds, and the subsequent scaffold architecture enhanced aqueous solution uptake beyond either macro- or micro-channels alone, achieving a maximum volumetric flow rate of $1782.1 \pm 48 mm^3/s$.

By combining 3DP and directional freezing, we can control both the micro- and macro-architecture of the scaffold so that it is more biomimetic and offers different regions corresponding to the zonal architecture of native cartilage and the underlying bone. The precisely controlled micro- and macro-channels also have the potential to assist immediate endogenous bone marrow uptake, model biomimetic osteochondral zones, stimulate chondrogenesis and osteogenesis, and encourage vascularization in the bone region of an osteochondral scaffold.

5.2 Introduction

Cartilage regeneration is a promising field with many attempts at creating a tissue-engineered cartilage substitute. While many tissue-engineered skin and bone products exist and continue to enter the market, there remains no FDA-approved, tissue-engineered solution to regenerate the avascular, aneural cartilage tissue other than autologous chondrocyte implantation (ACI), which is both costly and requires weeks of cell culture time, not to mention healthy cartilage from which to harvest the chondrocytes.[1-3] Many attempts to create biomaterial scaffolds for implantation are being made, yet these technologies still often require seeded cells.[4-6] Major problems persist with the cell-based approaches. Insufficient chondrogenic differentiation cues lead to un- or dedifferentiated cells, hypertrophy, osteogenesis, and senescence.[7] Another obstacle with current cell-based strategies is the uncontrolled loss of transplanted cells. Cell delivery is often inefficient and inhomogeneous, and furthermore stressors can induce chondrogenic apoptosis.[7] Moreover, distributing high densities of cells within scaffolds uniformly has remained a persistent challenge, yet the only Food and Drug

Administration-approved cell seeding method involves using a Petri dish, which has yielded poor uniformity deep within the scaffold.[8] Instead of seeding cells prior to implantation, this project proposes using channels within the scaffold to wick up and distribute endogenous mesenchymal stem cells from the underlying bone marrow.

When considering a material from which to fabricate an osteochondral tissue-engineered scaffold, chitosan-alginate (Ch-Al) was deemed an optimal selection due to its ability to promote both osteogenesis and chondrogenesis, both *in vitro* and *in vivo*.[9,10] Our previous work has also shown that Ch-Al supports chondrogenesis by chondrocytes and serves as a template for sustained growth factor delivery. Lyophilizing Ch-Al creates generates porous, hydrophilic scaffolds with significant mechanical strength, approximately three times the compressive modulus and yield strength of pure chitosan.[9] Ch-Al scaffolds have been used in cartilage tissue engineering particularly because they are naturally occurring polysaccharides similar in chemical structure to articular cartilage extracellular matrix (ECM) glycosaminoglycans (GAGs) like chondroitin sulfate, keratan sulfate, and hyaluronic acid.[11] Further, Ch-Al scaffolds can be prepared at neutral pH, allowing growth factors and drugs to be uniformly incorporated without denaturation.[10]

Three-dimensional printing (3DP) was chosen as the fabrication method to create macro-channeled scaffolds. 3DP of scaffolds for tissue engineering offers many advantages over mold-based fabrication techniques since the resulting scaffolds can be tailored to be patient- and site-specific. Also 3DP scaffolds can have complex geometries, such as undercuts, curvatures, and channels, while maintaining a relatively high throughput fabrication process.[12] However, 3DP can be limited to what materials are compatible with the printer type, and often sugars, starches, and plasters are the only materials used in some powder-based 3D printers. Selective laser sintering (SLS) printers often implement more biologically relevant powders, such as β-tricalcium phosphate (β-TCP)[13,14] or hydroxyapatite particles[15-18], but both these powders and the 3DP itself can be very expensive. Other types of 3D printers like fused deposition modeling (FDM) printers extrude plastics that have low porosity and thus limited cell infiltration.

Two 3DP approaches, indirect and direct, were implemented to fabricate simple and more complex macro-channeled scaffolds, respectively. For negative molding using a 3DP preform (indirect 3DP), FDM was chosen due to its high resolution, ease of use, and strength of high aspect ratio parts. Specifically, we hoped to produce Ch-Al scaffolds with long, uniaxial channels using FDM printed negative molds. For positive molding using a 3DP preform (direct 3DP), powder-based 3DP was selected due to its high resolution, fast printing time, use of cost-effective sugar as a preform material, and the ability to infuse in any polymer of choice into the sugar print. More explicitly, we hoped to fabricate Ch-Al scaffolds with complex, tri-directional channels from sugar preforms using a poly(L-lactic acid) (PLLA) coating to protect the sugar from dissolving in the aqueous environment of the Ch-Al solution. This positive molding method would allow the fabrication of any aqueous-based polymer scaffold by centrifuge infusion into the PLLA preform, followed by freeze-drying, thus creating a porous, channeled scaffold based on a 3DP design.

To date, none of the present tissue-engineered cartilage replacement techniques have generated cartilage tissue that meets the functional demands of an *in vivo* environment.[19] The cartilage generated within tissue engineered implants—if there is proper cartilage regeneration and not fibrocartilage production—often lacks the zonal organization that gives native cartilage its unique structural and functional properties.[19] No clinical trials have been preformed with zonally engineering cartilage, and several of the most common approaches for regeneration, such as ACI, matrix-induced ACI (MACI), and microfracture, result in tissue that lacks zonal organization, as seen by 1 and 2 year follow up investigations.[19] A few research studies are moving toward a more zonal architecture, however, such as a 3DP osteochondral scaffold with two zones of different pore size and preferential binding of chondrocytes to the top cartilage zone during seeding.[20] A collagen gradient hydrogel that recruits mesenchymal stem cells to the center of the construct using haptotaxis has been implanted in the patellar groove in a rabbit knee model.[21] Other strategies of creating two separate cartilage and bone layers, joined after fabrication by suturing, gluing, press fitting, or external fixation have been limited by inferior integration between cartilage and bone tissues, resulting in eventual separation.[22-25] Single integrated, biphasic or multi-layered osteochondral scaffolds have been engineered, but they fail to capture the micro-scale features and properties of the cartilage zonal microenvironment.[26-30]

Directional freezing of scaffolds prior to freeze-drying has been applied to a few different materials for a variety of applications, mostly to increase strength beyond simply porous scaffolds.[31,32] By placing the scaffold solution in a mold on a cold surface, or cold finger, and controlling the rate (in C/min) at which that solution freezes using a thermocouple, heater and liquid nitrogen cooling source, the direction of ice crystal growth in the freezing scaffold solution can be forced to be anisotropic.[31] This directional freezing results in lamellar pores with an extremely high aspect ratio, and the size and shape of the pores as well as the compressive strength can be altered by altering the exact freezing rate.[32] Another outcome of directional freezing is a complex microstructure where the majority of the scaffold has lamellar pores, yet there is a seamless transition to a cellular or spherical pore zone near the base of the freezing front and thus the ice crystal growth direction.[32] Here we proposed applying directional freezing to Ch-Al scaffolds to capture the zonal architecture of osteochondral tissue. Moreover, the micro-channels or lamellar pores resulting from directional freezing were hypothesized to further increase wicking beyond 3DP macro-channels alone.

We aim to develop an acellular scaffold implant with biomimetically designed micro- and macroarchitecture that promotes cartilage regeneration. This scaffold would be implanted into the joint during resurfacing and would facilitate the instant uptake of underlying bone marrow and residing mesenchymal stem cells. Our system would address the many challenges facing cartilage tissue engineers today, such as cell loss upon delivery and lack of zonal architecture, and has the potential to become an off-the-shelf solution for cartilage regeneration.

5.3 Materials and Methods

5.3.1 Materials

Mouse bone marrow stromal cells (mBMSCs, C57BL/6 mouse mesenchymal stem cells from Bone Marrow, Cat # S1502-100), antibiotic-antimycotic (ABAM, Cat # 15240-062), and Vybrant DiI Cell-Labeling Solution (Cat # V22885) were obtained from Life Technologies (Grand Island, NY).

Chitosan (practical grade, Cat # 41763), alginate from brown algae (Cat # A7003), calcium chloride ($CaCl_2$-$2H_2O$, Cat # 12022), 50% sodium hydroxide in water (Cat # 415413), α – Lactose monohydrate (Cat # L3625), and poly(acrylic acid) (PAA) (Cat # 535931) were obtained from Sigma-Aldrich (St. Louis, MO).

Acetic acid (glacial, Cat # A38 SI-212), chloroform (Cat # C298-4), optimal cutting temperature Compound (OCT, Tissue-Tek, Cat # 4583), Dulbecco's Modification of Eagle's Medium w/ 4.5 g/L glucose, L-glutamine & sodium pyruvate (DMEM 1X, Cellgro, Cat # 10-013-CV), and fetal bovine serum (FBS, Cat # MT35015CV) were obtained from Fisher Scientific (Waltham, MA).

Pure cane granulated white sugar was obtained from C&H (Crockett, CA), and Zb7 clear binder solution (Part # 05392) was obtained from Z Corporation (Rock Hill, SC). Poly(L-lactic acid) (PLLA, Cat # B6002-2) was obtained from Lactel (Birmingham, AL).

5.3.2 Scaffold Fabrication using Negative Molding

Negative molds were printed out of acrylonitrile butadiene styrene (ABS) plus plastic using a uPrint (Stratasys, Eden Prairie, MN) 3DP with 256um vertical step size. Cylindrical mold inner height was 20mm with an additional 2mm base, inner diameter was 10mm, and outer diameter was 14mm. For fabricating channeled scaffolds, cylindrical molds contained seven 1mm vertical rods running along the z axis, attached at the base. All six rods were spaced radially 3mm apart from the center rod, which was located in the exact center of the mold cross sectional area.

Adapted and modified from Li et al[9,10], Ch-Al scaffolds were fabricated with 2% w/v chitosan dissolved in 2% v/v acetic acid in dH_2O and 2% w/v alginate dissolved in dH_2O, mixed at 1:1 ratio. The Ch-Al solution was ultrasonically homogenized for 1min, titrated to pH 7.4 with 50% sodium hydroxide, ultrasonically homogenized for 5min, poured into 3DP negative molds, and frozen at -80C overnight. The resulting frozen scaffolds were lyophilized overnight, crosslinked for 15min with 1% w/v $CaCl_2$, washed three times with dH_2O, and lyophilized overnight. Ch-Al scaffolds were imaged using a Nova Nano scanning electron microscope (SEM) 230 (FEI, Hillsboro, OR), with 10keV accelerating voltage and 3.0 spot size.

5.3.3 Scaffold Fabrication using Positive Molding

Positive molds were printed out of a 1:1 sugar (50-106um sieved):lactose mixture using a Z402 (Z Corporation, Rock Hill, SC) 3DP with 178um vertical step size. Binder used to fuse the powder particles together was formulated from a 2:1 ratio of Zb®7 clear binder solution:poly(acrylic acid) (PAA) pH 5. Cylindrical mold height was 20mm, and diameter was 20mm. Cylindrical molds contained 3mm channels running along the x, y, and z axes. Z axis channels were spaced radially 6mm apart from the center channel, which was located in the exact center of the mold cross sectional area. X and y axis channels were spaced horizontally and vertically 6mm apart, creating a 3x3 array of channels on four faces around the cylinder.

Positive sugar-lactose molds were dip coated with 7.5 w/v% poly(L-lactic acid) (PLLA) in chloforom, allowed to dry overnight, and then soaked in water to leach out the sugar-lactose. Resulting PLLA preforms were laser cut (Versa Laser, Punchbowl, NSW, Australia) on all faces to produce 300um holes that allowed for Ch-Al solution, prepared as described above, infusion by centrifugation at 2500rpm for 10min. Once Ch-Al solution was infused into the PLLA preform, preforms were frozen at -80C overnight, lyophilized overnight, crosslinked for 15min with 1% w/v $CaCl_2$, washed three times with dH_2O, and lyophilized overnight. Next, preforms were soaked in chloroform overnight to dissolve the PLLA, followed by washing three times with dH_2O and final lyophilization to obtain Ch-Al scaffolds. Ch-Al scaffolds were imaged using a Nova Nano SEM 230, with low vacuum detector, 10keV accelerating voltage, and 3.0 spot size.

5.3.4 Scaffold Fabrication with Directional Freezing

Ch-Al solution, prepared as described above, was poured into PTFE cylindrical molds with 20mm inner diameter, 40mm height, and a copper base. The Ch-Al solution was directionally frozen by placing the copper base of the mold directly onto a copper cold finger that extended downward into a container of liquid nitrogen. The temperature of the freezing front was controlled using liquid nitrogen and a ring heater. A 5C/min cooling rate was selected based on previous studies of porosity and strength,[32] and the Ch-Al solution was cooled to -100C. Frozen Ch-Al was lyophilized for 48hrs, crosslinked for 15min with 1% w/v $CaCl_2$, washed three times with dH_2O, and lyophilized overnight. For SEM, scaffolds were flash frozen using liquid nitrogen and cut in half either along the z axis, parallel to the freezing front, or across the z axis, perpendicular to the freezing front. Ch-Al scaffolds were imaged using a Nova Nano SEM 230, with low vacuum detector, 15keV accelerating voltage, and 3.0 spot size.

5.3.5 Scaffold Fabrication with Directional Freezing using Negative Molding

Ch-Al solution, prepared as described above, was poured into ABS plus cylindrical 3DP negative molds printed by the uPrint, which were inserted into PTFE cylindrical molds, which were then placed on the copper cold fingers. 3DP negative mold height was 20mm, inner diameter was 16mm, and outer diameter was 19.6mm. To create channeled scaffolds, 3DP lids with seven 1mm vertical rods running along the z axis, attached at the base of lid, were placed on top of the cylindrical molds so the rods protruded into the scaffold solution. All six rods were spaced radially 3mm apart from the center rod, which was located in the exact center of the mold cross sectional area. Once the molds were filled and lids were put on to introduce channels if necessary, the Ch-Al solution was directionally frozen at 5C/min cooling rate. Frozen Ch-Al was lyophilized for 48hrs, crosslinked for 15min with 1% w/v $CaCl_2$, washed three times with dH_2O, and lyophilized overnight.

5.3.6 Fluid Uptake

Scaffolds with and without channels fabricated using negative 3DP molds were submersed in a 500ul pool of 0.1% w/v SafraninO in dH_2O or C57BL/6 mouse blood, with the meniscus measuring 1mm, so only 1mm of the scaffold bottom was initially submerged. SafraninO was used as a stain to visualize fluid uptake and did not increase viscosity beyond that of water alone. Directionally frozen scaffolds with and without channels fabricated using negative 3DP molds, which had greater volume, were submersed in a 2ml pool of 0.1% w/v SafraninO in dH_2O or C57BL/6 mouse blood, with the meniscus measuring 1mm. Directionally frozen scaffolds were inverted before submersion into fluid. The time for fluid to wick 50% of the scaffold height, which was approximately the maximum wicking observed, and 100% of the scaffold height was measured. Volumetric flow rate and wicking velocity were calculated at these two heights.

5.3.7 Cell Suspension Uptake

Scaffolds with and without channels fabricated using negative 3DP molds were submersed in a 500ul pool of DMEM with 10% FBS and 1% ABAM containing $5x10^5$ mouse bone marrow stromal cells (mBMSCs) fluorescently labeled with Vybrant DiI, with the meniscus measuring 1mm. Scaffolds with channels fabricated using positive 3DP molds, which had greater volume, were submersed in a 2ml pool of $2x10^6$ fluorescently labeled mBMSCs, with the meniscus measuring 1mm. After cell suspension uptake, scaffolds were fixed, embedded in OCT, and sectioned for viewing by fluorescent microscopy.

5.4 Results

5.4.1 Macro-channels by 3D Printed Negative Molds

Ch-Al scaffolds were cast in 3DP negative molds to be solid cylinders or have 1mm macro-channels (Figure 5.1). Figure 5.1a shows the computer aided design (CAD) model for the 3DP negative mold with rods and the resulting channeled Ch-Al scaffold. SEM images of channeled Ch-Al illustrated ~1mm diameter macro-channels and overall high porosity with ~100um pores in the internal region of the scaffold, as seen by taking the scaffold cross section (Figure 5.1b and 5.1c). The top and bottom surfaces of scaffolds appeared as a denser fibrous mat where scaffold struts ran perpendicular to the z axis (Figure 5.1d and 5.1e). This was most likely due to surface tension effects during freezing.

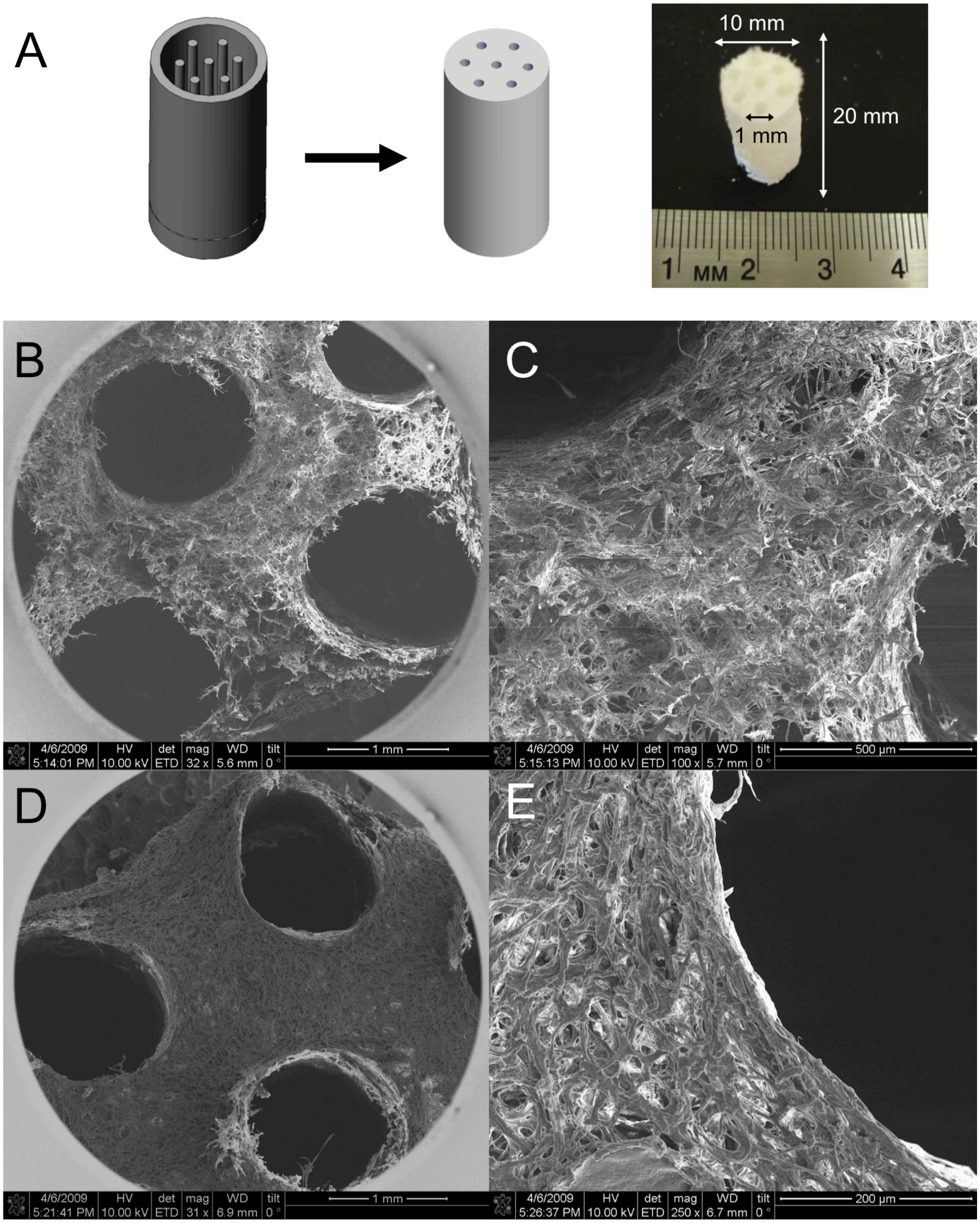

Figure 5.1 Computer aided design (CAD) model of three-dimensionally printed (3DP) negative mold and resulting channeled hypothetical scaffold (left) and actual chitosan-alginate (Ch-Al) scaffold (right) (a). Scanning electron microscope (SEM) images of a cross section of channeled Ch-Al at low (b) and high magnifications (c). SEM images of the top surface of channeled Ch-Al at low (d) and high magnifications (e). Low magnification reveals 1mm channels, as designed, and high magnification reveals 100um pores in the cross section.

5.4.2 Macro-channels by 3D Printed Positive Molds

In order to create more complex geometries beyond the capabilities of negative molding, Ch-Al scaffolds were fabricated from 3DP preforms in a positive molding process using centrifuge infusion, as shown in Figure 5.2a. 3DP sugar-lactose preforms with tri-directional 3mm macro-channels were dip coated in PLLA to preserve the architecture of the preform while allowing for aqueous-based polymer infusion. The sugar-lactose was leached away in water, leaving open space for infusion of Ch-Al. PLLA preforms were laser cut with 300um holes so that Ch-Al could successfully infuse into the preform during centrifugation (Figure 5.2b-d). Without these laser cut holes, PLLA was not inherently porous enough to allow any Ch-Al to penetrate the outer shell. Frozen, lyophilized, and crosslinked Ch-Al-PLLA was prepared as any normal Ch-Al scaffold, except as a final processing step, PLLA had to be dissolved away in chloroform to reveal the final Ch-Al scaffold. Ch-Al scaffolds resulting from this 3DP positive molding process maintained the complex macro-channeled shape of the original CAD model.

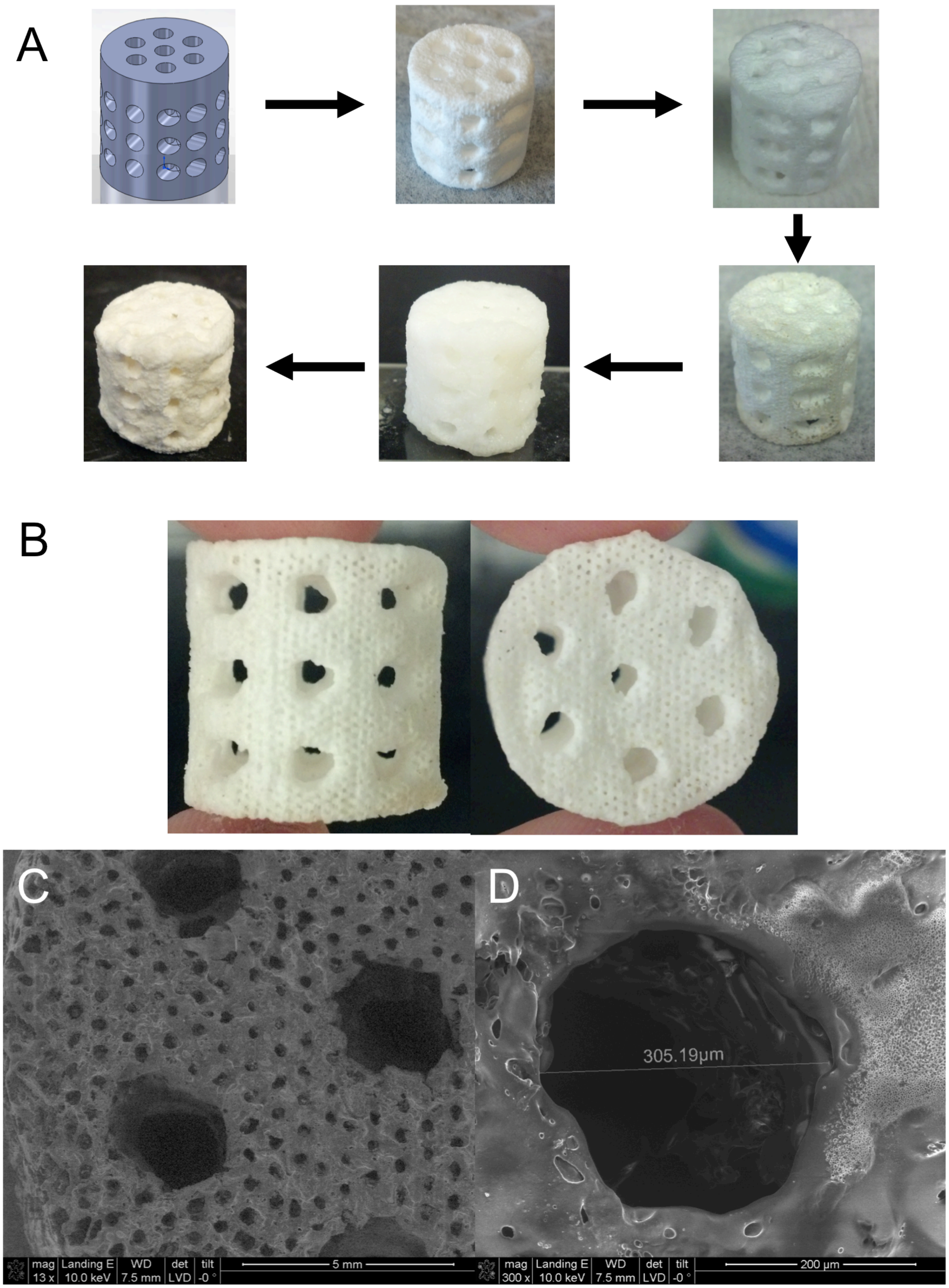

Figure 5.2 3DP positive molding process using centrifuge infusion, starting from CAD model, followed by 3DP of sugar-lactose preform, leached PLLA preform, laser cut PLLA preform, Ch-Al centrifuge infused preform, and final Ch-Al scaffold (a). Gross images of laser cut PLLA preform (b). SEM images of laser cut PLLA preform at low (c) and high magnifications (d). Low

magnification reveals 3mm channels, as designed, and high magnification reveals 300um laser cut holes.

5.4.3 Aqueous Solution Uptake by Macro-Channels

Ch-Al scaffolds created using 3DP negative molds with or without 1mm macro-channels were submersed in 0.1% SafraninO aqueous solution. Only the bottom 1mm of the scaffold was submerged, and the remaining height of the scaffold wicked the aqueous solution very quickly. Macro-channels improved volumetric flow rate to 50% height from 300mm^3/s to 450mm^3/s compared to scaffolds without channels, as shown in Figure 5.3a. Once normalized by cross sectional area with or without channels, the wicking velocity was 10mm/s for macro-channeled scaffolds and only 6mm/s for scaffolds without channels (Figure 5.3b). Both the volumetric flow rate and velocity started to plateau as fluid wicked beyond the 50% height mark, but the loss in speed was not dramatic.

A

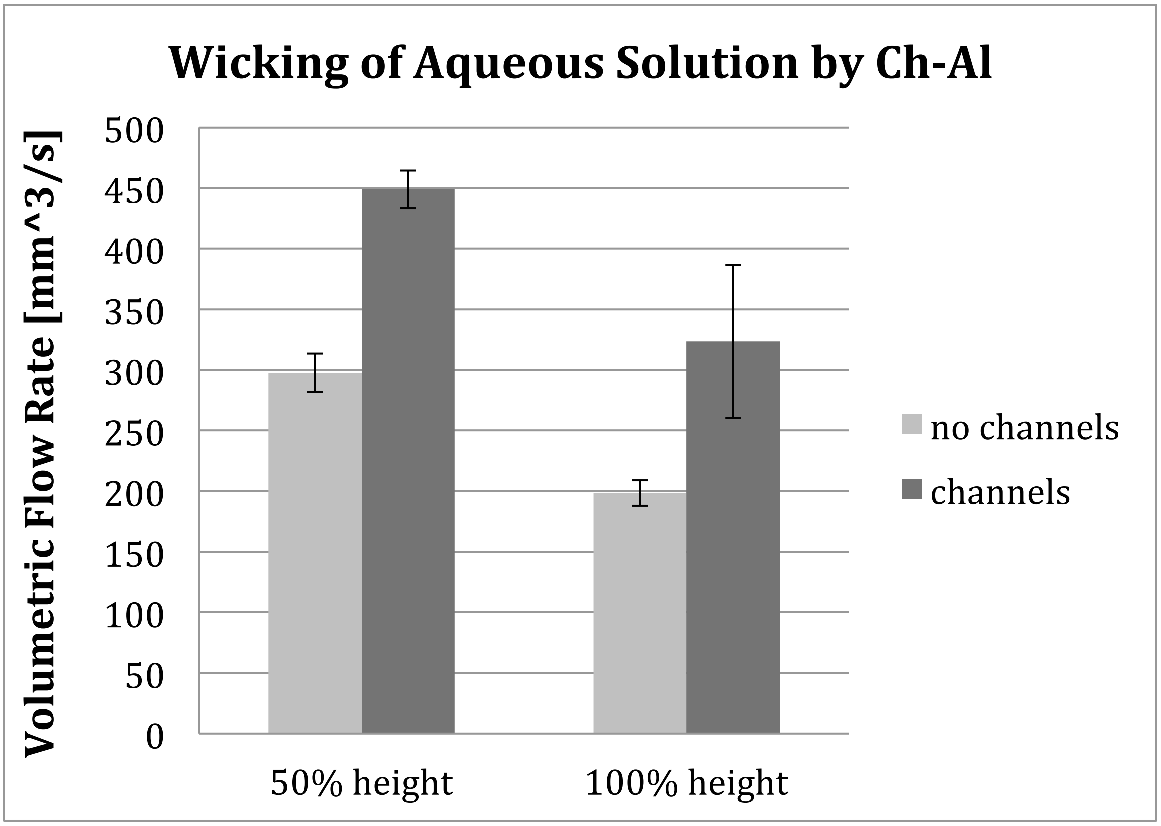
Wicking of Aqueous Solution by Ch-Al
Volumetric Flow Rate [mm^3/s]
500
450
400
350
300
250
200
150
100
50
0
50% height
100% height
no channels
channels

B

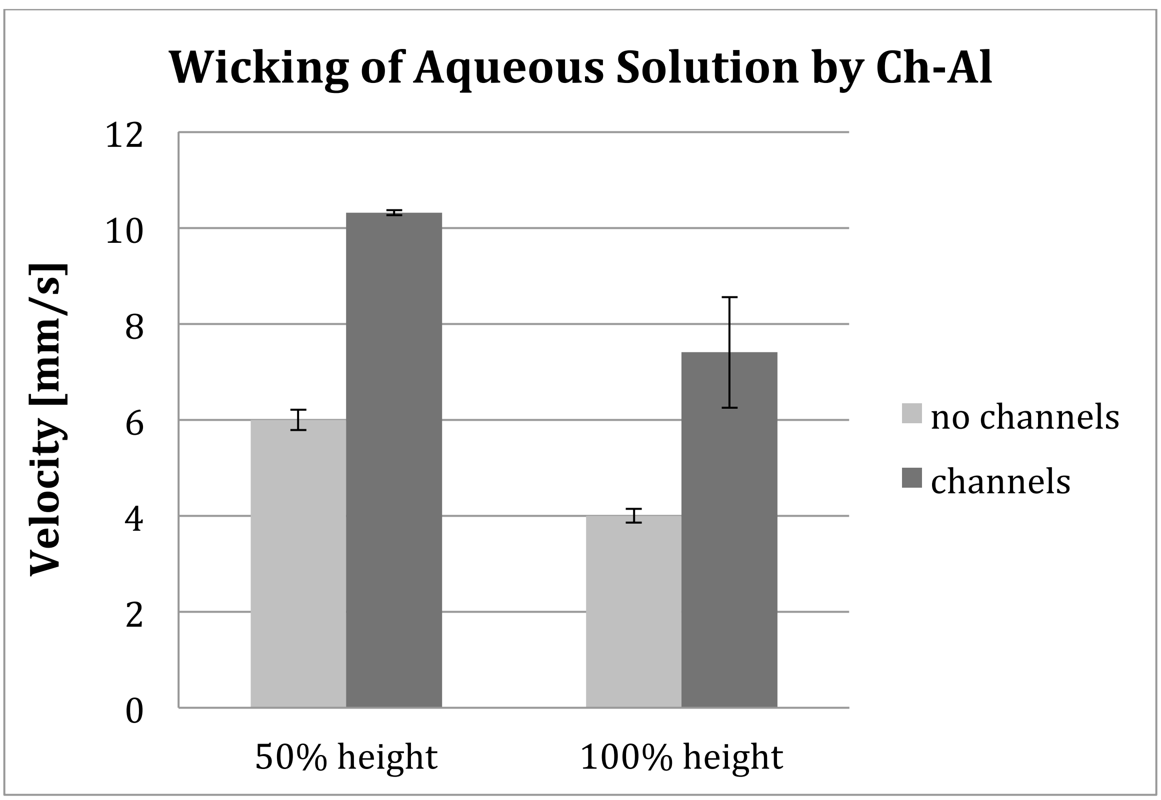
Wicking of Aqueous Solution by Ch-Al
Velocity [mm/s]
12
10
8
6
4
2
0
50% height
100% height
no channels
channels

Figure 5.3 Aqueous solution uptake by Ch-Al made from 3DP negative molds. Scaffolds with or without macro-channels wicked a 0.1% SafraninO aqueous solution. The time to wick 50% and 100% height was measured, and volumetric flow rate (a) and velocity were calculated (b).

5.4.4 Blood Uptake by Macro-Channels

Ch-Al scaffolds created using 3DP negative molds with or without 1mm macro-channels were submersed in blood from C57BL/6 mice. Only the bottom 1mm of the scaffold was submerged, and the remaining height of the scaffold wicked blood very quickly, but not as quickly as the purely aqueous solution, due to viscosity differences. Macro-channels improved volumetric flow rate to 50% height from $8mm^3/s$ to $170mm^3/s$ compared to scaffolds without channels, as shown in Figure 5.4a. Once normalized by cross sectional area with or without channels, the wicking velocity was 4mm/s for macro-channeled scaffolds and only 0.19mm/s for scaffolds without channels (Figure 5.4b). For macro-channeled scaffolds, both the volumetric flow rate and velocity started to plateau as blood wicked beyond the 50% height mark, but the loss in speed was not extreme, similar to what was seen in the aqueous solution wicking. However, due to the high viscosity of blood compared to that of water, scaffolds without any channels showed very poor wicking from the start, and in all cases did not even wick the full 100% height, indicating that this system captured a condition in which macro-channels drastically improve blood wicking. In fact, without channels, Ch-Al scaffolds barely wicked blood beyond 50% height.

A

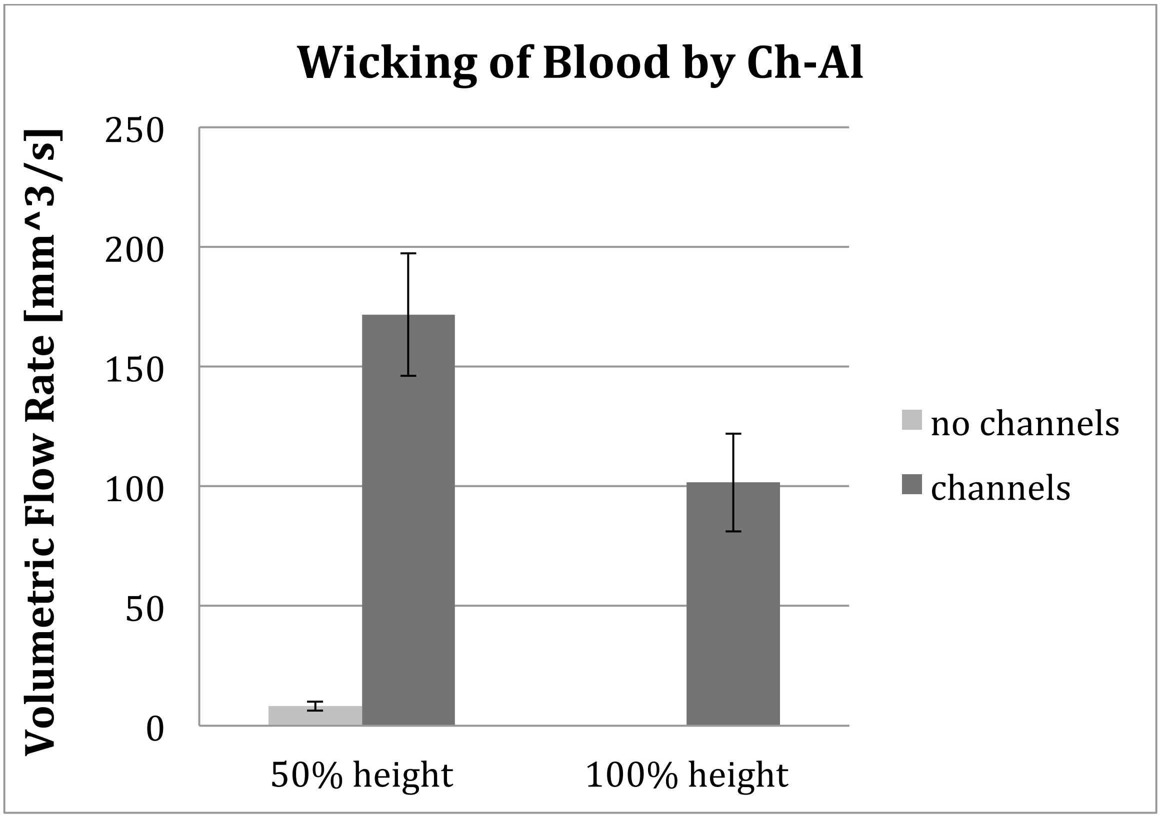

Wicking of Blood by Ch-Al
Volumetric Flow Rate [mm^3/s]
250
200
150
100
50
0
50% height
100% height
no channels
channels

B

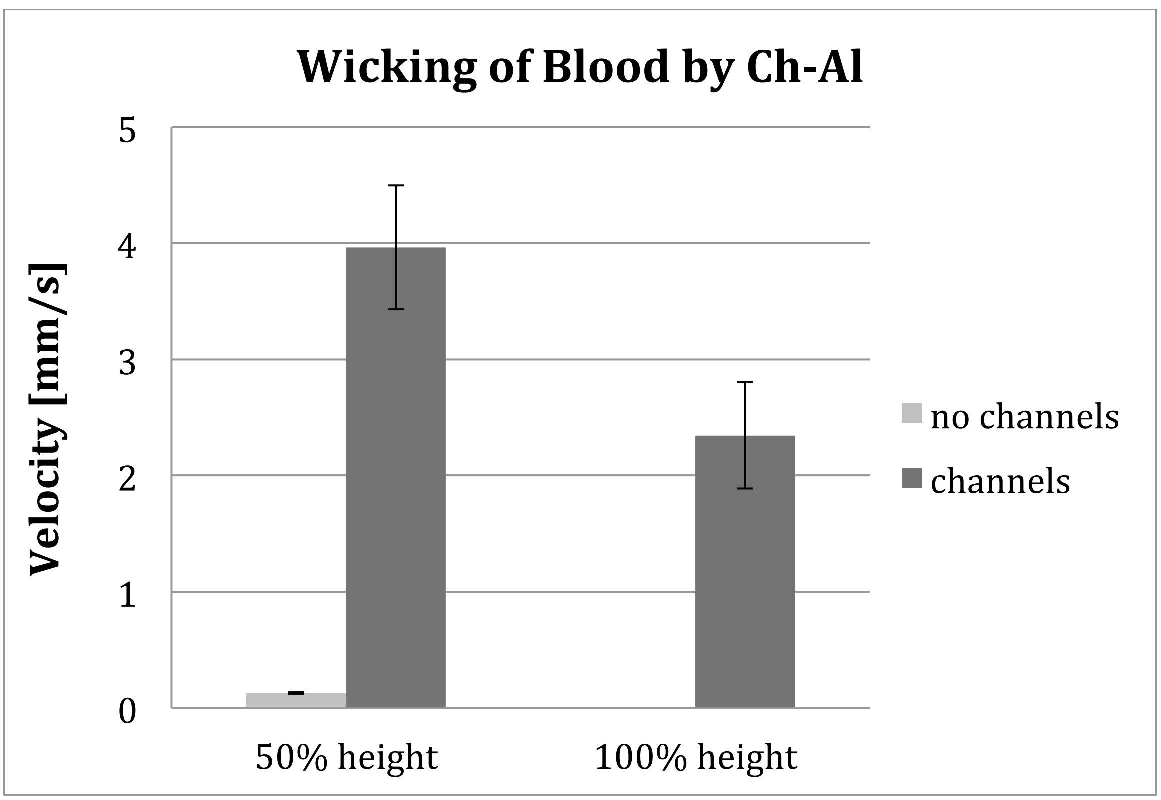

Wicking of Blood by Ch-Al
Velocity [mm/s]
5
4
3
2
1
0
50% height
100% height
no channels
channels

Figure 5.4 Blood uptake by Ch-Al made from 3DP negative molds. Scaffolds with or without macro-channels wicked C57BL/6 mouse blood. The time to wick 50% and 100% height was measured, and volumetric flow rate (a) and velocity were calculated (b).

5.4.5 Cell Suspension Uptake and Distribution by Macro-Channels

Macro-channels also facilitate cell uptake, as seen in *in vitro* studies where 3DP negatively molded Ch-Al scaffolds with 20mm height and 1mm macro-channels wicked a fluorescently labeled mBMSC suspension within 2.5s, consistent with wicking velocities seen with purely aqueous solutions (Figure 5.5a). Cell suspension uptake was also observed in 3DP positively molded Ch-Al scaffolds, as shown in Figure 5.5b. Thus, the centrifuge infusion processing steps did not hinder the hydrophilicity of Ch-Al. Sectioning showed that the cells were distributed throughout the entire height and diameter of the scaffolds, not just around the channel edges or at the scaffold bottom. In scaffolds without any macro-channels, cells remained in the bottom ¼ of the scaffold (data not shown), demonstrating that channels are required to deliver cells beyond a certain height in order to overcome filtering effects.

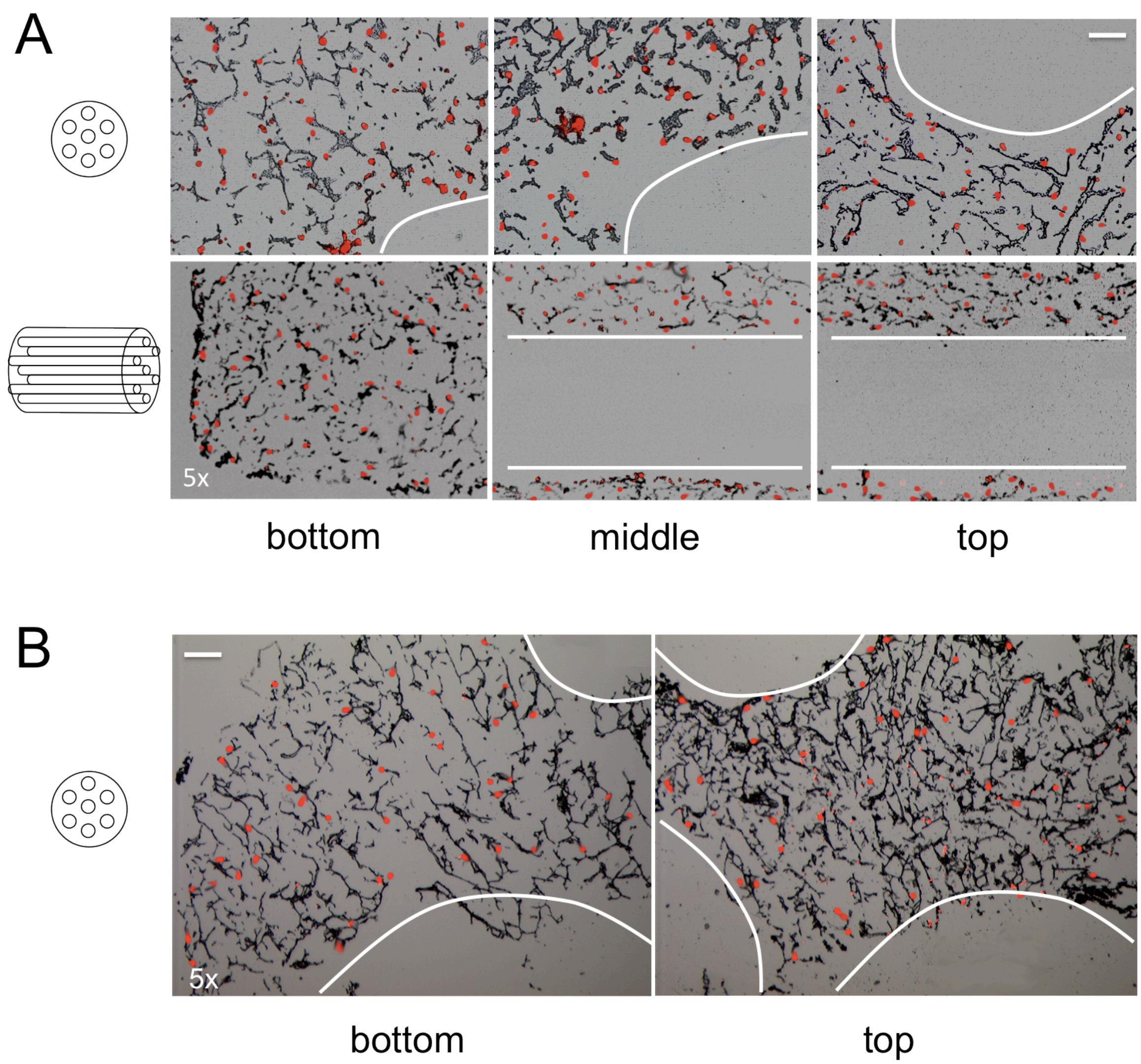

Figure 5.5 Cell suspension uptake by Ch-Al made from 3DP negative (a) or positive molds (b). Scaffolds with or without macro-channels wicked $1x10^6$ mBMSCs/mL cell suspension, where the cells were fluorescently labeled red with Vybrant DiI. Cross sections both perpendicular and parallel to the z axis are shown in (a), while only cross sections perpendicular to the z axis are shown in (b). Channels in (a) are 1mm diameter, while channels in (b) are 3mm diameter, as designed. Images shown are merged red fluorescence on top of bright field to show the scaffold structure. Magnification is 5x. Scale bar equals 250um.

5.4.6 Micro-Channels by Directional Freezing

Directional freezing at 5C/min was applied to Ch-Al scaffolds, and scaffolds with lamellar pores, or micro-channels, measuring 300um on the long axis and 50um on the short axis were achieved (Figure 5.6). Cross sectioning of both parallel and perpendicular (to the freezing front) planes of the scaffolds followed by SEM imaging yielded lamellar pores seen from the parallel cut (Figure 5.6a) and cellular pores seen from the perpendicular cut (Figure 5.6b), indicating successful directional freezing. In addition to the lamellar pore region, there was also a zone of 100um cellular pores at the bottom 500um of the scaffolds, corresponding to the region of the scaffold closest to the cold finger, as expected. Moreover, the bottom 100um of scaffolds exhibited a denser fibrous morphology, as seen with traditionally cast and frozen scaffolds, where scaffold struts ran perpendicular to the z axis, likely due to surface tension effects.

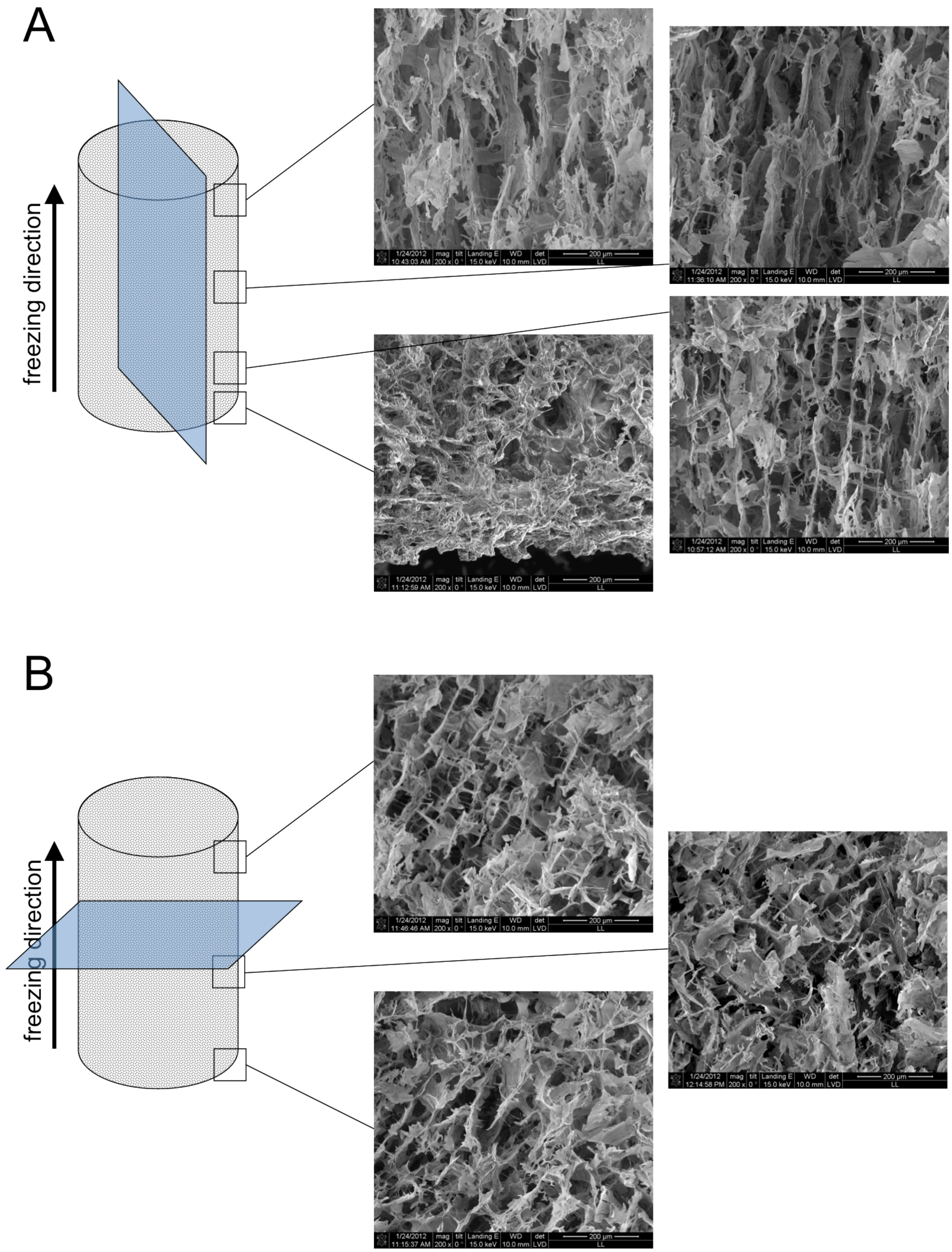

Figure 5.6 Directionally frozen Ch-Al scaffolds, cross sectioned parallel to the z axis (a) or perpendicular to the z axis (b). SEM images reveal a lamellar zone with 300um long axis and 50um short axis columnar pores and a cellular zone at the bottom 500um with 100um spherical pores (a). Ch-Al scaffolds were directionally frozen with a cooling rate of 5C/min down to -100C.

5.4.7 Aqueous Solution Uptake by Macro- and Micro-Channels

Ch-Al scaffolds were fabricated to have macro- and micro-channels by casting Ch-Al solution in a 3DP negative mold which was fitted on the cold finger during directional freezing. Scaffolds with or without 1mm macro-channels, with or without directionally frozen micro-channels, were submersed in 0.1% SafraninO aqueous solution. Directionally frozen scaffolds were inverted before submersion into fluid, so that the lamellar pore zone at the scaffold top was placed directly into the 1mm fluid meniscus, allowing the remaining height of the scaffold to wick the aqueous solution extremely quickly via micro-channels. Similar to before in Figure 5.3a, macro-channels improved volumetric flow rate to 50% height from 300mm^3/s to 450mm^3/s compared to scaffolds without channels, as shown in Figure 5.7a. However, micro-channels alone further improved volumetric flow rate to 50% height to 700mm^3/s, and the combination of macro- and micro-channels resulted in an extreme increase in volumetric flow rate to nearly 1800mm^3/s. Once normalized by cross sectional area with or without channels, the wicking velocity was only 3mm/s for scaffolds without channels, 5mm/s for macro- or micro-channeled scaffolds, and an astonishing 15.5mm/s for macro- and micro-channeled scaffolds (Figure 5.7b). Both the volumetric flow rate and velocity started to plateau as fluid wicked beyond the 50% height mark, but the loss in speed was not considered problematic due to the already high values.

A

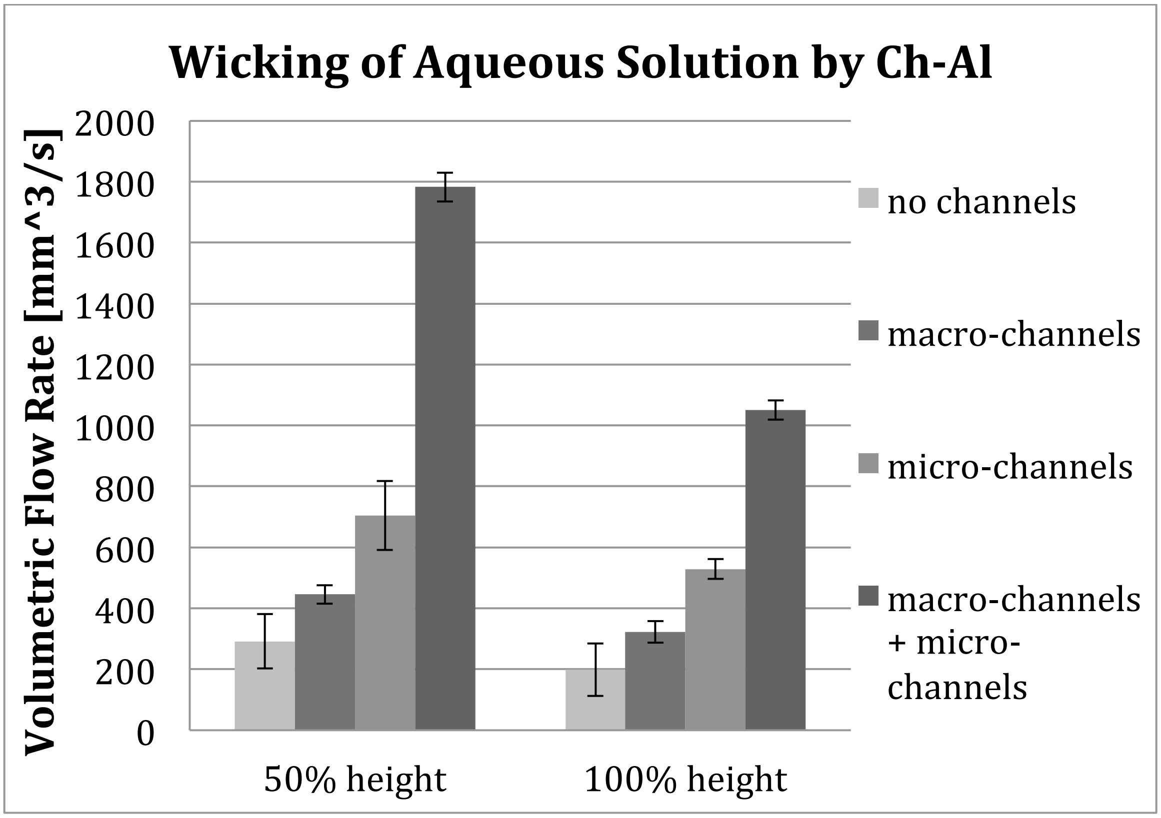
Wicking of Aqueous Solution by Ch-Al
Volumetric Flow Rate [mm^3/s]
2000
1800
1600
1400
1200
1000
800
600
400
200
0
50% height
100% height
no channels
macro-channels
micro-channels
macro-channels + micro-channels

B

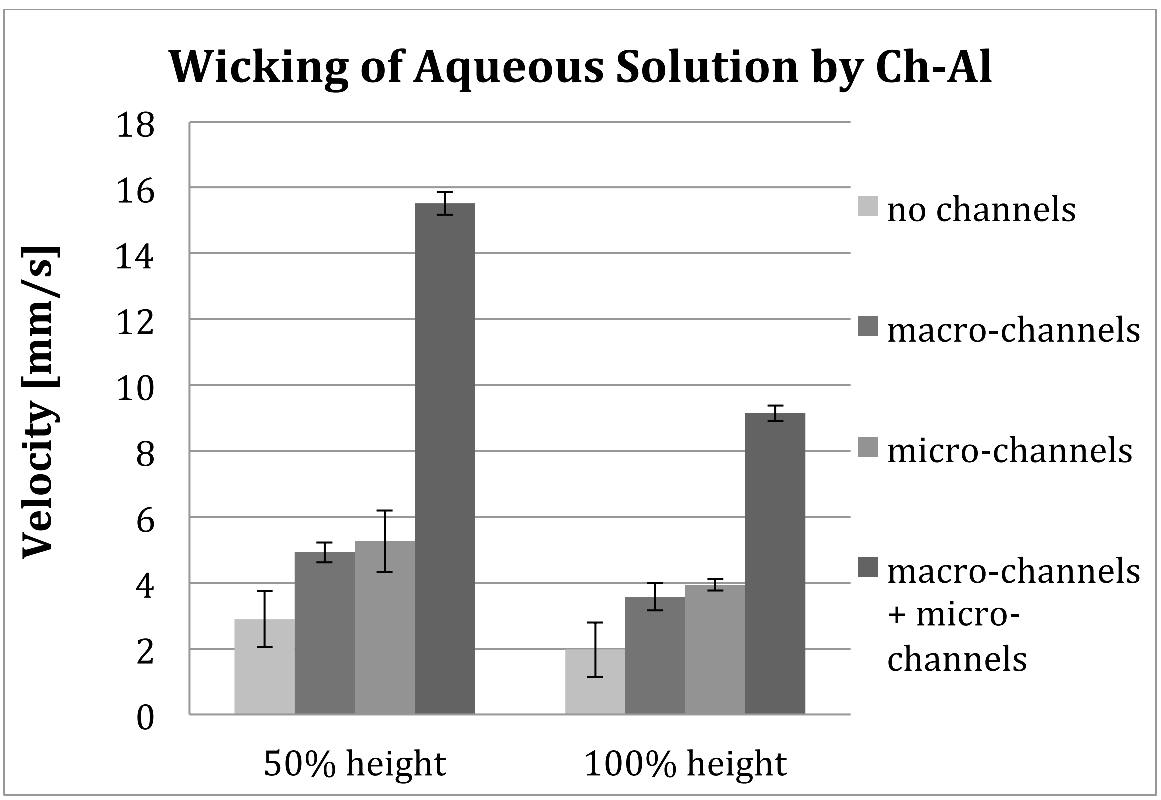
Wicking of Aqueous Solution by Ch-Al
Velocity [mm/s]
18
16
14
12
10
8
6
4
2
0
50% height
100% height
no channels
macro-channels
micro-channels
macro-channels + micro-channels

Figure 5.7 Aqueous solution uptake by directionally frozen Ch-Al made from 3DP negative molds. Scaffolds with or without macro-channels, with or without directionally frozen micro-channels, wicked a 0.1% SafraninO aqueous solution. The time to wick 50% and 100% height was measured, and volumetric flow rate (a) and velocity were calculated (b).

5.4.8 Blood Uptake by Macro- and Micro-Channels

Ch-Al scaffolds created to have macro- and micro-channels using 3DP negative molds with or without 1mm macro-channels and directional freezing were submersed in blood from C57BL/6 mice. Directionally frozen scaffolds were inverted before submersion into fluid, so that the lamellar pore zone at the scaffold top was placed directly into the 1mm fluid meniscus, allowing the remaining height of the scaffold to wick the aqueous solution very quickly via micro-channels, but not as quickly as the purely aqueous solution, due to viscosity differences. Similar to Figure 5.4a, macro-channels improved volumetric flow rate to 50% height from $18mm^3/s$ to $177mm^3/s$ compared to scaffolds without channels, as shown in Figure 5.8a. However, micro-channels alone further improved volumetric flow rate to 50% height to $225mm^3/s$, and the combination of macro- and micro-channels resulted in an extreme increase in volumetric flow rate to nearly $450mm^3/s$. Once normalized by cross sectional area with or without channels, the wicking velocity was only 0.14mm/s for scaffolds without channels, 1.75mm/s for macro- or micro-channeled scaffolds, and an impressive 3.5mm/s for macro- and micro-channeled scaffolds (Figure 5.8b). Both the volumetric flow rate and velocity started to plateau as blood wicked beyond the 50% height mark, similar to behavior seen in aqueous solution wicking, but the loss in speed was not considered an issue. As before, due to the high viscosity of blood compared to that of water, scaffolds without any channels showed very poor wicking from the start, and in all cases did not even wick the full 100% height, indicating that this system captured a condition in which macro- and micro-channels drastically improve blood wicking. Consistent with Figure 5.4, without channels, Ch-Al scaffolds barely wicked blood beyond 50% height. These results point to the need for channels in physiological situations such as bone marrow uptake.

A

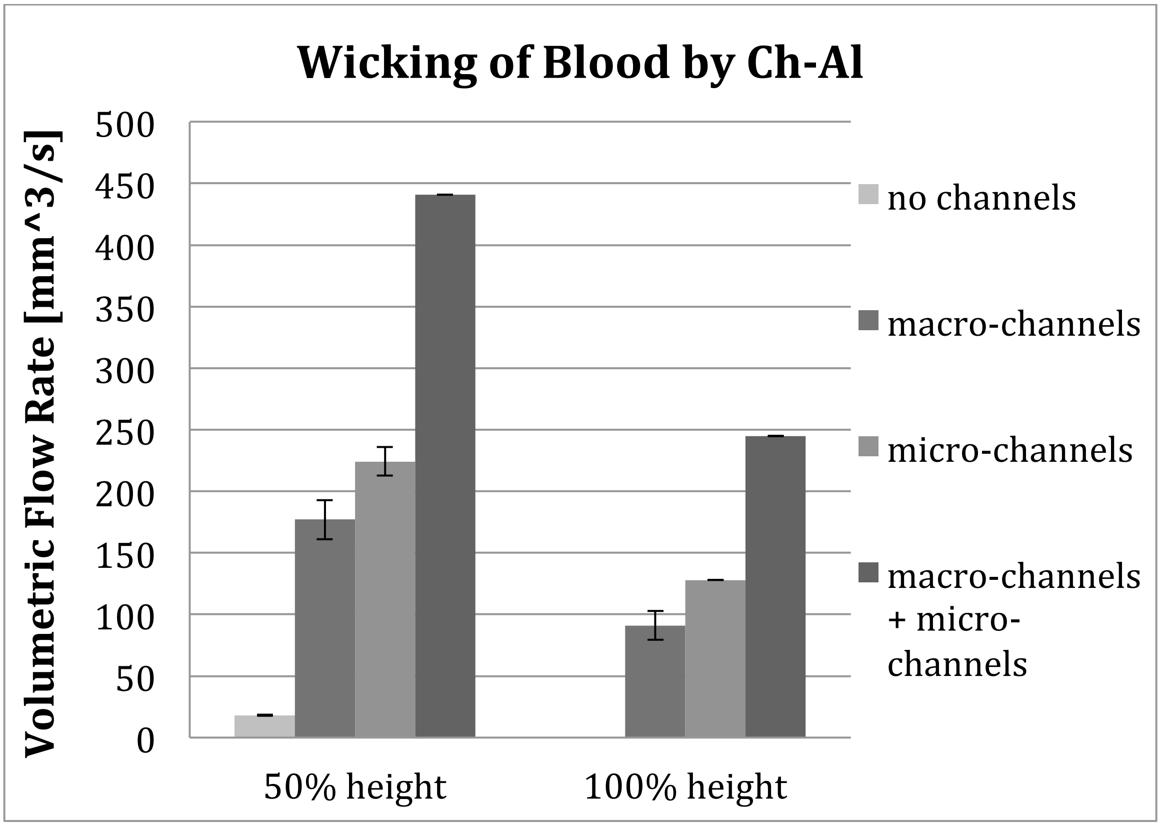

B

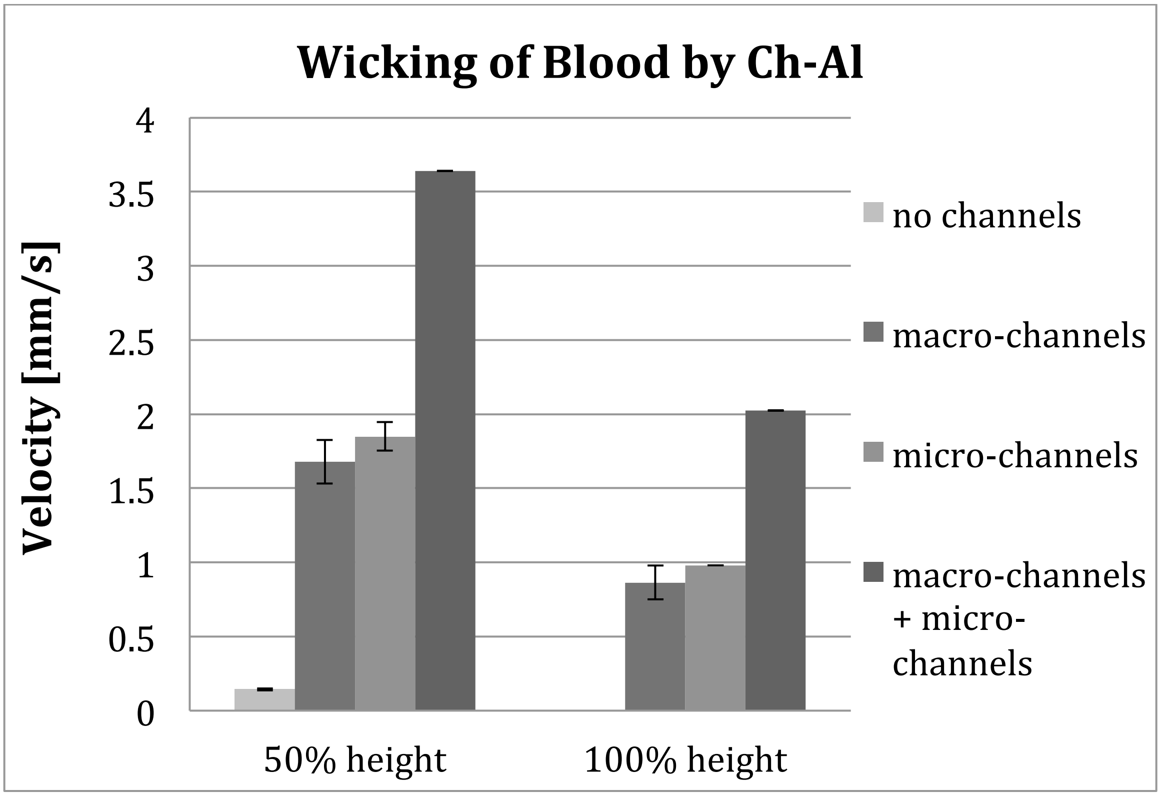

Figure 5.8 Blood uptake by directionally frozen Ch-Al made from 3DP negative molds. Scaffolds with or without macro-channels, with or without directionally frozen micro-channels, wicked C57BL/6 mouse blood. The time to wick 50% and 100% height was measured, and volumetric flow rate (a) and velocity were calculated (b).

5.5 Discussion

It was observed that the top and bottom surfaces of Ch-Al scaffolds exhibited denser fibers, oriented perpendicular to the z axis, than in the cross sectioned scaffold center, where scaffold struts were randomly oriented. This is hypothesized to be due to surface tension effects during freezing and freeze-drying. Similar behavior was seen with pure chitosan lyophilized scaffolds, where SEM revealed an ionic complex membrane on the outer scaffold surface while the internal porous structure was retained.[33] If the temperature during lyophilization is not low enough, freeze-drying often results in the formation of a surface skin due to the collapse of the matrix at the scaffold-air or scaffold-solid interface, which is driven by interfacial tension during solvent evaporation.[34]

Directionally frozen scaffolds only displayed this behavior on the bottom surface, not the top, since ice crystal growth during directional freezing was severe and likely overshadowed any surface tension effects, dominating pore formation.

Ch-Al scaffolds wicked both aqueous solution and blood extremely quickly. This can be explained by the hydrophilicity of both Ch and Al, whose contact angles have been shown to be 20 degrees and 10 degrees, respectively, as measured during layer-by-layer assembly of Ch-Al films.[35] Blood uptake was not as fast as aqueous solution uptake because of the difference in viscosity. The viscosity of blood, a non-Newtonian fluid, at 37C is normally 3-4cP, while the viscosity of water is 0.91cP at 25C and 1.0cP at 20C.[36] Fluid uptake was maximum up to around 80% of the scaffold height, and then the volumetric flow rate and velocity started to plateau. To illustrate this, volumetric flow rate and velocity were calculated up to 50% and 100% height. This is consistent with general knowledge about imbibement by porous solids, specifically how fluid uptake is nonlinear and decreases over time in the presence of gravity.[37] The slower speed after the 50% height mark was still faster than the time scale to activate plasma coagulation, ~30-45s, which is the physiologically relevant parameter to be concerned with when considering what may hinder bone marrow uptake *in vivo*.[38]

The zone closest to the cold finger exhibited cellular or spherical pore morphology, and this zone was located at the bottom 500um of the scaffold. Beyond this region, a lamellar zone was maintained all the way through the remaining height. This cellular zone forms because directional freezing kinetics involves a progressive transition of the freezing front morphology from planar to cellular followed by cellular to lamellar or dendritic.[32] This transition is caused by the progressive build up of supercooling ahead of the freezing front and may also be influenced by morphological instabilities induced by the Ch-Al slurry particles.[32] After the transition occurs, a steady regime is achieved, which was confirmed experimentally by the lamellar region persisting through the remaining height. The first zone in contact with the cold finger demonstrates faster freezing kinetics, and at this point the heat transfer equilibrium has not yet been reached. This accounts for the unstable cellular morphology in this region of the scaffold.[32] Directional freezing is a competition between heat transfer and mass transfer kinetics, and the presence of dendrites achieved by directional freezing indicates the system resides in diffusion limited ice crystal growth. While previous work demonstrated directional freezing with a dispersed phase in a continuous phase, or ceramic particles distributed in water, this system demonstrates directional freezing of a continuous phase in a continuous phase, or polymers dissolved in water. Instead of ceramic particles being pushed out of ice crystals during ice crystal nucleation and growth, Ch-Al polymer is pushed out via phase separation and must occur very quickly. The presence of the 3DP mold within the cold finger introduces a third material with a different thermal conductivity, and this third materials affects the heat transfer during directional freezing. However, the thermal conductivity of the 3DP ABS mold is likely very low, similar to the PTFE cylindrical mold of the cold finger, so the heat transfer was likely preferential into the Ch-Al aqueous solution, which has a much higher thermal conductivity. This explains why the presence of the 3DP mold did not interfere with lamellar pore formation.

Because the 3DP negative molds used for directionally freezing (Figures 5.7 and 5.8) were larger than those used in previous aqueous solution and blood uptake experiments (Figures 5.3 and 5.4), the diameters of the scaffolds were larger, resulting in a cross-sectional area slightly more than twice as large. This explains why although the volumetric flow rates of scaffolds with no channels and macro-channels are the same across experiments, the wicking velocities differ by a factor of at least 2. For example in Figure 5.7, scaffolds have twice the volume and wick half as fast, so the volumetric flow rates appear equal with those in Figure 5.3. However, for velocity, scaffold cross-sectional area is divided out, so the velocity relies solely on the height and time to wick, which corresponds to scaffolds in Figure 5.7 wicking at a velocity 2x as slow because they had a 2x greater cross sectional area to fill.

The next phase of this research naturally entails applying directional freezing to 3DP positive molding by implementing directional freeze casting after centrifuge infusion. With these two approaches, complex, patient-specific macro-geometry and finely controlled, biomimetic micro-geometry can be achieved. In the future, 3D printed, directionally frozen Ch-Al scaffolds can be translated to an *in vivo* rabbit knee joint model, where an osteochondral implant may enhance vascularization of the bone portion due to the channeled architecture and may improve chondrogenesis in the cartilage region due to the precisely controlled, biomimetic design.

5.6 Conclusion

Macro- and micro-designed Ch-Al scaffolds, based on 3DP and directional freezing, were successfully fabricated to increase aqueous solution uptake, blood uptake, and cell distribution. Macro-channels were created using both 3DP negative molds and more complex 3DP positive molds, which utilized a centrifuge infusion process into a PLLA preform made from the original sugar 3D print. Micro-channels parallel to the z axis were obtained by directional freezing using a cold finger apparatus, and the resulting lamellar pores were 300um long by 50um diameter. A 100um diameter cellular pore zone was seen at the bottom 500um of the scaffold, with an integrated transition from lamellar to spherical pore regions. The top and bottom surfaces of scaffolds traditionally cast and frozen at -80C as well as the bottom surfaces of directionally frozen scaffolds demonstrated a denser fibrous morphology where scaffold struts ran perpendicular to the z axis. The combination and orientation of parallel lamellar pores, cellular pores, and perpendicular scaffold struts in a single integrated scaffold may serve to mimic the zonal architecture seen in native articular cartilage. Further, the remarkable fluid uptake ability by scaffolds with macro- and micro-channels may allow for an off-the-shelf, acellular osteochondral implant that does not require cell seeding.

References

1. Gomoll AH, Farr J. Autologous chondrocyte implantation (ACI). Cartilage Restoration 2014;143-152.
2. McGowan KB, Stiegman G. Regulatory challenges for cartilage repair technologies. Cartilage 2013;4(1):4-11.
3. Ruano-Ravina A, Jato Diaz M. Autuologus chondrocyte implantation: a systematic review. Osteoarthritis and Cartilage 2009;14:47-51.
4. Diekman BO, Guilak F. Stem cell-based therapies for osteoarthritis: challenges and opportunities. Current Opinion in Rheumatology 2013;25(1):119-126.
5. Gardner OF, Archer CW, Stoddart MJ, et al. Chondrogenesis of mesenchymal stem cells for cartilage tissue engineering. Histology and Histopathology 2013;28(1):23-42.
6. Roelofs AJ, Rocke JPJ, De Bari C. Cell-based approaches to joint surface repair: a research perspective. Osteoarthritis and Cartilage 2013;21(7):892-900.
7. Steinert AF, Ghivizzani SC, Tuan RS, Noth U, et al. Major biological obstacles for persistent cell-based regeneration of articular cartilage. Arthritis Research & Therapy 2007;9:213-227.
8. Yeong WY, Chua CK, Chandrasekaran M, et al. Rapid prototyping in tissue engineering: challenges and potential. Trends in Biotechnology 2004;22(12):643-652.
9. Li Z, Zhang M, et al. Chitosan-Alginate Hybrid Scaffolds for Bone Tissue Engineering. Biomaterials 2005;26:3919-3928.
10. Li Z, Zhang M. Chitosan-Alginate as Scaffolding Material for Cartilage Tissue Engineering. J Biomed Mater Res 2005;75A:485-493.

11. Wan Y, Wu H, Wen D. Porous-Conductive Chitosan Scaffolds for Tissue Engineering, 1: Preparation and Characterization. Macromol Biosci 2004;4:882-890.

12. Lee M, Wu BM. Recent advances in 3D printing of tissue engineering scaffolds. Computer-Aided Tissue Engineering, Methods in Molecular Biology 2012;868:257-267.

13. Shuai C, Zhuang J, Liu J, et al. *In vitro* bioactivity and degradability of β-tricalcium phosphate porous scaffold fabricated via selective laser sintering. International Union of Biochemistry and Molecular Biology 2013;00(0):1-8.

14. Simpson RL, Wiria FE, Hansen UN, et al. J. Biomed. Mater. Res. 2008;84B:17-25.

15. Shuai C, Gao C, Peng S. Structure and properties of nano-hydroxyapatite scaffolds for bone tissue engineering with a selective laser sintering system. Nanotechnology 2011;22:285703(9pp).

16. Shuai C, Yang B, Li Z, et al. Development of composite porous scaffolds based on poly(lactide-co-glycolide)/nano-hydroxyapatite via selective laser sintering. Int. J. Adv. Manuf. Technol. 2013

17. Eosoly S, Brabazon D, Looney L, et al. Selective laser sintering of hydroxyapatite/poly-ε-caprolactone scaffolds. Acta Biomaterialia 2010;6:2511-2517.

18. Zhou WY, Lee SH, Ip WY, et al. Selective laser sintering of porous tissue engineering scaffolds from poly(L-lactide)/carbonated hydroxyapatite nanocomposite microspheres. J. Mater. Sci: Mater. Med. 2008;19:2535-2540.

19. Klein TJ, Malda J, Hutmacher DW, et al. Tissue engineering of articular cartilage with biomimetic zones. Tissue Engineering: Part B 2009;15(00):1-15.

20. Sherwood J, Riley S, Ratcliffe A, et al. A three-dimensional osteochondral composite scaffold for articular cartilage repair. Biomaterials 2002;23:4739-4751.

21. Mimura T, Imai S, Matsusue Y, et al. A novel exogenous concentration-gradient collagen scaffold aguments full-thickness articular cartilage repair. Ostoearthritis Cartilage 2008;16(9):1083-1091.

22. Brittberg M, SjogrenJansson E, Peterson L, et al. Influence of fibrin sealant (Tisseel®) on osteochondral defect repair in the rabbit knee. Biomaterials 1997;18(3):235-242.

23. Shao XX, Hutmacher DW, Lee EH, et al. Evaluation of a hybrid scaffold/cell construct in repair of high-load-bearing osteochondral defects in rabbits. Biomaterials 2006;27(7):1071-1080.

24. Schaefer D, Martin I, Freed LE, et al. Tissue-engineered composites for the repair of large osteochondral defects. Arthritis Rheum 2002;46(9):2524-2534.

25. Kreklau B, Sittinger M, Gross U, et al. Tissue engineering of biphasic joint cartilage transplants. Biomaterials 1999;20(18):1743-1749.

26. Holland TA, Bodde EWH, Jansen JA, et al. Osteochondral repair in the rabbit model utilizing bilayered, degradable oligo(poly(ethylene glycol) fumarate) hydrogel scaffolds. J. Biomed. Mater. Res. A 2005;75A(1):156-167.

27. Chen GP, Sato T, Tateishi T, et al. Preparation of a biphasic scaffold for osteochondral tissue engineering. Mater. Sci. Eng. C 2006;26(1):118-123.

28. Levingstone TJ, Matsiko A, Gleeson JP, et al. A biomimetic multi-layered collagen-based scaffold for osteochondral repair. Acta Biomaterialia 2014 (in press).

29. Harley BA, Lynn AK, Gibson LJ, et al. Design of a multiphase osteochondral scaffold III: Fabrication of layered scaffolds with continuous interfaces. J. Biomed. Mater. Res. 2010;92A:1078-1093.

30. Shimomura K, Moriguchi Y, Nakamura N, et al. Osteochondral tissue engineering with biphasic scaffold: Current strategies and techniques. Tissue Engineering Part B 2014 (in press).

31. Deville S, Saiz E, Tomsia AP, et al. Freezing as a path to build complex composites. Science 2006;311:515-518.

32. Deville S, Saiz E, Tomsia AP. Freeze casting of hydroxyapatite scaffolds for bone tissue engineering. Biomaterials 2006;27:5480-5489.

33. Madihally SV, Matthew HWT. Porous chitosan scaffolds for tissue engineering. Biomaterials 1999;20:1133-1142.

34. Ho MH, Kuo PY, Wang DM, et al. Preparation of porous scaffolds by using freeze-extraction and freeze-gelation methods. Biomaterials 2004;25(1):129-138.

35. Yuan W, Dong H, Zhou Q, et al. pH-controlled construction of chitosan/alginate multilayer flim: Characterization and application for antibody immobilization. Langmuir 2007;23:13046-13052.

36. Elert G. The Physics Hypertextbook. Viscosity. 2014.

37. Masoodi R, Pillai KM. Wicking in porous materials: Traditional and modern modeling approaches. CRC Press 2013:317.

38. Oslakovic C, Cedervall T, Dahlback B, et al. Polystyrene nanoparticles affecting blood coagulation. Nanomedicine: Nanotechnology, Biology, and Medicine 2012;8:981-986.

<u>Chapter 6</u>

6. Characterizing Chitosan-Alginate Microaggregates for Sustained Growth Factor Delivery in Tissue Engineering

6.1 Abstract

Tissue engineering often employs the delivery of growth factors from scaffolds to signal cellular activities such as proliferation, differentiation, extracellular matrix (ECM) deposition, and ultimately, tissue regeneration. However, the mechanism of growth factor delivery is non-trivial. Chemical conjugation of proteins to a scaffold surface can result in a small burst release followed by permanent presentation of the bioactive molecule, and a gradual release is achieved as the bulk material degrades. Still, common problems of are often encountered with this approach, such as conjugation inefficiency, protein biological inactivity due to blocked binding sites, and inability to internalize the growth factor for subsequent activation of signaling cascades. Many varieties of diffusion-based systems have been implemented, but most still suffer from an uncontrollable, large burst release, poor encapsulation efficiency, and do not provide a spatiotemporal sustained release longer than a couple weeks. For cartilage regeneration, the timescale of healing can take up take up to many months, thus it is crucial that an engineered growth factor release profile be synchronized with this timeline in order to enhance and sustain chondrogenesis. This study demonstrates a delivery system based on ionic complexation that releases a variety of proteins in a sustained manner over the course of multiple months.

Chitosan-alginate (Ch-Al) microaggregates encapsulated 10ug to 10mg model proteins bovine serum albumin (BSA) at 90% to 99% loading efficiency, respectively. Further, release from microaggregates was <10% over 60 days for all doses of BSA with <5% burst release, exhibiting an inverse dose dependent release behavior. Ch-Al microaggregates also sustained the release of both

positively and negatively charged proteins of varying molecular weights, such as histone, fibrinogen, avidin, and biotin. 100ug histone, fibrinogen, avidin, and biotin loaded in microaggregates gradually released over 30 days, with small molecule biotin burst releasing the most at 24% on day 3, and the other three proteins burst releasing <5%. Compared to nonspecific adsorption of 100ug BSA on Ch-Al scaffolds, Ch-Al microaggregates on Ch-Al scaffolds reduced the burst release from 5% to 2% and total release at day 30 from 60% to 30%. Moreover, compared to nonspecific adsorption of 10mg BSA on Ch-Al scaffolds, microaggregates on scaffolds reduced the burst release from 30% to 2% and total release at day 30 from 60% to 16%. Thus, it can be concluded that Ch-Al microaggregates offer an extreme advantage over nonspecific adsorption at high doses, doses similar to those required for human *in vivo* studies.

When characterizing Ch-Al microaggregates, it was discovered that they self assemble into polyionic complexes that form hierarchical structures with fiber-like morphology. Ch-Al fiber diameter based on scanning electron microscopy (SEM) was around 1um with 5um length, but also a larger flake morphology was observed with up to 50um length. This bimodal population and self-assembly over time was confirmed with dynamic light scattering (DLS). Ch-Al microaggregate morphology allowed greater persistence within Ch-Al scaffolds during washing compared to polystyrene microspheres or even Ch-Al microparticles fabricated to have granular morphology. This increased persistence has implications in the *in vivo* environment where it is advantageous to have a growth factor carrier that does not easily migrate or wash away from the scaffold or implant site. Together, these results point to the potential of Ch-Al microaggregates as a sustained release system to deliver chondrogenic growth factors to promote cartilage regeneration.

6.2 Introduction

Lots of recent focus has been given to growth factor delivery from within scaffolds to assist cartilage tissue regeneration, specifically to signal proliferation, metabolism, adhesion, chemotaxis, gene expression, differentiation, and extracellular matrix (ECM) production by chondrocytes and stem cells.[1-5] Cartilage is a particularly difficult tissue to regenerate due to the senescent nature of chondrocytes, lack of vascularization, and the fact that <1% of cartilage volume is made up of cells.[6] Thus, signaling molecules are delivered to enhance regenerative activity by cells, both native and exogenous, to improve healing within the wound site. However, the mechanism in which these bioactive molecules are delivered requires careful and thoughtful engineering as well as timing.

Materials with growth factors chemically conjugated to their surface through a covalent bond offer some advantage of a gradual release as the bulk material degrades and permanent presentation of the bioactive molecule, but certain growth factors require internalization for activation of their signaling cascades and conjugation chemistry to surfaces can be inefficient or render the protein biologically inactive.[7] Alternatively, non-covalent approaches that rely on diffusion may be implemented, but most diffusion-based growth factory delivery systems suffer from a large burst release[8], have problems with protein stability and immunogenicity[9], and do not provide a sustained release over the course of many weeks[8], which is required for cartilage production. In fact, cartilage healing in canine defects is characterized by a proliferative phase at 1.5 months followed by a remodeling phase lasting 3-6 months.[10] Here we aim to develop a delivery system that releases chondrogenic growth factors in a sustained manner to promote cartilage regeneration.

Chitosan-alginate (Ch-Al) scaffolds were selected as a platform for growth factor delivery, since our previous research shows Ch-Al can support chondrogenesis by chondrocytes and also can be fabricated into biomimetic osteochondral scaffolds based on three-dimensional printing and directional freezing. Other studies have shown that Ch-Al has the ability to promote both osteogenesis and chondrogenesis, both *in vitro* and *in vivo*.[11,12] Lyophilizing Ch-Al creates generates porous, hydrophilic scaffolds with significant mechanical strength, approximately three times the compressive modulus and yield strength of pure chitosan.[11] Ch-Al scaffolds have been used in cartilage tissue engineering particularly because they are naturally occurring polysaccharides similar in chemical structure to articular cartilage extracellular matrix (ECM) glycosaminoglycans (GAGs) like chondroitin sulfate, keratan sulfate, and hyaluronic acid.[13] Further, Ch-Al scaffolds can be prepared at neutral pH, allowing growth factors and drugs to be uniformly incorporated without denaturation.[12]

In previous studies we have shown that there is an inherent ability of chitosan-alginate scaffolds to bind proteins quite strongly, resulting in a sustained release of both model and chondrogenic proteins at low doses. This is due to nonspecific adsorption of the protein to the charged surface of the scaffold. The net charge of Ch-Al scaffolds, which are fabricated at pH 7.4, is likely negative based on both polymers' isoelectric points, but the scaffold surface is likely zwitterionic since it can be loaded at high efficiency with both positively and negatively charged proteins followed by a subsequent slow release over many weeks. Unfortunately, at high doses in the milligram range, which is more physiologically relevant, this sustained release breaks down, and a 30% burst release of model protein bovine serum albumin (BSA) was seen on day 0, followed by 60% total release by day 30.

Thus, there is a need for a better growth factor release mechanism from Ch-Al scaffolds beyond nonspecific adsorption and beyond the current release techniques. We proposed creating a diffusion-based delivery system also out of chitosan and alginate, due to the strength of ionic interaction between the two polymers. However, instead of creating three-dimensional scaffolds out of Ch-Al, alginate mixed with the desired protein was added dropwise to a stirring chitosan solution, creating Ch-Al microaggregates. This type of ionic complexation between chitosan and alginate, resulting in polyionic complexes, has been thoroughly studied for growth factor release[14-17]. Ch-Al microparticles, with and without hydroxyapatite coating, have also been used for growth factor delivery, but using different ratios of chitosan to alginate and with calcium chloride crosslinker.[18] It was shown that Ch-Al microparticles alone did not exhibit high encapsulation efficiency or sustain release.[18] Using a modified protocol from fabricating Ch-Al microparticles, this study creates a new form factor for growth factor delivery—microaggregates. This research attempts to improve sustained protein release beyond microparticles and demonstrate that the morphology of microaggregates compared to microparticles is critical for persistence within scaffolds. In the future, using this Ch-Al microaggregate release system, Ch-Al scaffolds may be able to support chondrogenesis by stem cells, an accomplishment never before achieved using simple nonspecific adsorption.

6.3 Materials and Methods

6.3.1 Materials

Histone H1 from calf thymus Alexa Fluor 488 conjugate (Cat # H-13188), fibrinogen from human plasma Alexa Fluor 488 conjugate (Cat # F13191), avidin Texas Red conjugate (Cat # A-820, Life Technologies), biotin-4-Fluorescein (Cat # B-10570), and antibiotic-antimycotic (ABAM, Cat # 15240-062) were obtained from Life Technologies (Grand Island, NY).

Chitosan (practical grade, Cat # 41763), alginate from brown algae (Cat # A7003), alginic acid sodium salt from brown algae (viscosity of 2% solution at 25C ~250cps, Cat # A2158), calcium chloride ($CaCl_2$-$2H_2O$, Cat # 12022), 50% sodium hydroxide in water (Cat # 415413), bovine serum albumin fluorescein isothiocyanate conjugate (BSA-FITC, Cat # A9771), Pluronic F-68 (Cat # P-1300), sodium chloride (Cat # S9888) were obtained from Sigma-Aldrich (St. Louis, MO).

Dulbecco's phosphate buffered salt solution (PBS 1X with calcium and magnesium, Mediatech, Cat # 21-030-CM), acetic acid (glacial, Cat # A38 SI-212), Dulbecco's Modification of Eagle's Medium w/ 4.5 g/L glucose, L-glutamine & sodium pyruvate (DMEM 1X, Cellgro, Cat # 10-013-CV), fetal bovine serum (FBS, Cat # MT35015CV), and 0.22um polyethersulfone (PES) membrane filters (Cat # 50-202-045) were obtained from Fisher Scientific (Waltham, MA). Nile Red polystyrene microspheres with 1.7-2.2um diameter (Cat # 556261) were obtained from BD Biosciences (San Jose, CA).

6.3.2 Microaggregate Preparation

Both 0.1% w/v chitosan in 0.05% v/v acetic acid in dH_2O and 0.1% w/v alginic acid sodium salt in dH_2O solutions were mixed separately and filtered separately through a 0.2um media filter. 6ml of the chitosan solution was set stirring at 1000rpm in a 20ml scintillation vial using a 1cm length stir bar. 300ul 0.1N sodium hydroxide was added to the stirring chitosan to bring the pH up to 5.5. Next, the alginate solution was mixed with protein to a total of 1.8ml, and this was added dropwise to the stirring chitosan. The combined solution was allowed to stir for 2min, followed by sonication using an ultrasonic homogenizer for 30s. The mixture was divided into eight microcentrifuge tubes for centrifugation at 14,500rpm for 15min. Pellets of microaggregates formed, and the supernatant was collected for encapsulation efficiency. The remaining supernatant was aspirated, and pellets were resuspended in dH_2O and sonicated again for 10s for dispersion.

6.3.3 Scaffold Fabrication

Adapted and modified from Li et al[11,12], Ch-Al scaffolds were fabricated with 2% w/v chitosan dissolved in 2% v/v acetic acid in dH_2O and 2% w/v alginate dissolved in dH_2O, mixed at 1:1 ratio. The Ch-Al solution was ultrasonically homogenized for 1min, titrated to pH 7.4 with 50%

sodium hydroxide, ultrasonically homogenized for 5min, pipetted into a 96-well plate as a mold, and frozen at -80C overnight. The resulting frozen scaffolds were lyophilized overnight, crosslinked for 15min with 1% w/v $CaCl_2$, washed three times with dH_2O, and lyophilized overnight.

6.3.4 Protein Release

For protein release from Ch-Al microaggregates, 0ug, 10ug, 100ug, 1mg, or 10mg BSA, or 100ug histone, fibrinogen, avidin, or biotin, was loaded into microaggregates, which were resuspended after centrifugation in 200ul dH_2O as release medium. The 0ug release profile served as a baseline for subtraction of the background. For nonspecific adsorption of protein on Ch-Al scaffolds, 100ug or 10mg BSA in 50ul PBS was pipetted onto scaffolds, which were lyophilized overnight and then suspended in 200ul dH_2O as release medium. For the addition of protein-loaded Ch-Al microaggregates on Ch-Al scaffolds, 100ug or 10mg BSA was loaded into microaggregates, which were resuspended after centrifugation in 50ul dH_2O and pipetted onto scaffolds. Scaffolds with microaggregates were lyophilized overnight and then suspended in 200ul dH_2O, 2N NaCl in dH_2O, PBS, or complete DMEM with 10% FBS and 1% ABAM as release media. Release from microaggregates alone, nonspecific adsorption on scaffolds, and microaggregates on scaffolds was captured over time by collecting and measuring the fluorescence of supernatants using a plate reader (Tecan, Männedorf, Switzerland).

6.3.5 Persistence within Scaffolds

For comparing persistence of Ch-Al microaggregates within Ch-Al scaffolds to Ch-Al microparticles or polystyrene microspheres, 10mg BSA was loaded into microaggregates, which were resuspended after centrifugation in 210ul dH_2O to create at 1% w/v solution, and 50ul of this suspension was pipetted onto scaffolds. Ch-Al microparticles were prepared the same as Ch-Al microaggregates, except 18mg of surfactant Pluronic was dissolved in the alginate-BSA solution, creating a 1% w/v Pluronic solution in alginate-BSA, prior to dropwise addition into chitosan. Also, these microparticle pellets were resuspended with 210ul 1% w/v Pluronic in dH_2O, and 50ul of this 1% w/v microparticle suspension was pipetted onto scaffolds as before. For polystyrene microspheres, 50ul of the 1% w/v stock solution was pipetted onto scaffolds. All scaffolds with microaggregates, microparticles, or microspheres were lyophilized overnight and then washed three times with 200ul dH_2O at release medium. The release of microaggregates, microparticles, or microspheres from scaffolds during each wash was captured by collecting and measuring the fluorescence of supernatants using a plate reader. In parallel, dynamic light scattering (DLS) by a ZetaSizer Nano-ZS (Malvern, Worcestershire, UK) immediately after suspension sonication was used to confirm microaggregate, microparticle, and microsphere size. Also, microaggregates, microparticles, and microspheres were flash frozen using liquid nitrogen and lyophilized overnight before imaging using a Nova Nano scanning electron microscope (SEM) 230 (FEI, Hillsboro, OR) with 10keV accelerating voltage and 3.0-4.0 spot size. Microaggregates were gold sputter coated for 1min prior to imaging, but both other samples were imaged using the SEM low vacuum detector.

6.4 Results

6.4.1 Dose Dependent Encapsulation Efficiency and Release

For the encapsulation of protein, the Ch-Al mixture was pHed to 5.5 for maximum ionic interaction between the positively charged amine and negatively charged carboxylic acid groups. This lead to very high encapsulation efficiencies, despite protein dose, and also very slow protein release profiles, as expected. Doses of BSA (66.5kDa, negative) ranging from 10ug to 10mg encapsulated in Ch-Al microaggregates at 90% to 99% efficiency, respectively (Figure 6.1a). Further, release from microaggregates was sustained over at least 60 days with less than 5% burst release and 10% or less total release for all doses (Figure 6.1b). Both the encapsulation efficiency and release profiles of BSA from Ch-Al microaggregates exhibited an inverse dose-dependent behavior, with higher doses displaying increased encapsulation and decreased release. Figure 6.1c illustrates how freshly-made microaggregates in suspension were centrifuged into pellets and the supernatant was collected for encapsulation efficiency calculations. Pellets were resuspended during the course of release and spun down at each time point for collecting the supernatant for release calculations. Microaggregates retained fluorescently labeled BSA, as seen by the yellow hue of pellets on day 0 and 60.

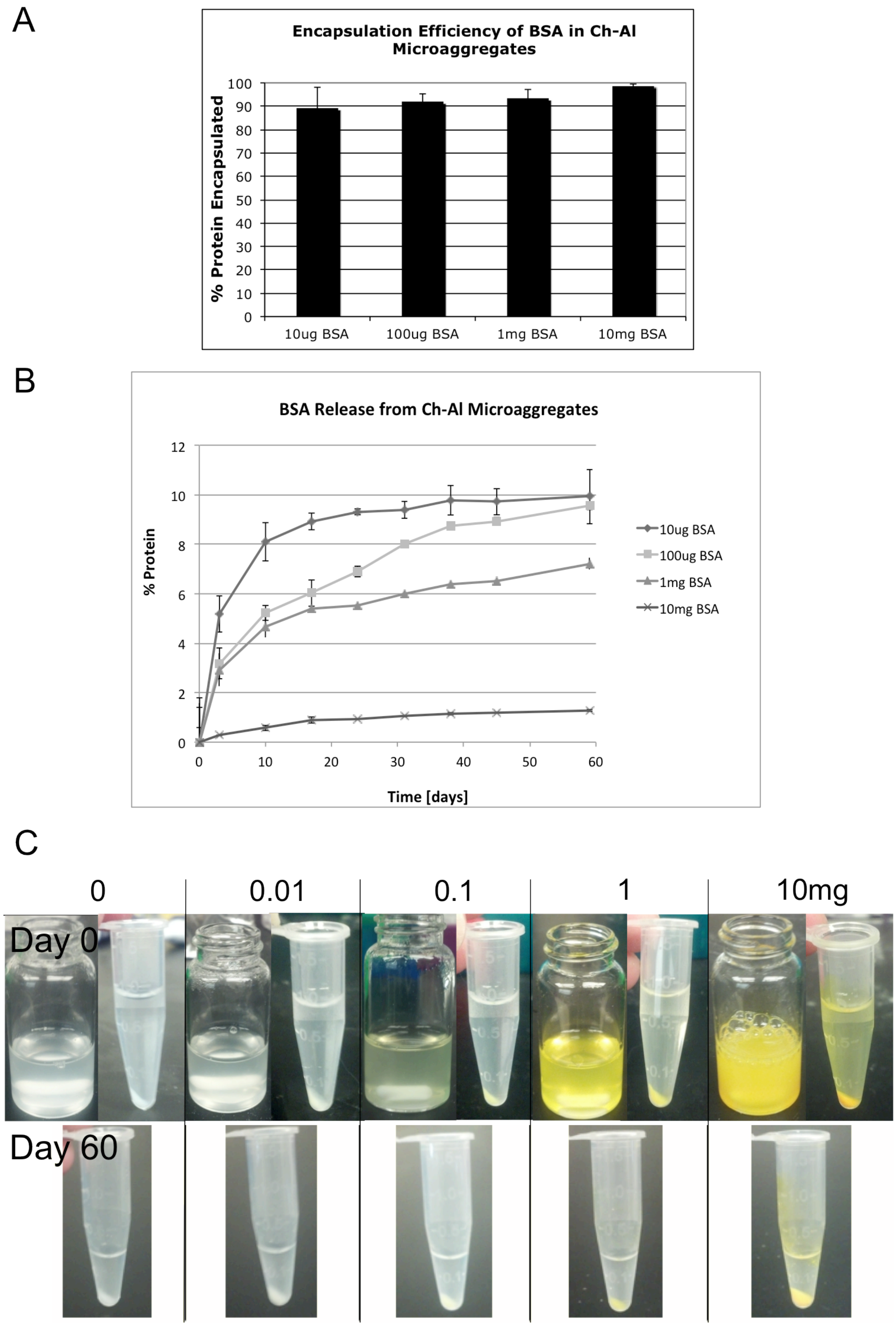
A
Encapsulation Efficiency of BSA in Ch-Al Microaggregates
% Protein Encapsulated
100
90
80
70
60
50
40
30
20
10
0
10ug BSA
100ug BSA
1mg BSA
10mg BSA
B
BSA Release from Ch-Al Microaggregates
% Protein
12
10
8
6
4
2
0
0
10
20
30
40
50
60
Time [days]
10ug BSA
100ug BSA
1mg BSA
10mg BSA
C
0
0.01
0.1
1
10mg
Day 0
Day 60

Figure 6.1 Encapsulation efficiency of different doses of BSA in chitosan-alginate (Ch-Al) microaggregates (a). Release profiles of different doses of BSA from Ch-Al microaggregates (b). Sonicated Ch-Al microaggregates in solution (left) and after centrifugation (right) releasing BSA over the course of 60 days (c).

6.4.2 Release of Various Proteins

Proteins of various molecular weights and isoelectric points were also encapsulated within and released from Ch-Al microaggregates. 100ug histone (21.5kDa, positive), fibrinogen (340kDa, negative), avidin (66-69kDa, positive), and biotin (small molecule, negative) were encapsulated within microaggregates at efficiencies of >94%, except biotin which only encapsulated at 45% (Figure 6.2a). Histone, fibrinogen, and avidin release profiles exhibited 5% or less burst release and 5%, 5%, and 12% total release after 25 days, respectively (Figure 6.2b). On the other hand, biotin burst released 24% and released a total of nearly 30% after 25 days, indicating that microaggregates may not be the best choice for encapsulation and sustained release of small molecules.

A

B

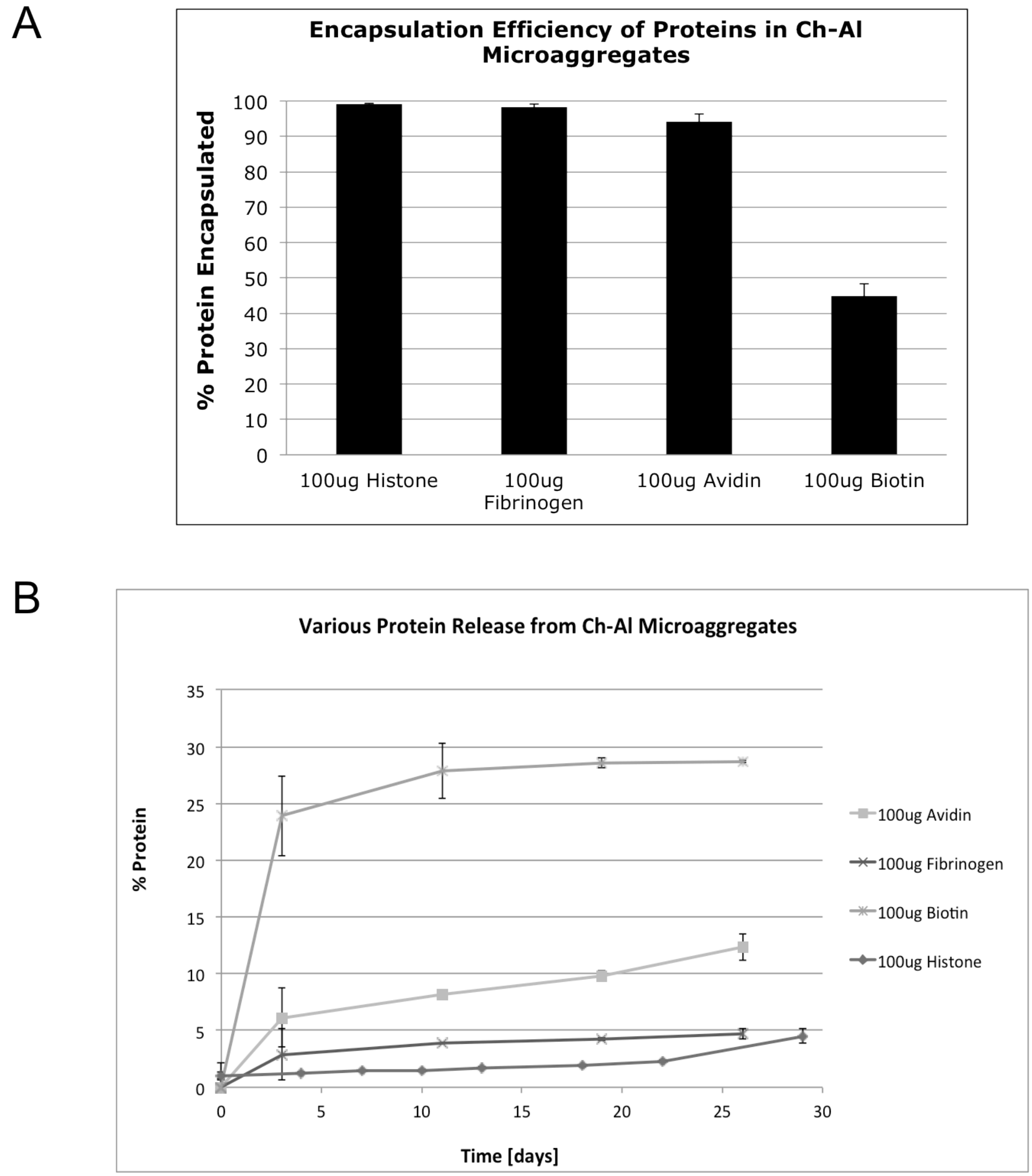

Figure 6.2 Encapsulation efficiency of 100ug of various proteins in Ch-Al microaggregates (a). Release profiles of 100ug of different proteins from Ch-Al microaggregates (b).

6.4.3 Microaggregates vs. Nonspecific Adsorption on Scaffolds

Low dose of 100ug and high dose of 10mg of BSA was either loaded into Ch-Al microaggregates which were then added to Ch-Al scaffolds, or else loaded onto Ch-Al scaffolds directly through nonspecific adsorption. At low dose of BSA, the release profile from nonspecific adsorption was deemed sufficient for tissue engineering purposes due to its sustained release of 60% over 30 days with only 5% burst release. When this lose dose of BSA was loaded into microaggregates, the burst release was reduced to 2% and total release after 30 days was reduced to 30%, as seen in Figure 6.3a. However at high doses such as 10mg of BSA, burst release from nonspecifically adsorbed protein was 30%, followed by a total release of 60% after 30 days. Microaggregates improved the sustained release of high dose of BSA, demonstrating a 2% burst release and 16% total release after 30 days, as shown in Figure 6.3b. Figure 6.3c illustrates the loss in yellow color over 50 days when a high dose of fluorescently labeled BSA was loaded onto Ch-Al scaffolds via nonspecific adsorption. In contrast, much less protein was released, as indicated by remaining yellow hue, when the same high dose of BSA was loaded into microaggregates on scaffolds.

A

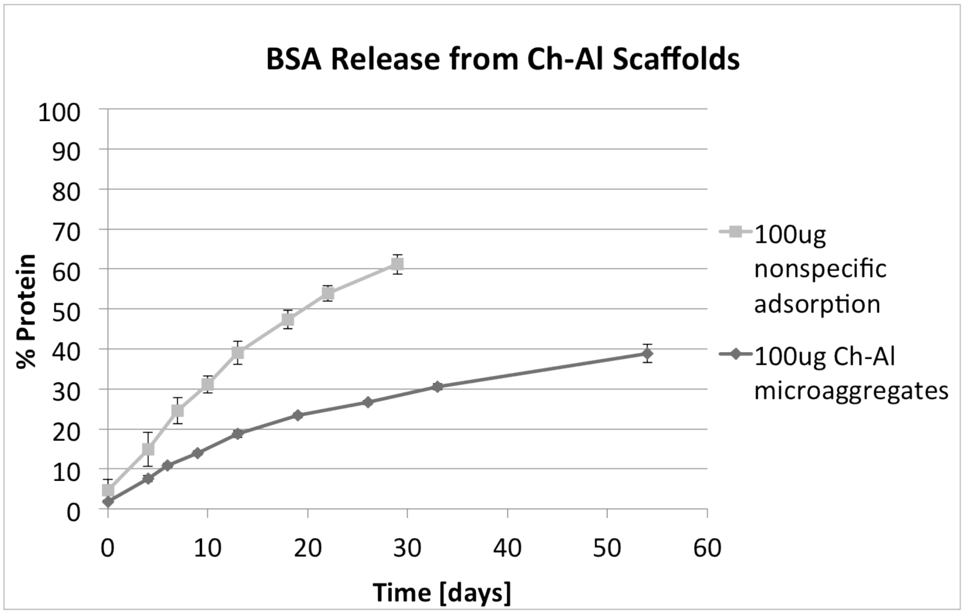
BSA Release from Ch-Al Scaffolds
% Protein
Time [days]
100ug nonspecific adsorption
100ug Ch-Al microaggregates

B

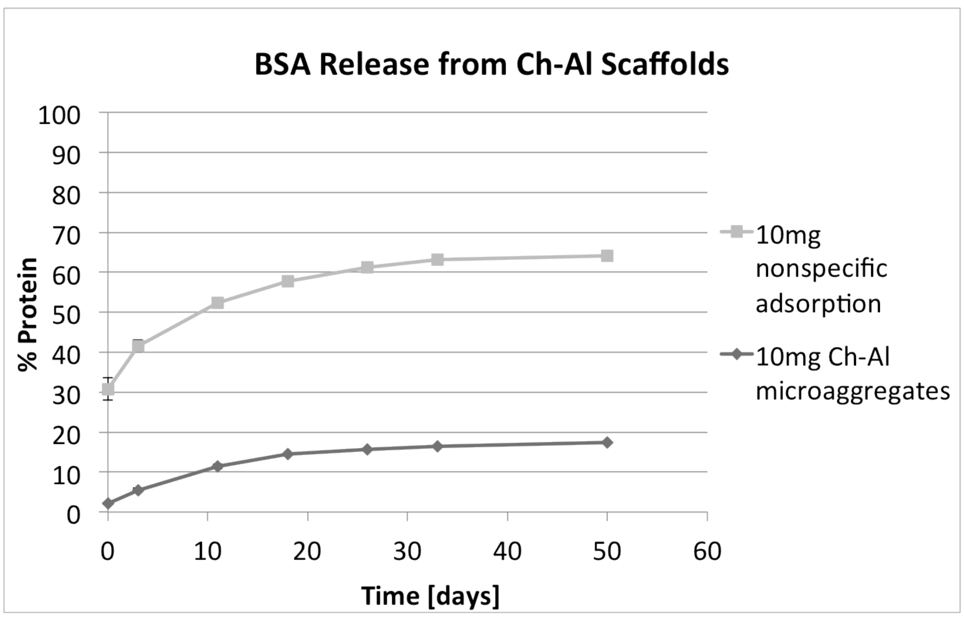
BSA Release from Ch-Al Scaffolds
% Protein
Time [days]
10mg nonspecific adsorption
10mg Ch-Al microaggregates

C

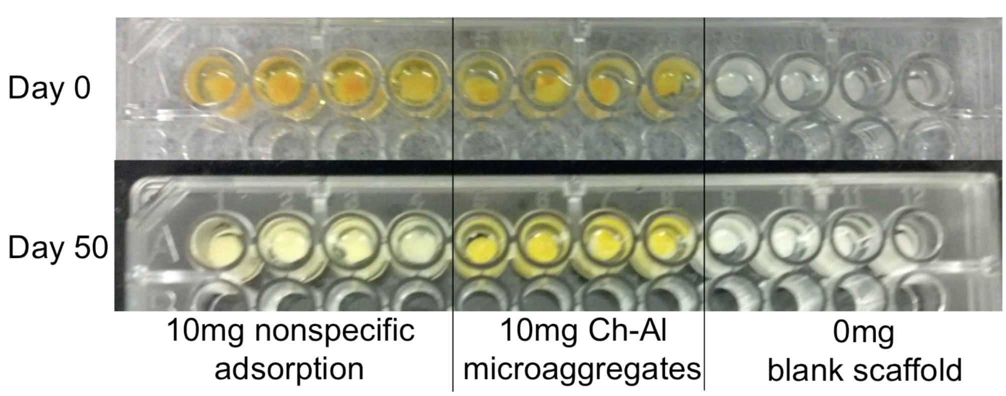
Day 0
Day 50
10mg nonspecific adsorption
10mg Ch-Al microaggregates
0mg blank scaffold

Figure 6.3 Release profile of low dose of BSA from Ch-Al scaffolds via nonspecific adsorption or Ch-Al microaggregates (a). Release profile of high dose of BSA from Ch-Al scaffolds via nonspecific adsorption or Ch-Al microaggregates (b). Ch-Al scaffolds releasing high dose BSA via nonspecific adsorption or Ch-Al microaggregates on days 0 and 50 (c).

6.4.4 Ionic Complexation Effect

Release of 10mg of BSA from Ch-Al microaggregates within Ch-Al scaffolds was modulated by the type of release medium in which the scaffolds were incubated (Figure 6.4). Microaggregate-loaded scaffolds were incubated in either dH_2O, 2N NaCl, PBS, or complete DMEM. It was hypothesized that the mechanism of protein encapsulation and release from microaggregates was dictated by ionic complexation between charged moieties on the protein and free charged functional groups on both chitosan and alginate, specifically amines and carboxylates, respectively. This proved to be likely since a strong ionic solution of 2N NaCl displaced BSA very readily, leading to greater BSA release than scaffolds in dH_2O, PBS, or complete DMEM. Release in 2N NaCl resulted in a burst release of 8% and a total release of 30% by day 7. Contrastingly, burst release in dH_2O was merely 0.1% with a total release of 7% by day 7. BSA release in PBS and complete DMEM fell in the middle, with a burst release of 1% and a total release of 9% in PBS, and an increased burst release of 5% and a total release of 25% in complete DMEM on day 7.

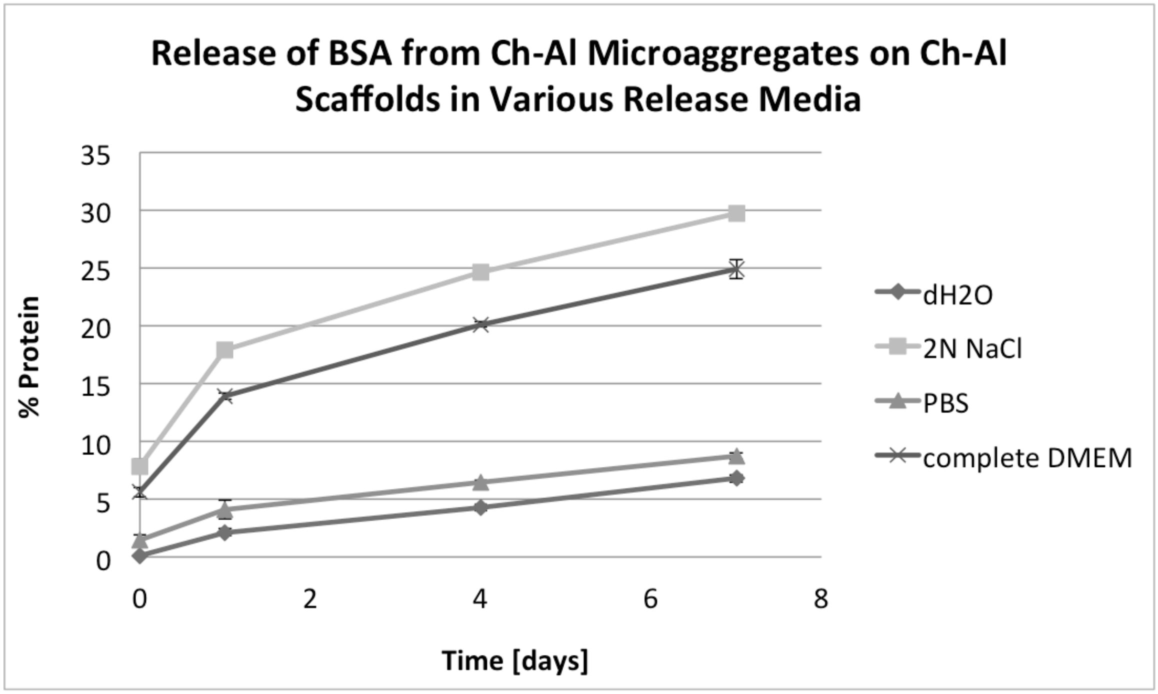

Figure 6.4 Release profile of high dose of BSA from Ch-Al microaggregates on Ch-Al scaffolds using various release media such as dH_2O, 2N NaCl in dH_2O, PBS, and complete DMEM.

6.4.5 Persistence within Scaffolds

Using DLS, it was discovered that Ch-Al microaggregate size changes over time from a single peak 500nm-1um population to a two peak 500nm-1um and 5um bimodal population (data not shown). The appearance of the second peak indicating larger sized microaggregates only appeared if samples were allowed to sit at room temperature for 5min or more before DLS measurement. However, if samples were measured using DLS immediately after sonication, only the smaller peak appeared. This led to the hypothesis that microaggregates in solution aggregate over time. Upon viewing by SEM, it was revealed that Ch-Al microaggregates exhibited a fibrous morphology, with approximately 1um diameter and 5um length fibers. Another flake-like type of morphology was seen alongside the fibers, with the longest dimension measuring around 50um. Based on these size and morphology data, it was postulated that Ch-Al microaggregates self assemble into polyionic complexes that form larger hierarchical structures with fiber-like morphology over time. This likely occurs during the initial dropwise addition of alginate and protein into stirring chitosan and continues in solution even after sonication. The fiber-like morphology of microaggregates was suspected to increase their persistence within scaffolds during washing compared to other protein delivery mechanisms with lower aspect ratios like microparticles and microspheres. Thus, microparticles were made of Ch-Al by adding in the surfactant Pluronic during fabrication to arrest fiber growth and create a more granular morphology. These Ch-Al microparticles were similar to Ch-Al microaggregates from a chemical standpoint, but morphologically the two were very different, and therefore they could be used as a comparison to demonstrate the effect of morphology on persistence within scaffolds. The encapsulation efficiency of BSA within Ch-Al microparticles was still ~98% for 10mg loading (data not shown). For further comparison, polystyrene microspheres with perfectly round morphology were also tested for their persistence within scaffolds. Figure 6.5 illustrates the size as measured by DLS (Figure6. 5a) and morphology as imaged by SEM (Figure 6.5b) of Ch-Al microaggregates, Ch-Al microparticles, and polystyrene microspheres. It was confirmed that microaggregates persisted within scaffolds during washing significantly better than microparticles or microspheres (Figure 6.5c). Only 5% of microaggregates were washed away after three washes, while 30% and 80% of microspheres and microparticles were lost, respectively. However it is important to note that while the burst release of BSA from microaggregates is <2% upon washing and the expected burst release of Nile Red from microspheres is likely to be very low as well, the burst release of BSA from microparticles was not characterized, and thus the fluorescent signal in the wash may be due to released BSA alone and not microparticles themselves leaving.

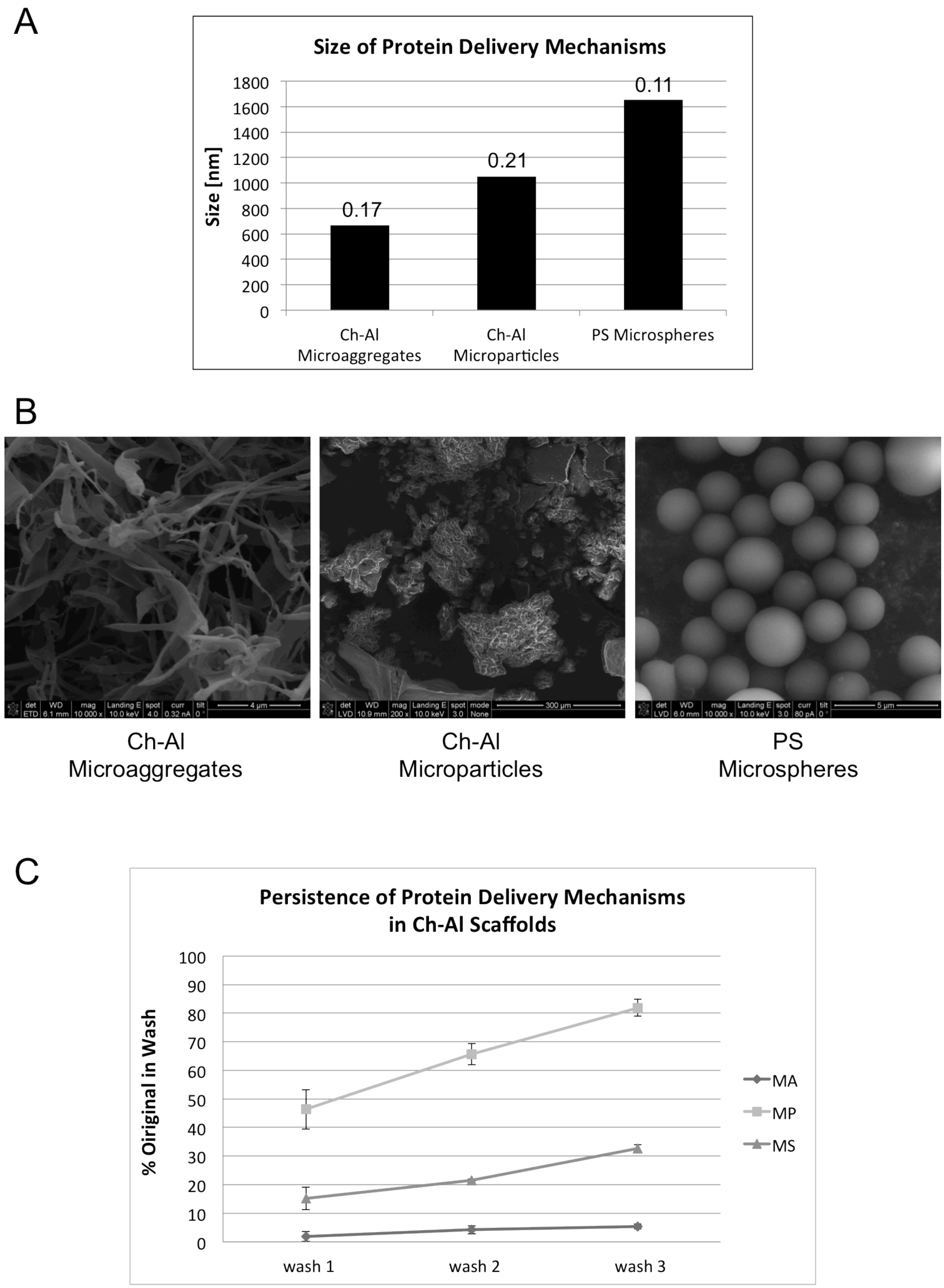

Figure 6.5 Dynamic light scattering (DLS) size measurements of the different protein delivery mechanisms: Ch-Al microaggregates, Ch-Al microparticles, and polystyrene microspheres (a). Scanning electron microscopy (SEM) of Ch-Al microaggregates, Ch-Al microparticles, and

polystyrene microspheres demonstrating the morphology of these different protein delivery mechanisms (b). Persistence of Ch-Al microaggregates (MA), Ch-Al microparticles (MP), or polystyrene microspheres (MS) on Ch-Al scaffolds after three washes (c).

6.5 Discussion

Interestingly, with increasing dose, the encapsulation efficiency of BSA increases while the burst release and slope of release decrease, which may be due to an increasing complexation between the protein and the chitosan-alginate microaggregates during mixing as the protein content increases. Typically in other drug loading systems and even ionic complexation systems that use chitosan and tripolyphosphate (TPP), encapsulation efficiency drops off with increasing dose. The fact that microaggregates encapsulate more protein at higher doses may be due to alginate chains trapping proteins between the chitosan and alginate polymer backbones during ionic complexation. This kind of entrapment would not occur when using small molecule TPP to ionically complex with chitosan chains. Moreover, other proteins with various isoelectric points, and thus charges, as well as different molecular weights all encapsulated at high efficiency and released with little burst and minimal total release over many weeks. This points to the versatility of Ch-Al microaggregates as a protein release system. Based on the fact that differently charged proteins behave similarly in terms of encapsulation and release, it may be likely that both positively and negatively charged moieties within the protein interact with the negatively and positively charged functional groups of alginate and chitosan, respectively, during the microaggregate fabrication process. The negative alginate solution is first mixed with protein and then added dropwise to a positive stirring chitosan solution, so there are multiple opportunities for ionic complexation between proteins of various charges with branches of the polymer chains. This ionic complexation extends beyond net positive proteins electrostatically interacting with negative alginate, or net negative proteins interacting with positive chitosan. Net neutral or even like-charged proteins have the potential to interact with both chitosan and alginate due to the fact that charge distribution within a protein is not usually uniform.

However, small molecule biotin, which has a negative carboxylate group at neutral pH, displayed poor encapsulation efficiency and a large burst release, which suggests that microaggregates may not be a good choice of delivery mechanism for small molecules. Nevertheless, based on the excellent performance of model proteins in this study, therapeutic proteins for chondrogenesis and osteogenesis like TGF-β1 (44.3 kDa, positive) and NELL1 (130 kDa monomer, negative) may be successfully encapsulated and delivered with desired efficiency.

Nonspecific adsorption release kinetics were not as sustained as microaggregate release kinetics, despite the fact that both the microaggregates and the scaffolds were made of Ch-Al. This may be due to the pH difference between the two environments during protein loading. Ch-Al scaffolds were at pH 7.4 when BSA was loaded, and Ch-Al microaggregates were at pH 5.5 when BSA was loaded during fabrication. The acid dissociation constants of chitosan and alginate are 6.3 and 3.4-3.7, respectively.[14] At pH 7.4, alginate is negatively charged and chitosan is neutral, resulting in an overall negative charge of the scaffold surface to which proteins were nonspecifically adsorbed. At pH 5.5, alginate is negatively charged and chitosan is positively charged, resulting in an overall neutral charge of the microaggregates, but a maximum region of ionic interaction due to charge density matching between the two polymers. Previously, Ch-Al polyelectrolyte complexes in various forms have been used to encapsulate and deliver proteins or drugs by manipulating the degree of association between the two polymers' functional groups as well as their pH-dependent charge density.[14,15] So if proteins can be loaded into microaggregates during this pH-dependent zone of maximized ionic interaction, they will likely encapsulate at a very high efficiency with little burst release, which was confirmed in this study. Further, in this pH range of maximum ionic interaction around 5.5, ionic complexes between chitosan and alginate exist in a shrunken state, compared to above 6.3 or below 3.4, where the polymer chains exist in a swollen state and are less able to trap proteins.

In an attempt to verify that ionic compexlation was the driving mechanism behind protein encapsulation and release, protein-loaded microaggregates were added to scaffolds and incubated in various release media with varying concentrations of ions and other proteins. Microaggregates on scaffolds in 2N NaCl release medium released BSA faster than in any other release medium. This is due to its high concentration of ions compared to dH_2O, PBS, or complete DMEM. dH_2O contains no ions, while complete DMEM contains 10% FBS, 1% ABAM, 4.5g/L glucose, 110mg/L sodium pyruvate (1mM), 584mg/L L-glutamine (4mM), 3.7g/L $NaHCO_3$ (44.04mM), 6.4g/L NaCl (109.5mM), and negligible amounts of other inorganic salts, amino acids, and vitamins. PBS contains 136.9mM NaCl, and this is the mostly highly concentrated salt in PBS by at least two orders of magnitude. Thus, 2N NaCl has nearly 15 times higher concentration of NaCl than PBS, and this difference led to a 5 times greater burst release and 4 times greater total release over the course of just 7 days. Incubation in 2N NaCl also exhibited greater burst and total release than in complete DMEM, which contained serum proteins in addition to salts comparable in concentration to PBS, affirming the importance of ionic complexation in protein retention within microaggregates. Just as any proteins in the release medium compete away the loaded protein of interest, any ions in the release medium will displace the loaded protein as well, and here the ion competition was demonstrated to have a greater effect than the protein competition. Release in complete DMEM was greater than in PBS due to the presence of serum proteins in addition to salts, yet release in 2N NaCl was still more significant than either.

It is important to remember that release *in vivo* may be much greater than what is demonstrated in these *in vitro* experiments, so while it may seem like the release profile curves are too shallow, *in vivo* the release profiles may be steeper due to the presence of bodily fluids containing high concentrations of proteins and ions. Total plasma protein concentration in human blood ranges from 60-80g/L, while Na^+ concentration is around 140mM and Cl^- concentration is around 100mM in human blood.[19] Further, even though some curves appear to plateau *in vitro*, there was still steady release of some protein even after the course of many weeks.

There has been a lot of research studying the interactions between chitosan and alginate and how they form polyion complexes.[20-22] Charge ratio, molecular weight, ionic strength, pH, mixing order, mixing speed, and diameter of the dispersing element all influence particle size, zeta potential, and stability of Ch-Al polyelectrolyte complexes.[22] Previously, Ch-Al polyelectrolyte complexes in various forms have been used to encapsulate and deliver proteins or drugs by manipulating the degree of association between the two polymers' functional groups as well as their pH-dependent charge density.[14,15] For example, Ch-Al self-assembling polyelectrolyte multilayer films have been used to immobilize antibodies[15], Ch-Al blend gel beads with dual crosslinking were shown to have gastrointestinal site-specific protein release[16], and drug-loaded, polyelectrolyte complexed Ch-Al fibers released charged compounds such as bovine serium albumin (BSA), platelet-derived growth factor-bb (PDGF-bb), and avidin over the course of 3 weeks.[17] Chitosan-gellan polyion complexes, which can be related to Ch-Al polyion complexes, have been shown to self assemble at the aqueous solution interface.[23,24] Polyionic complexation occurs through electrostatic interactions between cationic and anionic polymers, forming structures that possess a counterion pairing structure.[23,24] Other studies show that fibers and fibrils can self assemble via monomers aggregating into fibers through specific interactions then forming higher order structures through hierarchical assembly.[25] Hydrogen bonds and hydrophobic interactions between the monomer molecules are thought to be responsible for this assembly process.[25] These previous studies support for the hypothesis that Ch-Al microaggregates are polyionic complexes formed through ionic complexation that self assemble into fibrous networks. An alternative or perhaps cooperative idea is that microaggregates were formed through phase separation, since previous research has shown that phase separation followed by gelation can form nanofibrous networks.[26] With this theory, a multicomponent system becomes thermodynamically unstable and separates into more than one phase to lower the system free energy. This results in a polymer lean and a polymer rich phase, and subsequently the polymer rich phase solidifies to form the nanofibrous network.[26] This kind of phase separation may also serve to explain why and how Ch-Al microaggregates obtained their fibrous morphology.

By adding the surfactant Pluronic to the Ch-Al microaggregate fabrication process, Ch-Al microparticles were created instead. Surfactants are amphiphilic molecules that readily adhere to surfaces and consequently lower the interfacial tension.[27] With lower interfacial free energy, fiber self assembly may be arrested, and results confirmed that a more truncated, granular morphology was observed when surfactant was included. Ch-Al microparticles exhibited a greater size variability than microaggregates, and their fabrication also resulted in granular microparticles that washed away more easily than fibrous microaggregates. The SEM image in Figure 6.5b illustrates an extreme size range, but in reality most microparticles were around 20um. DLS measurements claimed a 1um population, but this is likely because DLS cannot detect very large particles over a few microns, which was the majority of the Ch-Al microparticles.

Ch-Al microaggregate persistence in scaffolds during washing was improved over Ch-Al microparticles or polystyrene microspheres *in vitro*. This data has implications in an *in vivo* environment where blood and fluid flow may disrupt or dislodge the protein delivery system from its carrier. Moreover, macrophages tend to engulf particles of a particular size range (4-80um) and transport them to nearby lymphatic system, resulting in the inadvertent migration of particles away from the targeted injury site, as seen in periurethral injection studies.[28,29] Therefore, having a protein delivery mechanism with distinct morphology and size may be useful for persistence *in vivo*.

In the future, once stem cell chondrogenesis can be established on Ch-Al scaffolds using Ch-Al microaggregates to deliver chondrogenic growth factors *in vitro,* this system can be translated to *in vivo* implantation in a rabbit knee joint model. Mesenchymal stem cells in the underlying bone marrow can be wicked up into the scaffold using controlled macro- and micro-channeled architecture, and stem cells encountering growth factor releasing from the microaggregates can be guided to differentiate down the chondrogenic pathway and regenerate the cartilage tissue.

6.6 Conclusion

This study demonstrates the successful efficient encapsulation and sustained delivery of various model proteins using novel Ch-Al microaggregates. Microaggregates outperformed nonspecific adsorption on scaffolds at both low and high doses, but the most convincing evidence to use microaggregates is the significantly reduced burst release at high doses relevant for human treatment. Ch-Al microaggregates can be used to deliver therapeutic proteins with extremely minimal loss upon loading and with a gradual release over the course of multiple months. Due to their fiber-like morphology, microaggregates persisted within scaffolds during washing *in vitro* compared to microparticles or microspheres which both exhibited significant loss upon washing, and it can be expected that these benefits of microaggregates will translate to an *in vivo* environment as well.

References

1. Langer R, Moses M. Biocompatible controlled release polymers for delivery of polypeptides and growth factors. Journal Cellular Biochemistry 1991;45:340-345.
2. Tayalia P, Mooney DJ. Controlled growth factory delivery for tissue engineering. Advanced Materials 2009;21:3269-3285.
3. Chen FM, Wu ZF, et al. Toward delivery of multiple growth factors in tissue engineering. Biomaterials 2010;31:6279-6308.

4. Santo VE, Gomes ME, Reis RL, et al. Controlled release strategies for bone, cartilage, and osteochondral engineering—part I: recapitulation of native tissue healing and variables for the design of delivery systems. Tissue Engineering Part B: 2013;19(4)308-326.
5. Santo VE, Gomes ME, Reis RL, et al. Controlled release strategies for bone, cartilage, and osteochondral engineering—part II: challenges on the evolution from single to multiple bioactive factor delivery. Tissue Engineering Part B 2013;19(4):327-352.
6. Temenoff JS, Mikos AG. Review: tissue engineering for regeneration of articular cartilage. Biomaterials 2000;21:431-440.
7. Reed S, Wu BM. Sustained growth factor delivery in tissue engineering applications. Annals of Biomedical Engineering 2013 [ahead of print]
8. Madry H, Rey-Rico A, Cucchiarini M, et al. Transforming growth factor beta-releasing scaffolds for cartilage tissue engineering. Tissue Engineering: Part B 2013 [ahead of print]
9. Jiskoot W, Randolph TW, et al. Protein instability and immogenicity: roadblocks to clinical application of injectable protein delivery systems for sustained release. J Pharm Sci 2012;101(3):946–954.
10. Breinan HA, Minas T, Spector M, et al. Histological evaluation of the course of healing of canine articular cartilage defects treated with cultured autologous chondrocytes. Tissue Engineering 1998;4(1):101-113.
11. Li Z, Zhang M, et al. Chitosan-Alginate Hybrid Scaffolds for Bone Tissue Engineering. Biomaterials 2005;26:3919-3928.
12. Li Z, Zhang M. Chitosan-Alginate as Scaffolding Material for Cartilage Tissue Engineering. J Biomed Mater Res 2005;75A:485-493.
13. Wan Y, Wu H, Wen D. Porous-Conductive Chitosan Scaffolds for Tissue Engineering, 1: Preparation and Characterization. Macromol Biosci 2004;4:882-890.

14. Lawrie G, Keen I, Grondahl L, et al. Interactions between alginate and chitosan biopolymers characterized using FTIR and XPS. Biomacromolecules 2007;8:2533-2541.

15. Yuan W, Dong H, Zhou Q, et al. pH-controlled construction of chitosan/alginate multilayer film: characterization and application for antibody immobilization. Langmuir 2007;23:13046-13052.

16. Xu Y, Zhan C, Zheng H, et al. Preparation of dual crosslinked alginate-chitosan blend gel beads and in vitro controlled release in oral site-specific drug delivery system. International Journal of Pharmaceuticals 2007;336:329-337.

17. Liao IC, Wan ACA, Leong KW, et al. Controlled release from fibers of polyelectrolyte complexes. Journal of Controlled Release 2005;104:347-358.

18. Lee M, Li W, Wu BM, et al. Biomimetic apatite-coated alginate/chitosan microparticles as osteogenic protein carriers. Biomaterials 2009;30:6094-6101.

19. Rao DA, Le T, and Bhushan V. First Aid for the USMLE Step 1 2008 (First Aid for the Usmle Step 1). McGraw-Hill Medical. 2007.

20. Mitrevej A, Sinchaipanid N, Kositchaiyong V, et al. Multiunit controlled-release diclofenac sodium capsultes using complex of chitosan with sodium alginate or pectin. Pharmaceutical Development and Technology 2001;6(3):385-392.

21. Sakai S, Ono T, Kawakami K, et al. Control of molecular weight cut-off for immunoisolation by multilayering glycol chitosan-alginate polyion complex on alginate-based microcapsules. J Microencapsulation 2000;17(6):691-699.

22. Hamman JH. Chitosan based polyelectrolyte complexes as potential carrier material in drug delivery systems. Marine Drugs 2010;8:1305-1322.

23. Yamamoto H, Senoo Y. Polyion complex fiber and capsule formed by self-assembly of chitosan and gellan at solution interfaces. Macromol Chem Phys 2000;201:84-92.

24. Ohkawa K, Kitagawa T, Yamamoto H. Preparation and characterization of chitosan-gellan hybrid capsules formed by self-assembly at an aqueous solution interface. Macromol Mater Eng 2004;289:33-40.

25. Binder WH, Smrzka OW. Self-assembly of fibers and fibrils. Agnew Chem Int Ed 2006;45:7324-7328.

26. Ma PX. Scaffolds for tissue fabrication. Materials Today 2004;30-40.

27. Ziani K, Henrist C, Cloots R, et al. Effect of nonionic surfactant and acidity on chitosan nanofibers with different molecular weights. Carbohydrate Polymers 2011;83:470-476.

28. Malizia AA, Reiman HM, Utz WJ, et al. Migration and granulomatous reaction after periurethral injection of polytef (Teflon). JAMA 1984;251(24):3277-3281.

29. Henly DR, Barrett DM, Wein AJ, et al. Particulate silicone for use in periurethral injections: local tissue effects and search for migration. J Urology 1995;153:2029-2043.

Chapter 7

7. Future Aims

7.1 Mesenchymal Stem Cell Chondrogenesis

The main aim of this project is create a scaffold implant that recruits endogenous bone marrow stem cells and provides an environment that drives their chondrogenesis. Ch-Al scaffolds are robust, easy to handle, and highly elastic under extreme compressive strains, so they may serve as a suitable implant for cartilage resurfacing and large defects. However, two crucial pieces of information are still needed to confirm the plausibility of this goal. The first is to ensure that the mixed cell population within bone marrow contains enough mesenchymal stem cells and that they respond strongly enough to the provided cues to synthesize cartilage. Mesenchymal stem cells comprise a minor fraction of the total cell population in bone marrow with an approximate frequency of 1 in 5000 bone marrow mononuclear cells.[1] Moreover, bone marrow is made up of plasma proteins, hematopoietic stem cells, blood cells, and stromal cells that may form ectopic tissue. Interfering signals may be present in bone marrow or even the surrounding lesion, and the effect of the delivered growth factor could be diluted or quenched. To study this, bone marrow aspirate from New Zealand white rabbits can be cultured *in vitro* on Ch-Al scaffolds with chondrogenic growth factor delivery from microaggregates. Chondrogenic differentiation can be observed through sectioning and histology as performed previously on constructs. Different growth factors such as TGF-β1 or TGF-β3 as well as different delivery methods and concentrations may need to be employed to achieve the desired chondrogenic response. Ch-Al scaffolds can be functionalized with integrins specific to mesenchymal stem cells to bias attachment kinetics. In this regard, Ch-Al surfaces can be functionalized with antibodies specific to mesenchymal stem cell surface markers.

The second important element is to prove that channeled scaffolds absorb bone marrow readily and within seconds before the clotting cascade propagates. While cell suspension and blood uptake has been studied in the past, bone marrow is more viscous, and the capillary action and diffusion forces will be altered. Blood's viscosity at physiological temperature typically ranges from 3 to 4 mPa-s, while the viscosity of water at room temperature is 1 mPa-s. Like blood, red bone marrow is a non-Newtonian fluid whose viscosity decreases with shear. Human calcaneus bone marrow, which is mostly yellow and Newtonian, has a viscosity measured to be 37.5 mPa-s, yet bovine femoral and mostly red bone marrow viscosity was found to be 123 mPa-s.[2] Dry, channeled Ch-Al scaffolds can be implanted in a rat or rabbit femoral or tibial defect *in vivo* before sacrifice, and bone marrow uptake and distribution can be quantified bench-side and histologically. In the past, bone marrow uptake was studied *ex vivo* through implantation in a sacrificed rabbit knee joint., but the deceased rabbit did not have sufficient blood volume and pressure to achieve bone marrow uptake. Channel diameter and number may need to be optimized to encourage faster marrow uptake. However, it is important to keep in mind that open space within the scaffold will eventually need to be filled by cell-excreted matrix, so highly vacuous scaffolds may be a challenge for cells.

7.2 In Vivo *Validation*

An *in vivo* rat model may serve as a first pass trial to examine how Ch-Al scaffolds behave in the knee joint. Basic observations such as handling, toxicity, immune response, wear, and degradation can be addressed in this relatively inexpensive model. The size limitation with rat knee joint implantation, which has been done by collaborators and requires 2mm diameter and 1mm deep defects, may force the choice of implanting at larger site like the rib cage or intervertebral disc. Even though these sites contain fibrocartilage, the environment is still more representative of the knee joint in terms of cell type, tissue architecture, blood supply, and native enzymes than subcutaneous implantation.

Our lab has recently demonstrated a New Zealand white rabbit articular cartilage injury model. Critical size 3 mm patellofemoral groove defects were created by punch biopsy, and previously described alginate hydrogels containing Nell1 within chitosan microparticles were implanted.[3] Some defects with blank alginate scaffolds healed completely, but the incidence of healing with Nell1 delivery was more frequent. Explant histology revealed ECM and lacunae morphology typically seen in native cartilage in healed defects. Other defects exhibited fibrocartilage production and poor healing. Immune response to alginate hydrogels was severe in some cases, with fibrous encapsulation and bone ingrowth around and between alginate pieces. This patellofemoral groove injury model can be applied to Ch-Al scaffolds with and without TGF-β1. Cartilage production and integration with the defect edge will be critical in determining effectiveness of bone marrow mesenchymal stem cell repair of the lesion. One potential issue may be delayed degradation of Ch-Al, which could lead to chronic inflammation and disruption of cartilage healing. MMP-cleavable peptide sequences may be functionalized onto chitosan or alginate polymers during mixing or during crosslinking to assist scaffold breakdown in the joint by local enzymes.

A few osteoarthritic animal models have been employed to study pharmaceutical agents for the prevention and treatment of osteoarthritis in humans.[4,5] The two major types of models are spontaneous and induced osteoarthritis. The spontaneous category is a naturally occurring model, and the disease develops over time as the animal ages. Hartley albino guinea pigs, Syrian hamsters, and mice have all been used, but the medial compartment of the guinea pig knee is the most common model. Within the induced category, a protein mutation can be introduced in a transgenic model to cause osteoarthritic phenotype, or joint structure can be transected, damaged, or removed in a surgical model to cause joint instability. Another option is the injection of an exogenous substance to induce damage. Induced models have the advantage of accelerated disease progression and known origin and timing of induction. Common surgical models include mouse anterior cruciate ligament damage, rat and guinea pig unilateral medial meniscal tear, Beagle dog and rabbit partial medial meniscectomy, and dog anterior cruciate ligament transection.

A naturally occurring osteoarthritis Hartley albino guinea pig model can be treated with Ch-Al constructs containing growth factor releasing microaggregates implanted in the patellofemoral groove. The symptoms of osteoarthritis typically start around 3 months of age and 700 g weight and progress to severe lesions around 12 months.[5] Unlike rats and mice, guinea pigs express MMP1 and MMP13 in cartilage wound sites, making them a good model for the pathogenesis of human osteoarthritis. Healthy stem cells within bone marrow may be able to repair cartilage in the degenerative environment as chondrogenic growth factor gradually releases from microaggregates. Release kinetics *in vivo* will differ as ion, protein, and enzyme levels fluctuate within the joint. Mesenchymal stem cell response to TGF-β1 release can be evaluated by stem cell differentiation and matrix synthesis. Diffusion-based release can be compared to covalent, permanent presentation of TGF-β1. This osteoarthritic guinea pig model will provide the most accurate likeness to the human condition while remaining on the small scale of a rodent trial.

7.2.1 Aim 1: In Vivo *Validation of Chitosan-Alginate Scaffolds Implanted Both Subcutaneously and in the Knee Joint Incite a Limited Host Inflammatory Response*

Both chitosan and alginate polymers have been studied thoroughly *in vivo* for their inflammatory properties; however the blend of the two together has been much less investigated. The host response to chitosan alone ranges from acute to sub-acute inflammatory reaction. Chitosan is known to activate the complement system via the alternative pathway (C3 and C5), likely due to its positively charged amine functional groups.[6] Also, macrophages are known to interact with the acetylated residues of chitosan, so a higher degree of deacetylation can reduce macrophage response.[7] Chitosan is also a chemoattractant for neutrophils lasting for the first 7 days.[8] Overall, most studies cite a minimal foreign body reaction with few foreign body giant cells, no chronic inflammation or chronic lymphocyte presence, and little to no fibrous encapsulation.[8] Chitosan is further known to accelerate angiogenesis and coagulation, and the polymer is degraded by lysozyme and plasma.[9] Similarly, alginate is known to have an acute inflammatory reaction with the presence of neutrophils, macrophages, lymphocytes, eosinophils, and mastocytes.[8,10] However, some studies claim alginate causes persistent fibroblast presence, fibroplasia, and fibrosis.[8,11] Negatively charged surfaces have been shown to activate complement in a calcium dependent manner and thus via the classical pathway[12], and this may be expected of alginate due to its negatively charged carboxylate functional groups. Alginate is degraded via hydrolysis. As for a blend of the two polymers together, Ch-Al blended scaffolds were first infused with bone marrow and then implanted in the gluteus maximus muscle pouch of adult Sprague-Dawley rats (2 months old). These blend scaffolds shows a foreign body reaction at weeks and 1 and 2 shown by neutrophil presence. No fibrotic layer was seen at week 12, and there was good integration with the surrounding tissue at week 12. Moreover, blood vessels and collagen deposition were seen at weeks 4 and 12.[13]

These studies all indicate that Ch-Al blends have the potential to elicit an immune response, at least at the acute level, and it will be critical to assess inflammation over the course of many weeks. Our preliminary studies of Ch-Al scaffolds subcutaneously implanted on the abdomens of adult Sprague-Dawley rats have shown a severe neutrophil infiltration within the first week that persists up until 6 weeks, as indicated by some surviving but mostly dead neutrophils and neutrophilic debris at 6 weeks. Further, granulation tissue reminiscent of a fibrotic layer with loose collagen deposition and also blood vessels was seen surrounding the scaffolds as early as 1 week. Immunohistochemistry for CD68+ monocytes illustrated persistent monocyte presence from weeks

1 through 6. To determine if there was a species-specific inflammatory response, we moved to a dorsal subcutaneous C57BL/6 mouse model comparing Ch-Al scaffolds to Ch-Al scaffolds crosslinked with CS and also a baseline scaffold commonly used in cartilage tissue engineering, in this case fibrin. With this model we gathered information about "normal" amounts of inflammation generated in response to a relatively benign scaffold material like fibrin. At weeks 1 and 2, Ch-Al scaffolds in mice demonstrated much less neutrophil and monocyte infiltration than in rats, and much less fibrosis was seen as well. Moreover, Ch-Al scaffolds crosslinked with CS demonstrated no fibrosis at all and even less neutrophil and monocyte invasion. The control fibrin scaffolds implanted subcutaneously in mice degraded quickly, and in the remaining fragments there was no evidence of neutrophils, monocytes, or fibrosis, as expected.

These preliminary experiments point to the fact that Ch-Al can be tolerated *in vivo*, depending on the animal model and implant site. If Ch-Al scaffolds implanted in the rabbit knee turn out to be much less tolerated by the animals over the course of many weeks, the scaffold surface charges may be altered. Positively charged surfaces are known to activate the complement alternative pathway, while negatively charged surfaces are known to activate the complement classical pathway.[12] Our Ch-Al scaffolds are likely negatively charged, since the scaffold solution is neutralized to pH 7.4 before freeze-drying, and at this pH the carboxylic acid functional groups on alginate are negatively charged while the amine functional groups on chitosan are neutrally charged. One approach to shield the surface charge would be to coat the scaffold in a thin layer of poly(ethylene glycol) (PEG), which reduces interaction with blood proteins and thus reduces complement activation. Another approach would be to nonspecifically adsorb a protein, either general serum proteins or a therapeutically selected protein, to the surface of the scaffold to neutralize any charges before implantation.

7.2.2 Aim 2: In Vivo *Validation of Sustained Release of Chondrogenic Growth Factor using Chitosan-Alginate Microaggregates on Chitosan-Alginate Scaffolds Enhances Chondrogenesis when Implanted in the Knee Joint*

We have demonstrated that Ch-Al microaggregates, pHed to 5.5 for maximum ionic interaction between the positively charged amine and negatively charged carboxylic acid groups, produce a sustained release of model protein bovine serum albumin (BSA) with a <5% burst for doses of 10ug to 10mg initial load. Interestingly, with increasing dose, the burst release and slope of the release decreases, which may be due to an increasing aggregation between the protein and the Ch-Al microaggregates during mixing. Similar release kinetics--<5% burst and <50% released at 6 weeks--were seen with both positively and negatively charged proteins of varying molecular weights, such as histone, fibrinogen, avidin, and biotin. There is, however, an inherent ability of Ch-Al scaffolds to bind proteins quite strongly, also resulting in a sustained release with <5% burst and 60% released at 6 weeks for 100ug of BSA initial dose. This is due to nonspecific adsorption of the protein to the charged surface of the scaffold. 100ug of BSA loaded via nonspecific adsorption onto Ch-Al scaffolds was compared to 100ug of BSA loaded into Ch-Al microaggregates seeded on Ch-Al scaffolds, and the former demonstrated a sustained release but with a slope twice as steep as the system using microaggregates. The release kinetics of both systems at this dose are useful for cartilage tissue engineering. However, at much higher doses, such as 10mg of BSA, the nonspecific adsorption system results in a burst release of 30% and 60% released by 6 weeks. Thus, it can be concluded that the microaggregates offer an advantage over nonspecific adsorption at high doses, doses similar to those required for human *in vivo* studies.

Another dictating factor of release is the release medium and temperature. The release of chondrogenic protein TGF-β1, with 200ng nonspecifically adsorbed onto Ch-Al scaffolds, was tested at 37C in complete media (containing serum proteins and antibiotics). Because TGF-β1 is positive at physiological pH, it was expected that the protein bind strongly to the likely negative surface of Ch-Al, and results showed 2% burst release and 20% total release at 6 weeks using an ELISA assay. With this system of 200ng TGF-β1 nonspecifically adsorbed onto Ch-Al, chondrocytes or mouse bone marrow stromal cells (mBMSCs) were seeded onto the growth factor-loaded scaffolds and allowed to culture for 4 or 8 weeks. With TGF-β1, chondrocytes produced cartilage ECM within 4 weeks, and without TGF-β1 chondrocytes produced similar ECM at 8 weeks. mBMSCs excreted an immature ECM, likely collagen type I, at both 4 and 8 weeks with TGF-β1, but no cartilaginous ECM was generated. Ch-Al microaggregates releasing TGF-β1 were compared to nonspecific adsorption of the growth factor on Ch-Al scaffolds, and mouse adispose derived stem cells (mADSCs) or mBMSCs were seeded at a high density on the growth factor loaded scaffolds. At week 4, microaggregates promoted the greatest cartilaginous ECM laydown compared to nonspecific adsorption or no growth factor at all, for both cell types. These preliminary results were the first demonstration of stem cell chondrogenesis on Ch-Al scaffolds. Once stem cell chondrogenesis has been thoroughly established *in vitro,* this system can be translated to an *in vivo* implantation in the New Zealand white rabbit knee joint where mesenchymal stem cells in the underlying bone marrow are wicked up and differentiate down the chondrogenic pathway once in contact with TGF-β1 releasing from microaggregates within the scaffold.

7.2.3 Aim 3: In Vivo *Validation of Three Dimensionally-Printed, Micro- and Macro-Channeled Chitosan-Alginate Scaffolds Implanted in the Knee Joint Assist Mesenchymal Stem Cell Uptake, Vascularization, and Development of Cartilage Zonal Architecture*

Three dimensional printing (3DP) of scaffolds for tissue engineering offers many advantages over mold-based fabrication techniques since the resulting scaffolds can be tailored to be patient- and site-specific. Also 3DP scaffolds can have complex geometries, such as undercuts, curvatures, and channels, while maintaining a relatively high throughput fabrication process. However, 3DP can be limited to what materials are compatible with the printer, and often sugars and starches are the only materials used in some 3DPs. We developed a method of fabricating Ch-Al scaffolds from sugar preforms using a poly(L-lactic acid) (PLLA) coating to protect the sugar from dissolving in the aqueous environment of the Ch-Al solution. This method allows the fabrication of any aqueous-based polymer scaffold by infusion into the PLLA preform, followed by freeze-drying.

Directional freezing of scaffolds prior to freeze-drying has been applied to a few different materials for a variety of applications, mostly to increase strength. By placing the scaffold solution in a mold on a cold surface, or cold finger, and controlling the rate (in C/min) at which that solution freezes using a thermocouple and a heater, the direction of ice crystal growth in the freezing scaffold solution can be forced to be anisotropic, and thus also the aspect ratio of the resulting scaffold pores can be controlled. This directional freezing results in lamellar pores with an extremely high aspect ratio, and the size and shape of the pores can be altered by altering the freezing rate. We applied directional freezing to Ch-Al scaffolds and were able to achieve scaffolds with lamellar pores measuring 300um on the long axis and 30um on the short axis. Cross-sectioning of both parallel and perpendicular (to the freezing front) planes of the scaffold followed by SEM imaging yielded lamellar pores seen from the parallel cut and cellular pores seen from the perpendicular cut, indicating successful directional freezing.

By combining 3DP and directional freezing, we can control both the micro- and macro-architecture of the scaffold so that it is more biomimetic and offers different regions corresponding to the zonal architecture of native cartilage. Micro- and macro-channels also facilitate cell and blood uptake, as seen in *in vitro* studies the combination of the two resulted in the fastest wicking. Finally, we next plan to translate these 3DP, directionally frozen scaffolds to an *in vivo* New Zealand white rabbit knee joint model where we expect enhanced vascularization of the bone portion of the osteochondral scaffold due to the channeled architecture and improved chondrogenesis in the cartilage region due to the precisely controlled, biomimetic design.

References

1. Kastrinaki MC, Papadaki HA, et al. Functional, molecular and proteomic characterisation of bone marrow mesenchymal stem cells in rheumatoid arthritis. Ann Rheum Dis 2008;67(6):741-749.
2. Gurkan UA, Akkus O. The mechanical environment of bone marrow: a review. Annals of Biomedical Engineering 2008;36(12):1978-1991.
3. Lee M, Wu B, et al. Effect of Nell-1 delivery on chondrocyte differentiation. Tissue Engineering Part A 2010;16(5):1791-1800.
4. Stimpson SA, Kraus VB, Han B. Use of animal models of osteoarthritis in the evaluation of potential new therapeutic agents. In Vivo Models of Inflammation 2006;1:65-82.
5. Bendele AM. Animal models of osteoarthritis in an era of molecular biology. J Musculoskel Neuron Interact 2002;2(6):501-503.
6. Minami S, Suzuki H, Shigemasa Y, et al. Chitin and chitosan activate complement via the alternative pathway. Carbohydrate Polymers 1998;36(2-3):151-155.
7. Benesch J, Tengvall P. Blood protein adsorption onto chitosan. Biomaterials 2002;23(12);2561-2568.
8. Atala A, Lanza R, Nerem R, et al. Principles of regenerative medicine. 2011.
9. Okamoto Y, Yano R, Minami S, et al. Effects of chitin and chitosan on blood coagulation. Carbohydrate Polymers 2003;53(3):337-342.
10. Robitaille R, Dusseault J, Halle JP, et al. Inflammatory response to peritoneal implantation of alginate-poly-L-lysine microcapsules. Biomaterials 2005;26(19):4119-4127.

11. Atala A, Lanza R. Methods of Tissue Engineering. 2002.
12. Chonn A, Cullis PR, Devine DV. The role of surface charge in the activation of the classic and alternative pathways of complement by liposomes. J of Immunology 1991;146(12):4234-4241.
13. Li Z, Zhang M, et al. Chitosan-Alginate Hybrid Scaffolds for Bone Tissue Engineering. Biomaterials 2005;26:3919-3928.